

DESIGN OF A TUNNEL BY NEW AUSTRIAN TUNNELING METHOD (NATM)

A MAJOR PROJECT REPORT
SUBMITTED IN PARTIAL FULFILLMENT OF THE REQUIREMENTS
FOR THE CREDITS
OF

MASTER OF TECHNOLOGY
IN
GEOTECHNICAL ENGINEERING

Submitted by:

ABHISHEK KAUSHIK 2K19/GTE/01

Under the supervision of

Dr. RAJU SARKAR



**DEPARTMENT OF CIVIL ENGINEERING
DELHI TECHNOLOGICAL UNIVERSITY**

(Formerly Delhi College of Engineering)
Bawana Road, Delhi-110042

JULY 2021

DEPARTMENT OF CIVIL ENGINEERING

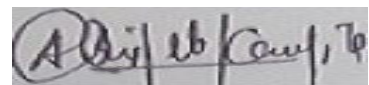
DELHI TECHNOLOGICAL UNIVERSITY

(Formerly Delhi College of Engineering)

Bawana Road, Delhi-110042

CANDIDATE'S DECLARATION

I, Abhishek Kaushik (2K19/GTE/01) of M.Tech (Geotechnical Engineering), hereby declare that the Project Dissertation titled " Design Of A Tunnel By New Austrian Tunneling Method(NATM)" which is submitted by me to the Department of Civil Engineering, Delhi Technological University, Delhi is submitted in partial fulfillment of the requirement for the award of the degree of Master of Technology, is original and not copied from any source without proper citation. This work has not previously formed the basis for the award of any Degree, Diploma Associateship, Fellowship or other similar title or recognition.



(ABHISHEK KAUSHIK)

Place: Delhi

Date:

2K19/GTE/01

CERTIFICATE

I hereby certify that the Project Dissertation entitled "DESIGN OF A TUNNEL BY NEW AUSTRIAN TUNNELING METHOD(NATM)" which is submitted by Abhishek Kaushik (2K19/GTE/01) of MTech (Geotechnical Engineering), Delhi Technological University, Delhi submitted in partial fulfillment of the requirement for the award of Master of Technology, is a record of the project work carried out by the student under my supervision. To the best of my knowledge, this work has not been submitted in part or full for any Degree or Diploma to this University or elsewhere.

Place: Delhi
Date: 04/08/2021
Department of Civil Engineering



(Dr. RAJU SARKAR)
SUPERVISOR & PROFESSOR

ABSTRACT

There are several methods for designing rock supports in tunnels. The Q-system is one of such methods, which is based on the rock mass classification. The Q-system was developed at Norwegian Geotechnical Institute (NGI) between 1971 and 1974 (Barton et al. (1974)). The rock supports recommendations from Q-system are based on the Q-value of the rock mass, which is calculated from 6 rock parameters. The rock parameters for calculating Q-values are based on the orientation and number of discontinuity sets present in the rock mass, surface condition of discontinuities, groundwater conditions and insitu stress state in the rock mass. For a known Q-value and span/height of the tunnel, the Q-system recommends rock support in terms of thickness of fibre reinforced sprayed concrete layer, rock bolts, reinforced ribs of sprayed concrete (RRS) and in some cases cast concrete lining (CCA). There are several types of fibres available to reinforce the sprayed concrete, however it is chosen to use steel fibres for the present work. The reinforced ribs of sprayed concrete (RRS) are similar to a reinforced concrete beam and generally recommended for a very poor quality of rock mass. Based on the quality of rock mass, the Q-system recommends thickness and the reinforcement in the RRS.

The installation of rock supports is a risky task, especially when the rock mass quality is very poor as the rock blocks may fall during installation. Moreover, the reinforcement for RRS need be placed during installation, which makes the construction of tunnel difficult, time consuming and expensive.

Several research papers are published to assess the validity of Q-system's supports recommendations, one such study was conducted by Palmstrom and Broch (2006). The authors concluded that the Q-system is a optimum method to design the supports for fair to very good rock masses, but it may provide impractical, unrealistic and conservative outcome for poor rock masses.

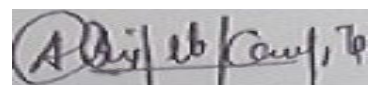
The rock supports from Q-system are compared with the outcome from numerical analysis in this thesis aiming to obtain the optimized rock supports and subsequently improving the safety and pace of construction. The main objective set for this study is to check the possibility of reducing the requirement of reinforcement in the RRS focusing mainly on the poor quality of rock masses in general, having Q- values less than 1.

The results from numerical analysis show that the rock supports recommended by Qsystem for the very poor rock mass ($Q < 1$) are conservative and can be optimised in terms of reducing the reinforcement in RRS, given that the detailed rock-lining interaction analysis is carried out.

ACKNOWLEDGEMENT

I would like to thank my esteemed supervisor – Dr. Raju Sarkar for his invaluable supervision, support and tutelage during the course of my MTech degree. My gratitude extends to the Faculty of Civil engineering to support my studies at the Department of Civil Engineering, Delhi Technological University.

Additionally, I would like to thank my friends, lab mates, colleagues and research team, for a cherished time spent together in the lab, and in social settings. My appreciation also goes out to my family and friends for their encouragement and support all through my studies



(ABHISHEK KAUSHIK)

Place: Delhi

Date:

2K19/GTE/01

CONTENTS

CANDIDATE'S DECLARATION	i
CERTIFICATE	2
ABSTRACT	iii
ACKNOWLEDGEMENT	iv
LIST OF FIGURES.....	viii
LIST OF TABLES.....	xii
NOMENCLATURE.....	xv
Chapter 1	1
INTRODUCTION	1
1.1 Objective of the thesis	1
1.2 State of the art.....	2
1.3 Methodology.....	4
Chapter 2	5
THEORY	5
2.1 Mechanical behaviour of rocks	5
2.2 Failure criteria.....	6
2.2.1 Mohr-Coulomb failure criterion.....	6
2.2.2 Hoek-Brown and generalised Hoek-Brown failure criterion	8
2.2.3 Drucker-Prager failure criterion	10
2.3 Design methods.....	10
2.3.1 The design methods based on the rock mechanical model.....	10
2.3.2 The methods based on the rock mass behavior	11
2.3.3 The methods based on rock classification system.....	11
(i) Rock quality designation (RQD).....	11
(ii) Rock mass rating (RMR)	11
(iii) Q-system.....	11
(iv) Geological strength index (GSI).....	12
(v) Rock mass index (RMi)	12
2.4 Numerical modelling approaches.....	13
2.5 Q-system.....	14
2.6 Strength parameters for joints in rock mass.....	19

2.7	Strength of young sprayed concrete	21
2.8	M-N interaction curves.....	23
2.8.1	For plain and reinforced concrete	24
2.8.2	For steel fibre reinforced concrete.....	25
Chapter 3	27
ROCK MASS CLASSIFICATION AND ROCKSUPPORT ASSESSMENT	27
3.1	Geological Lithologies	27
3.1.1	Quartz with Mica Minerals(Biotite and Muscovite) defining the schistosity inschistose quartzite) 27	
3.1.2	Porphyroblasts of Biotite and muscovite in schistose quartzite	27
3.1.3	Quartz II Porhyroblast in Quartz – Biotite Schist	28
3.2	Structural geology.....	28
3.3	Rock parameters for Q-system.....	28
3.3.1	Rock Quality Designation	29
3.3.2	Joint set numbers	29
3.3.3	Joint roughness numbers	30
3.3.4	Joint alteration numbers.....	31
3.3.5	Joint water reduction factors	31
3.3.6	Stress reduction factors.....	32
3.4	Q-values.....	32
3.5	Assessment of rock supports for the tunnel	33
Chapter 4	36
NUMERICAL ANALYSIS.....	36
4.1	Rock mechanical models	36
4.1.1	Geometry	38
4.1.2	Initial element loading.....	39
4.1.3	Strength and deformation properties of rock masses.....	39
4.1.4	Strength properties of joints in rock mass.....	49
4.1.5	Rock Supports	50
4.1.6	Hydraulic properties	57
4.1.7	Sign convention in rock mechanical models	57
4.1.8	Construction stages	58
4.1.9	Summery of supports and excavation stages	59

4.2	Structural models	60
4.2.1	Geometry	60
4.2.2	Material and sectional properties	60
4.2.3	Calibration	60
4.2.4	Loads and load combinations	61
4.2.5	Boundary conditions	62
4.2.6	Sign convention in structural models	64
4.3	Output of numerical analysis	66
4.3.1	Output of rock mechanical models	66
Chapter 5	69
DISCUSSION	69
Chapter 6	72
CONCLUSION	72
6.1	Future work.....	72
REFERENCES	74

LIST OF FIGURES

1.1	Cross section of Rohtang	2
1.2	Longitudinal section of Rohtang	2
1.3	Flowchart of methods used in the report	5
2.1	Post-peak behaviour of different rock masses (a) elastic-brittle plastic behaviour for very good quality rock mass, (b) strain-softening for average quality rock mass, (c) elastic-perfectly plastic for very poor quality rock mass (Hoek and Brown (1997))	7
2.2	Failure line of Coulomb's hypothesis drawn with Mohr circle in τ - σ plane	8
2.3	Disturbance factor based on different quality of blasting for tunnels (Hoek et al. (2002))	10
2.4	Geological strength index (GSI) chart from Marinos et al. (2005)	13
2.5	Application of continuum and discontinuum modelling approaches in relation to Q-values (Barton (1998))	15
2.6	Joint set numbers for different number of joint sets (NGI (2015):p .17) . .	16
2.7	Different types of joint surfaces and joint roughnesses (NGI (2015):p .20)	17
2.8	Support chart for estimating rock support for a tunnel using Q-system (NGI (2015):p 34) 20	
2.9	Rock support categories as per Q-system (NGI (2015):p 35)	21
2.10	Typical layout of RRS construction (NGI (2015))	21
2.11	(a) Roughness profiles of joints and corresponding JRC values (Barton and Choubey (1977)) (b) Joint roughness numbers J_r for several roughness profiles and corresponding JRC values for 20 cm and 100 cm long defects (subscript of JRC represents the length of defects (Bandis (1993))	22
2.12	Early strength development of sprayed concrete - The modified J2 curve (based on DS/EN-14487-1 (2005))	24
2.13	Compressive strength (σ) of sprayed concrete for 0 to 28 days after spraying	25
2.14	Young's modulus (E) of sprayed concrete for 0 to 28 days after spraying .	26
2.15	Rectangular stress distribution in reinforced concrete (from DS/EN-1992-1-1 (2005)), A_c is area of compression zone, A_s is cross-sectional area of reinforcement, λ and η are factors for defining effective height of compression zone (λx) and effective strength (ηf_{cd}), f_{cd} is design compressive strength of concrete, ϵ_s is maximum yield strain in reinforcement, ϵ_{cu3} is ultimate strain in concrete, F_c and F_s are total compressive and tensile forces respectively.	27
2.16	M-N interaction curve of C30/37 concrete grade for plain concrete and SFRC class 4c for 0.5 m x 0.55 m section	30
3.1	Rhombus-Porphiry with scattered and angled rhombi mapped at Skøttåstunnelen site (Jakobsen (2018))	31

3.2	Basalt (black rock at top) and latite lava (pink rock at bottom) mapped at Skøttåstunnelen site (Jakobsen (2018))	32
3.3	Conglomerate between latite lava and rhombus-porphyry mapped at Skøttåstunnelen site (Jakobsen (2018))	33
3.4	Support chart from Q-system handbook NGI (2015):p 34, horizontal blue line represents equivalent dimension of the tunnel and vertical green, yellow and pink boxes represent Q-values for exceptionally poor, extremely poor and very poor rock masses respectively, presented in Table 3.7	39
4.1	Modal boundaries, fixities at boundaries and finite element mesh for the rock mechanical models	43
4.2	Estimated GSI values presented in GSI chart (Marinos et al. (2005)) for exceptionally poor (red), extremely poor (green) and Very poor (blue) rock masses	46
4.3	Estimated disturbance factors according to quality of blasting (Hoek et al. (2002))	47
4.4	Field estimates of Hoek-Brown material parameter for intact rock (m_i) for different igneous rocks (Hoek (2006))	48
4.5	Field estimates of uniaxial compressive strength (σ_{ci}) for several rock types (Hoek (2006))	49
4.6	Modulus ratios (MR) for different igneous rocks (Hoek (2006))	53
4.7	Layout and design parameters of forepole: s_{cfp} is center to center spacing of forepoles, t_{fp} is thickness of forepoles, ϕ_{fp} is outer diameter of forepoles, L_{fp} is length of forepoles, L_{fpo} is overlap length of forepoles, L_{us} is unsupported angle of the forepoles (after Oke et al. (2014))	56
4.8	Longitudinal section of tunnel roof showing supports layout in 3D model and equivalent support in 2D model. Where, S_{RRS} is center to center spacing between RRS, L_{RRS} is length of RRS in longitudinal direction, t_{RRS} is thickness of RRS, t_{SF} is thickness of SFRC layer, L_{SF} is length of SFRC layer in longitudinal direction excluding RRS length, t_e is equivalent thickness of SFRC in 2D model (Not to scale)	51
4.9	Typical sketch of RRS showing following geometric parameters: L_{RRS} is length of forepoles, α_{fp} is inclination angle of forepoles, α_{fpa} is coverage length of RRS, t_{RRS} is thickness of RRS, S_b center of gravity of RRS, S_i ideal center of gravity of the RRS, z_{bt} is distance of center of gravity from top of RRS, z_{bb} is distance of center of gravity from bottom of RRS, z_{it} is distance of ideal center of gravity from top of RRS, z_{ib} is distance of ideal center of gravity from bottom of RRS, a_s is distance of center of gravity of steel from bottom of RRS.	52
4.10	Typical construction stages defined in rock mechanical models	56
4.11	Geometry and supports defined in rock mechanical models	57
4.12	Applied load in the structural models - cross-section view (left) and side view (right)	59
4.13	Typical spring beam model (Mayta et al. (2018))	50
4.14	Transverse and longitudinal direction in structural models	52
4.15	Description of geometry and supports elements in structural models	52

4.16 Vertical displacements in exceptionally poor rock mass from continuum model (Crown: 16 mm, Invert: 13 mm)	53
4.17 Vertical displacements in extremely poor rock mass from continuum model (Crown: 13 mm, Invert: 6 mm)	53
4.18 Vertical displacements in very poor rock mass from continuum model (Crown: 2 mm, Invert: 2 mm)	54
4.19 Vertical displacements in very poor rock mass from discontinuum model (Crown: 2 mm, Invert: 2 mm)	54
4.20 Horizontal displacements in exceptionally poor rock mass from continuum model (Max. at side wall: 7 mm)	54
4.21 Horizontal displacements in extremely poor rock mass from continuum model (Max. at side wall: 2 mm)	55
4.22 Horizontal displacements in very poor rock mass from continuum model (Max. at side wall: 0.4 mm)	55
4.23 Horizontal displacements in very poor rock mass from discontinuum model (Max at side wall: 0.5 mm)	55
4.24 Major principle stress (σ_1) in exceptionally poor rock mass from continuum model	56
4.25 Major principle stress (σ_1) in extremely poor rock mass from continuum model	56
4.26 Major principle stress (σ_1) in very poor rock mass continuum model	56
4.27 Major principle stress (σ_1) in very poor rock mass discontinuum model	57
4.28 Minor principle stress (σ_3) in exceptionally poor rock mass from continuum model	57
4.29 Minor principle stress (σ_3) in extremely poor rock mass from continuum model	57
4.30 Minor principle stress (σ_3) in very poor rock mass from continuum model	58
4.31 Minor principle stress (σ_3) in very poor rock mass from Continuum model	58
4.32 Out-of-plane principle stress (σ_z) in exceptionally poor rock mass from continuum model	58
4.33 Out-of-plane principle stress (σ_z) in extremely poor rock mass from continuum model	59
4.34 Out-of-plane principle stress (σ_z) in very poor rock mass from continuum model	59
4.35 Out-of-plane principle stress (σ_z) in very poor rock mass from discontinuum model	59
4.36 Strength factor and yielded elements (x for shear and o for tension) in exceptionally poor rock mass from continuum model	60
4.37 Strength factor and yielded elements (x for shear and o for tension) in extremely poor rock mass from continuum model	60
4.38 Strength factor and yielded elements (x for shear and o for tension) in very poor rock mass from continuum model	60
4.39 Strength factor and yielded elements (x for shear and o for tension) in very poor rock mass from discontinuum model	61
4.40 Axial force in rock bolts in exceptionally poor, extremely poor and very poor rock masses from continuum models	62
4.41 Axial force SCL in exceptionally poor, extremely poor and very poor rock masses from continuum models	63
4.42 Bending moments in SCL in exceptionally poor, extremely poor and very poor rock masses from continuum models	64
4.43 Displacements in SCL in exceptionally poor, extremely poor and very poor rock masses from continuum models	65

4.44 Deformed shapes of SCL (SLS) from structural models in exceptionally poor, extremely poor and very poor rock masses	
4.45 Transverse SLS axial forces (N_{yy}) in exceptionally poor, extremely poor and very poor rock masses	70
4.46 Transverse SLS bending moments (M_{yy}) in exceptionally poor, extremely poor and very poor rock masses	70
4.47 Longitudinal SLS axial forces (N_{xx}) in exceptionally poor, extremely poor and very poor rock masses	70
4.48 Longitudinal SLS bending moments (M_{xx}) in exceptionally poor, extremely poor and very poor rock masses	70
4.49 Transverse ULS bending moment (M_{yy}) and transverse ULS axial force (N_{yy}) in SCL after 12, 24 and 72 hours in exceptionally poor rock mass . .	71
4.50 Transverse bending moment (M_{yy}) and transverse axial force (N_{yy}) in SCL after 12, 24 and 72 hours in extremely poor rock mass	71
4.51 Transverse bending moment (M_{yy}) and transverse axial force (N_{yy}) in SCL after 12, 24 and 72 hours in very poor rock mass	71
4.52 Verification for transverse ULS bending moments (M_{yy}) and corresponding axial forces (N_{yy}) plotted in MN curves after 12, 24 and 72 hours for exceptionally poor rock mass	72
4.53 Verification for transverse ULS bending moments (M_{yy}) and corresponding axial forces (N_{yy}) plotted in MN curves after 12, 24 and 72 hours for extremely poor rock mass	72
4.54 Verification for transverse ULS bending moments (M_{yy}) and corresponding axial forces (N_{yy}) plotted in MN curves after 12, 24 and 72 hours for very poor rock mass	73
4.55 Maximum ULS transverse bending moments (M_{yy}) and corresponding axial forces (N_{yy}) in RRS for exceptionally poor rock mass	73
4.56 Maximum ULS transverse bending moments (M_{yy}) and corresponding axial forces (N_{yy}) in RRS for extremely poor rock mass	73
4.57 Maximum ULS transverse bending moments (M_{yy}) and corresponding axial forces (N_{yy}) in RRS for very poor rock mass	73
4.58 Verification for long-term transverse ULS bending moments ($M_{yy} = 134$ kNm/m) and corresponding axial forces ($N_{yy} = 860$ kN/m) plotted in MN curve for exceptionally poor rock mass	73
4.59 Verification for long-term transverse ULS bending moments ($M_{yy} = 80$ kNm/m) and corresponding axial forces ($N_{yy} = 915$ kN/m) plotted in MN curve for extremely poor rock mass	74
4.60 Verification for long-term transverse ULS bending moments ($M_{yy} = 35$ kNm/m) and corresponding axial forces ($N_{yy} = 538$ kN/m) plotted in MN curve for very poor rock mass	74

LIST OF TABLES

1.1	Dimensions of Rohtang tunnel , H.P. India.	3
2.1	Joint compressive strength (JCS) for different types of rocks (from Roc-Data (2019))	23
2.2	J2 values obtained from tests for first 24 hours	25
3.1	Three different sets of RQD values estimated from available boreholes loggings	34
3.2	Three different sets of joint set numbers estimated from available boreholes loggings	35
3.3	Three different sets of joint roughness numbers estimated from available boreholes loggings	36
3.4	Three different sets of joint alteration numbers estimated from available boreholes loggings	36
3.5	Three different sets of joint water reduction factors estimated from available boreholes loggings	37
3.6	Three different sets of stress reduction factors (SRF) estimated from available boreholes loggings	37
3.7	Summery of estimated rock parameters (Q-parameters), corresponding Q-values and rock mass qualities	38
3.8	Rock support recommendations from Q-system's support chart for exceptionally poor quality rock mass	39
3.9	Rock support recommendations from Q-system's support chart for extremely poor quality rock mass	40
3.10	Rock support recommendations from Q-system's support chart for very poor quality rock mass	40
4.1	Adopted modelling approach and post-peak material behaviour for rock mechanical models	42
4.2	Structure of the rock mass based on RQD and J_n for GSI estimation	45
4.3	Structure of the rock mass based on J_r and J_a for GSI estimation	45
4.4	GSI estimated from GSI chart (Figure 4.2) and equation (4.3)	47
4.5	Hoek-Brown material parameters for intact rock m_i , s , a and σ_{ci}	49
4.6	Material parameters for rock mass m_b , s and a for $D = 0$	50
4.7	Unit weight (γ) of igneous rocks from literature	51
4.8	Equivalent Mohr-Coulomb parameters calculated from Hoek-Brown parameters for exceptionally poor, extremely poor and very poor rock mass for $D = 0$	51
4.9	Friction angles (ϕ) and cohesion (c) for several igneous rock from literature	52

4.10	Rock mass moduli (E_{rm}) for exceptionally poor, extremely poor and very poor rock mass for $D = 0$	53
4.11	Estimated strength parameters of joints for very poor rock mass	54
4.12	Thickness and properties of concrete used for the analysis	55
4.13	Properties of rock-bolts defined in rock mechanical models	55
4.14	Range of design parameters for forepole umbrella (Oke et al. (2014))	57
4.15	Design parameters of forepole umbrella for exceptionally poor rock mass	57
4.16	Material quantities for calculating equivalent strength of 'reinforced rock' for exceptionally poor rock mass	58
4.17	Equivalent rock mass properties for 'reinforced rock' for exceptionally poor rock mass	58
4.18	Design parameters of forepole umbrella for extremely poor rock mass	59
4.19	Material quantities for calculating equivalent strength of 'reinforced rock' for extremely poor rock mass	59
4.20	Equivalent rock mass properties of 'reinforced rock' for extremely poor rock mass	59
4.21	Properties of reinforced ribs of sprayed concrete (RRS) and required reinforcement for exceptionally poor, extremely poor and very poor rock mass	60
4.22	Thicknesses of SFRC layer equivalent to SFRC and RRS to use in 2D models for exceptionally poor, extremely poor and very poor rock masses	64
4.23	Sign convention in RS2 software	65
4.24	Chosen finite element mesh size in structural models	68
4.25	Load cases used in structural models	69
4.26	Load combinations used in structural models	69
4.27	Spring stiffnesses for exceptionally poor, extremely poor and very poor rock masses	71
4.28	Spring stiffnesses of rock bolts for exceptionally poor, extremely poor and very poor rock mass	71
4.29	Compressive strength (σ) and Young's modulus of C30/37 concrete after 12, 24 and 72 hours	71
4.30	Maximum ULS bending moments and corresponding axial forces in RRS after 12, 24 and 72 hours for exceptionally poor, exceptionally poor and very poor rock masses	72
4.31	Maximum ULS bending moments and corresponding axial forces in RRS in long-term for exceptionally poor, exceptionally poor and very poor rock masses	72
A.1	Compressive strength (σ) and Young's modulus of concrete (E) from 0 to 28 days after casting	113
C.1	Structure of the rock mass based on RQD and J_n for GSI estimation (full range according to rock parameters and Q-values presented in Table 3.7)	117
C.2	Structure of the rock mass based on J_r and J_a for GSI estimation (full range according to rock parameters and Q-values presented in Table 3.7)	118
C.3	GSI estimated from GSI chart (Figure 4.2) and equation (4.3) (full range according to rock parameters and Q-values presented in Table 3.7)	118
C.4	Material parameters for rock mass m_b , s and a for $D = 0.8$ and $D = 0$ (full range according to rock parameters and Q-values presented in Table 3.7)	118

C.5	Mohr-Coulomb parameters calculated from Hoek-Brown parameters for exceptionally poor, extremely poor and very poor rock mass for $D = 0.8$ and $D = 0$ (Full range according to rock parameters and Q-values presented in Table 3.7)	119
C.6	Rock mass moduli (E_{rm}) for exceptionally poor, extremely poor and very poor rock mass for $D = 0.8$ and $D = 0$ (full range according to rock parameters and Q-values presented in Table 3.7)	119

NOMENCLATURE

Abbreviations

2D	2-Dimensional
3D	3-Dimensional
3DEC	3-Dimensional distinct element code
BEM	Boundary element method
CCA	Cast concrete lining
DEM	Distinct element method
DL	Dead load
DP	Drucker-Prager failure criterion
ESR	Excavation support ratio
FDM	Finite difference method FE
Finite element	
FEM	Finite element method
GSI	Geological strength index
HB	Hoek-Brown failure criterion JCS
Joint compressive strength JRC	Joint roughness coefficient
MC	Mohr-Coulomb failure criterion
MR	Modulus ratio
NGI	Norwegian geotechnical institute
PC	Plain concrete
RC	Reinforced concrete
RMi	Rock mass index RMR
Rock mass rating	
RP	Rock pressure
RQD	Rock quality designation
RRS	Reinforced ribs of sprayed concrete
SCL	Sprayed concrete lining
SFRC	Steel fibre reinforced concrete
SLS	Serviceability limit state
SRF	Stress reduction factor
UCS	Unconfined compressive strength of intact rock
UDEC	Universal distinct element code
UDL	Uniformly distributed load
ULS	Ultimate or collapse limit state

Greek Symbols

α_{fpa}	Coverage angle of the forepoles
α_{fp}	Inclination angle forepoles
α_{cc}	Factor for long-term effects and load application on compressive strength
γ	Unit weight of the rock mass
γ_F	Partial safety factor for SFRC
γ_G	Partial safety factor for SLS and ULS
γ_s	Partial safety factor for steel
γ_C	Partial safety factor for concrete
ϕ	Angle of internal friction
ϕ_b	Basic angle of internal friction
ϕ_{fp}	Outer diameter of forepoles
ϕ_r	Residual angle of internal friction

ψ	Dilation parameter
σ	Compressive strength of concrete after t days
σ_1	Major principle stress
σ_2	Intermediate principle stress
$\sigma_{3\max}$	Maximum confining stress
σ_3	Minor principle stress
σ_{cm}	Rock mass strength
σ_n	Normal stress
σ_t	Tensile strength
σ_z	Out-of-plane stress
σ_{ci}	Unconfined compressive strength of intact rock
τ	Shear stress/Strength
θ	Lode angle
ε_1	Major principle strain
ε_2	Intermediate principle strain
ε_3	Minor principle strain
ε_{c2} & ε_{c2}	Strains in concrete at reaching maximum strength
ε_{cu}	Ultimate strain in concrete
ε_s	Maximum yield strain in steel

Latin Symbols

A_b	Cross-sectional area of RRS
A_c	Area of compression zone
A_n	Net area
A_s	Total cross-sectional area of reinforcement
a_s	Distance of center of gravity of steel from bottom in RRS
A_t	Cross-sectional area of tunnel face
d_{2d}	Deformation in bending in 2D model
d_{3d}	Deformation in bending in 3D model
E_b	Bolt modulus
E_c	Young's modulus of concrete
E_i	Rock mass modulus of intact rock
E_{rm}	Rock mass modulus
E_s	Young's modulus of steel
f_{cd}	Design strength of concrete
f_{ck}	Characteristic compressive strength of concrete
f_{ctm}	Mean tensile strength of concrete
F_c	Compressive force
f_{R1k}	Characteristic flexural residual strength of SFRC in SLS

f_{R3k}	Characteristic flexural residual strength of SFRC in ULS F_s
Tensile force	
f_{yd}	Design strength of steel
f_{yk}	Characteristic yield strength of steel
H_t	Height of tunnel
h_t	Depth of tunnel from ground level
I_1 & J_2	Stress invariants
I_b	Moment of inertia of RRS
I_e	Moment of inertia of equivalent thickness of SFRC
I_{RRS}	Ideal moment of inertia of RRS I_{SF}
Moment of inertia of SFRC layer j_R	Joint roughness
J_a	Joint alteration number
j_A	Degree of weathering
J_{Cond89}	Ratings for joints
j_C	Joint condition factor
j_L	Persistence of discontinuities
J_n	Joint set number
j_P	Jointing parameter
J_r	Joint roughness number
J_w	Joint water reduction factor
K_b	Axial stiffness of bolt
K_i	Spring stiffness
k_n	Normal stiffness of joints k_s
Shear stiffness of joints	
L_t	Length of tunnel
L_b	Bolt length
L_e	Equivalent length of SFRC layer in 2D model in longitudinal direction
L_{fpo}	Overlap length of forepoles
L_{fp}	Length of forepoles
l_i	Contributory distance of the node "i"
L_{RRS}	Length of RRS in longitudinal direction
L_{SF}	Length of SFRC layer in longitudinal direction excluding RRS
L_{us}	Unsupported length of forepoles
m_b, s & a	Hoek-Brown material constants for rock mass m_i
Hoek-Brown material constant for intact rock	M_{xx}
Longitudinal bending moment	
M_{yy}	Transverse bending moment
N_{xx}	Longitudinal axial force
N_{yy}	Transverse axial force
R_i	Radius of the tunnel lining
S_t	Span of tunnel
S_b	Center of gravity of RRS
S_{cfp}	Center to center spacing of forepoles
S_i	Ideal center of gravity of the RRS
S_{RRS}	Center to center spacing between RRS
t_e	Equivalent thickness of the SFRC layer in 2D model
t_{fp}	Thickness of forepoles t_{RRS}
Thickness of RRS	
t_{SF}	Thickness of SFRC layer

u_s	Shear displacement
V_b	Block volume
z_{bb}	Distance of center of gravity from bottom in RRS
z_{bt}	Distance of center of gravity from top of RRS
z_{ib}	Distance of ideal center of gravity from bottom in RRS
z_{it}	Distance of ideal center of gravity from top in RRS
c	Cohesion
f_{Ftsd}	Design axial tensile strength of SFRC in SLS
f_{Ftsk}	Characteristic axial tensile strength of SFRC in SLS
f_{Ftud}	Design axial tensile strength of SFRC in ULS
f_{Ftuk}	Characteristic axial tensile strength of SFRC in ULS
n	Modular ratio
q & k	Material parameters for DP failure criterion a & c
Coefficients	in Change & stille's equations
b	Width of section
D	Disturbance factor
E	Young's modulus of concrete after t days h_w
Depth of section	
L	Length of joint
M	Bending moment
N	Axial force
Q	Rock mass quality index (Q-value)
s_j	Joint spacing t

Chapter 1

INTRODUCTION

Tunnel is an underground opening used for many purposes for instance transporting passengers, water and sewage etc. The tunnels are an efficient way of using underground land for redirecting traffic congestion from more populous town centers, reducing air pollution in residential areas, water supply in cities and waste management etc. The design and construction of tunnels is a challenging task for a rock engineer. There are many methods to design tunnels based on the use of tunnel, rock/soil type, size of tunnel. The Q-system is one of the most popular method to design a tunnel. The thesis is prepared to check the possibility to optimize the tunnel design from Q-system using numerical methods.

1.1 Objective of the thesis

The Q-system was introduced by Barton et al. (1974) to design the rock support system for a tunnel in the rock mass. According to Q-system, the rock masses are classified in to 7 types from A to E. The A represents the very good quality rock mass and the E represents the extremely poor quality of rock mass. The Q-system was published in an internal NGI report “*Handbook - Using the Q-system (Rock mass classification and support design)*” NGI (2015) with all the background information and recommendations for calculating Q-value also known as Tunnelling Quality Index or Q-index. The Q-values can be calculated for any given rock mass based on 6 rock parameters. The rock parameters and corresponding Q-values are discussed in detail further in Section 2.5.

The Q-system recommends rock supports based on the calculated Q-values and the span or height of the tunnel. The lowest possible value of Q could be 0.001 for extremely poor quality of rock mass and the highest 1000 for virtually unjointed intact rock mass. The rock supports include steel fibre reinforced sprayed concrete (SFRC) lining, rock bolts and in case of very poor to exceptionally poor rock mass, cast concrete lining (CCA) or reinforced ribs of sprayed concrete (RRS) along with SFRC layer and rock bolts.

In this thesis the rock support system designed using Q-system and numerical methods are compared aiming to optimize the rock supports and improve safety and pace of construction.

The longitudinal section presented in the Figure 1 shows the rock mass qualities along the tunnel alignment. From the figure, the zone number I to Va represents the rock mass quality, where zone Va is very poor rock mass. The thesis is prepared to design rock supports in very poor to exceptionally poor rock mass, therefore tunnel section only in zone Va is taken into account. The average depth of tunnel from the ground surface(h) in the zone Va is around 15 m which is used to calculate overburden in later chapters.

The boreholes data made available by BRO used to characterize the rock mass. The rock parameters obtained from borehole data is divided into three data sets aiming to obtain Q-value corresponding to exceptionally poor rock mass quality for set 1, extremely poor quality for set 2

and very poor for set 3. Thereafter, the corresponding Q-values are calculated, which are then used to estimate recommended rock supports from support chart provided in NGI (2015).

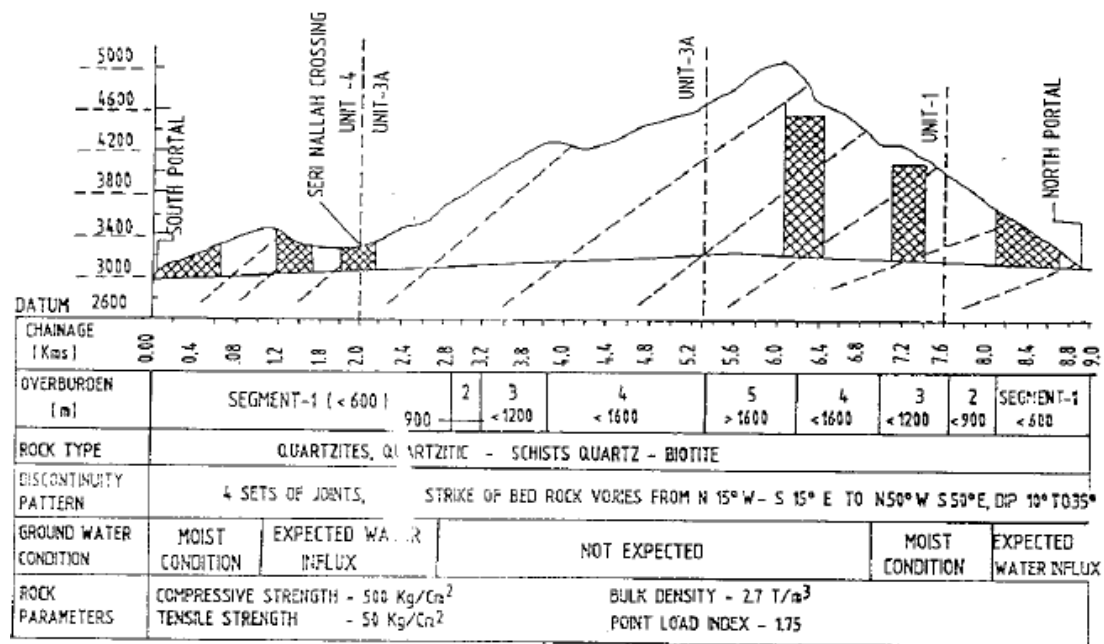


Figure 1 Longitudnal section of rohtang tunnel

For the numerical analysis, two types of numerical models are prepared - rock mechanical and structural, corresponding to each rock mass quality. The rock parameters calculated for Q-system and borehole data used to calculate the rock mass strength and deformation properties based on Hoek-Brown and Mohr-Coulomb failure criteria to use as a input in rock mechanical models.

The outputs of rock mechanical model are calibrated with corresponding structural model for 3-dimensional analysis of stresses. Eventually, the forces obtained from structural models used to verify the requirement of reinforcement in RRS using MN curves for plain concrete, reinforced concrete and SFRC.

1.2 State of the art

Since the Q-system was introduced by Barton et al. (1974), it has become a widely accepted rock mass classification system for designing primary support system for tunnels. The Q-system proved to be a systematic, easy to apply means for rock engineers to design rock supports. After introduction of Q-system in 1974, it has been updated in 1993 based on a thousand examples of underground excavations in Norway. Thereafter, it was updated again in 2002 based on some more examples of underground excavation in Norway, Switzerland and India according to NGI (2015). It is evident that the Q-system is checked and updated accordingly, mainly for the rock masses in Norway which is in general good quality rock masses. However, the Q-system also provides recommendations for very poor to extremely poor quality of the rock masses but it provides more of a general solution for Q values between 0.001 and 0.01. For instance, a tunnel with 10 to 15 m span (equivalent dimension as per Q-system) and Q-value of between 0.001 and 0.01, it recommends to use cast concrete lining or more than 25 cm thick SFRC along with reinforced ribs of sprayed concrete (RRS) and rock bolts. It is important to notice that the Q-value in this example has a change of one order of magnitude but the support recommendations are same. Therefore, to estimate more realistic support for tunnel it is necessary to use numerical methods keeping in mind that the principles of applied mechanics and structural engineering should be the basis of rock

support design. The range of Q-values between 0.001 to 1 is a particular area of interest of the thesis, thus available research and author's comments are described here as a basis for the present work.

In a study by [Palmstrom and Broch \(2006\)](#), the limitations and misuses of the Q-system are highlighted. The authors described that the Q-system works best for a Q-value approximately between 0.1 to 40, whereas the Q-system can provide support estimate for a Q-value anywhere between 0.001 to 1000. The authors stated that the use of Q-system for a Q-values less than 0.1 and more than 40 may result in unrealistic estimates of support for practical use. Therefore, authors advised to use Q-system in planning stage for the given range of Q-values. They do not support the use of Q-system for final design.

In recent years, many studies published where authors have compared the support for tunnels from Q-system and numerical methods. In a study by [Pells and Bertuzzi \(2007\)](#), the authors have compared some of the tunnels in Australia designed by numerical methods with support recommendations by Q-system. The authors seem to be agreed with the findings of [Palmstrom and Broch \(2006\)](#). In the comparison, they have discovered that for some cases the Q- system recommendations are not sufficient for the stability of the tunnel and numerical methods provide substantially higher support.

In another study by [Kanik and Gurocak \(2018\)](#), the authors have designed the rock supports by the empirical classification systems (RMR, Q-system and RMi) and compared it with the output of the numerical method i.e. Finite element method (FEM). The authors have concluded that the classification systems especially Q-system does not provide optimum support as required in numerical analysis.

[Rahmani et al. \(2012\)](#) also published a study about comparing results of empirical classification systems with numerical methods. The authors discovered, for a Q-value of 0.1 to 0.5, the support required from Q-system and numerical methods are the same. However, they have advised to use Q-system to estimate initial rock supports especially in the absence of laboratory results for strength and deformation parameters. In case of availability of laboratory results, the authors have advised to carry out detailed numerical analysis to calibrate the results obtained by Q-system.

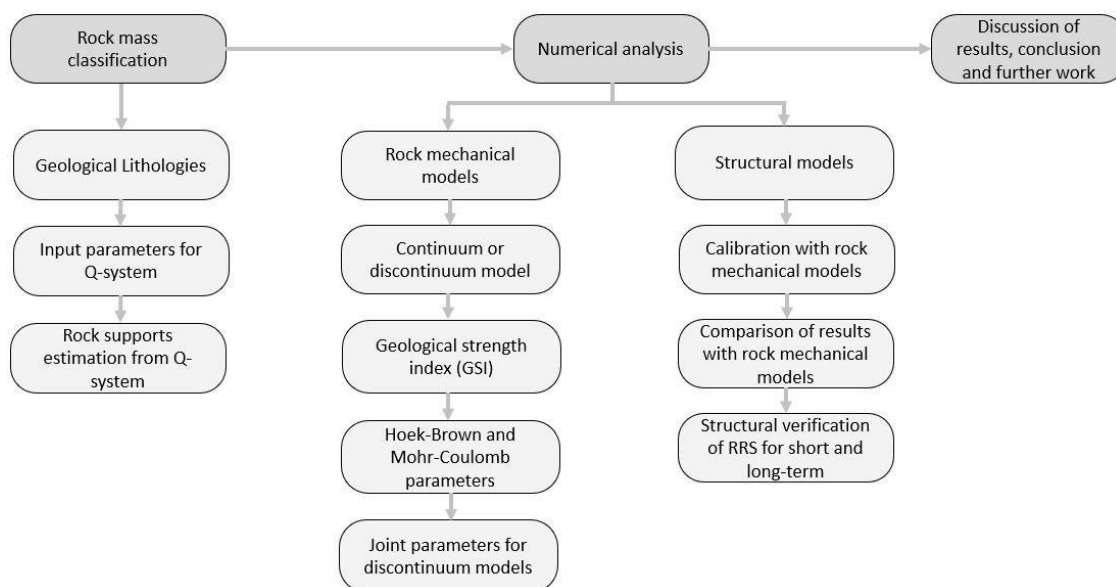
From all the available studies and researches, it is evident that the Q-system or any other classification system may or may not provide a good estimate of rock supports depending on many factors. One of the such factor is input parameters for Q-system. To completely trust the design by Q-system, the proper mapping of for Q-system parameters shall be done at site. In absence of the mapping, it could be really difficult to have a precise estimate of the input parameters especially RQD (Rock quality designation) and SRF (Stress reduction factor). These two parameters are difficult to estimate especially for poor to exceptionally poor quality rock masses. Another factor that may result in wrong estimation of the supports using Q-system in case of drill and blast tunnels are RQD and joint set number (J_n) after blasting. [Palmstrom and Broch \(2006\)](#) have provided references where it is recommended to include fractures due to blasting while estimating RQD and J_n . In this case, the Q-system will provide different supports system before and after blasting. [Palmstrom and Broch \(2006\)](#) have found it inconsistent as Q-system does not provide any recommendations to estimate these parameters in case of drill and blast tunnels.

As said earlier, the objective of the thesis is to analyse very poor to exceptionally poor quality of rock mass, therefore the input parameters for Q-system are carefully obtained from provided borehole loggings as the mapping data is not available for the study. Subsequently, the numerical analysis is performed for all the cases designed using Q-system and the results are compared.

1.3 Methodology

The assessment in the thesis starts with studying geology of the area where the tunnel is going to be built. The geological data is provided by BRO for the Rohtang Tunnel. The available rock cores from boreholes at construction site are studied to obtain mechanical properties of the rock and input parameters for the Q-system. Subsequently, the Q-values are calculated and the rock mass around the tunnel is classified. Eventually, the rock supports from Q-system based on calculated Q-values are estimated.

The next phase of the thesis starts with numerical modelling. The numerical analysis is subdivided into two parts - rock mechanical analysis and structural analysis. For the rock mechanical models, first of all the choice between continuum and discontinuum model is made based on the rock mass quality. Furthermore, the input parameters for the model i.e. GSI, Hoek-Brown parameters, Mohr-Coulomb parameters are calculated. For discontinuum modelling the joint parameters are also calculated. Thereafter, the output of rock mechanical models are calibrated with structural models for structural analysis. Eventually, the structural verification of RRS for short-term (Early-age strength of concrete) and long-term (28 days strength of concrete) case is presented for the design forces obtained from structural models followed by the discussion of results and conclusion. The methodology of the thesis is presented in the Figure 1.3.



Chapter 2

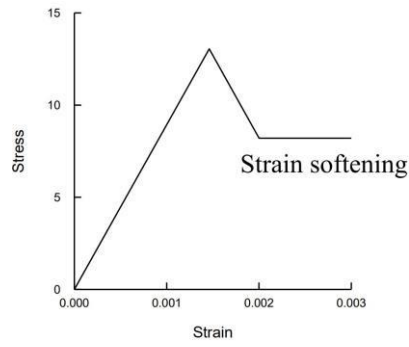
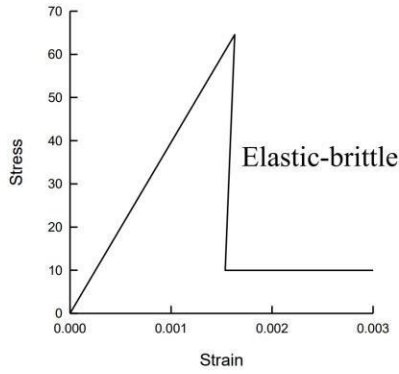
THEORY

Before starting to work on the thesis, the author focused on reading research articles and relevant books to gather background knowledge of the used topics. The present work involves designing rock supports using Q-system NGI (2015) and thereafter optimize it using numerical methods (rock mechanical and structural models). Therefore, the author focused on learning about mechanical behaviour of rock masses, failure criteria, existing design methods for rock support design, modelling techniques, early-age strength of concrete and structural verification of steel fibre reinforced concrete (SFRC). The brief description of studied topics is presented in this chapter.

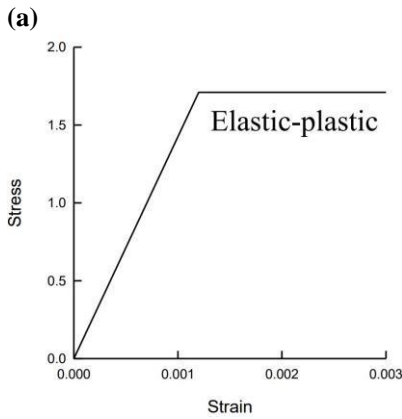
2.1 Mechanical behaviour of rocks

The different materials exhibit different types of behaviours when subjected to an external stress. The type of behaviour may be better understood by observing the strains in material with respect to applied stress until failure. The stress-strain relationship may be linear or non linear based on the material. Generally, most engineering materials (e.g. concrete) exhibit linear-elastic, non-linear elastic, plastic or brittle failure. The rocks also follow the same types of behaviour as other engineering materials. However, the rock mass behaviour is more complex than homogeneous materials because of its heterogeneous and porous nature. It is important to estimate the behaviour of rock mass after failure while using numerical models. The rock mass behaviour after failure is termed as 'post-peak behaviour' hereinafter in this report.

Hoek and Brown (1997) suggested that the post-peak behaviour of the rock masses depends upon the rock mass quality. The very good quality hard rock masses exhibit brittle post-peak behaviour. It means, the strength of very good quality rock mass suddenly drops after reaching the peak strength as presented in the Figure 2.1a. The strength drop results into significant dilation (increase in volume). The average quality rock masses shows a strain-softening post-peak behaviour, means the strength gradually drops to a residual values. Thereafter, the plastic strains show up in the rock mass. The stress strain relationship for average quality rock mass presented in the Figure 2.1b. Lastly, the very poor quality rock masses shows elastic-perfectly plastic post-peak behaviour. The strength in this case reaches to a peak value and remain same after failure with large plastic strains. That means the rock mass continues to deform without any increase in the stress after reaching peak strength. The very poor quality rock masses generally do not exhibit any volume change when fail. Therefore, it is a good practice to assume the dilation parameter 0 for these rock masses as recommended in PLAXIS 2D (2019). The stress-strain relationship for average quality rock mass presented in the Figure 2.1c.



(b)



(c)

Figure 2.1: Post-peak behaviour of different rock masses (a) elastic-brittle plastic behaviour for very good quality rock mass, (b) strain-softening for average quality rock mass, (c) elastic-perfectly plastic for very poor quality rock mass (Hoek and Brown (1997))

2.2 Failure criteria

The failure of rock masses is a complex process. From engineering point of view, it is paramount to have a good estimate of how and when a rock/rock mass will fail. Therefore, many failure criteria are developed to establish a relationship between stress and strength of rocks. Failure criteria describe a relationship between strength of material and stresses and strains in the material by means of mathematical formulas. Hudson and Harrison (1997) explains that a failure criterion can express strength of rocks as a function of principle stresses ($\sigma_1, \sigma_2, \sigma_3$) and principle strains ($\epsilon_1, \epsilon_2, \epsilon_3$) as presented in equation (2.1).

$$\text{Strength} = f(\sigma_1, \sigma_2, \sigma_3) \quad \text{or} \quad f(\epsilon_1, \epsilon_2, \epsilon_3) \quad \text{or} \quad f(\sigma_1, \sigma_2, \sigma_3, \epsilon_1, \epsilon_2, \epsilon_3) \quad (2.1)$$

Where, σ_1 is major principle stress, σ_2 is intermediate principle stress and σ_3 is minor principle stress and similarly ϵ_1, ϵ_2 and ϵ_3 are major, intermediate and minor principle strains respectively.

2.2.1 Mohr-Coulomb failure criterion

The Mohr-Coulomb (MC) failure criterion is a classical failure criterion that applies to many engineering materials. It is the conjunction of Mohr's graphical representation of shear and normal stresses with Coulomb's hypothesis. Coulomb's hypothesis is the simplest and widely used failure

criterion for soils and rocks. According to Coulomb's hypothesis, the failure in rock occurs at a plane due to shear stress (τ) acting along that plane. The sliding motion due to shear stress (τ) along the plane is resisted by normal stress (σ_n) acting perpendicular to that plane and cohesion (c) of the material. The MC failure criterion thereby expressed by equation (2.2).

$$\tau = c + \sigma_n \tan \phi \quad (2.2)$$

Where, ϕ is the internal friction angle of the material.

When Coulomb's hypothesis is drawn along with the Mohr's circle, Coulomb's failure line is a tangent of Mohr's circle as presented in the Figure 2.2. Using trigonometric relations MC failure criterion from equation (2.2) can be expressed in terms of principle stresses as shown in equation(2.3).

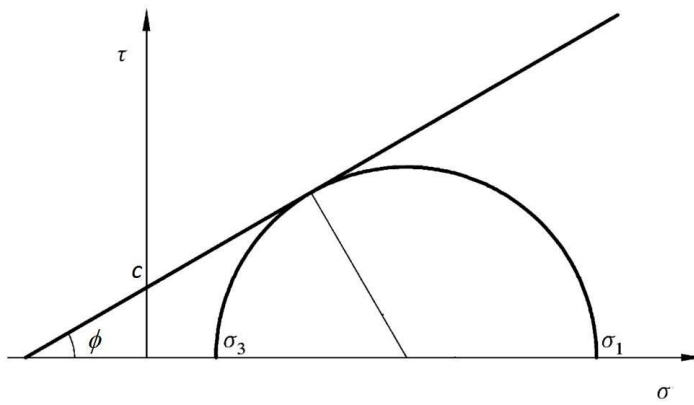


Figure 2.2: Failure line of Coulomb's hypothesis drawn with Mohr circle in τ - σ plane

$$F_s = \frac{1}{2} (\sigma_1 - \sigma_3) + \frac{1}{2} (\sigma_1 + \sigma_3) \sin \phi - c \cos \phi = 0 \quad (2.3)$$

The Mohr-Coulomb yield surface in terms of Lode angle (θ), first stress invariant (I_1) and second deviatoric stress invariant (J_2) can be expressed as:

$$F_s = \frac{I_1}{3} \sin \phi + \sqrt{J_2} \left[\cos \theta - \frac{1}{\sqrt{3}} \sin \theta \sin \phi \right] - c \cos \phi = 0 \quad (2.4)$$

The stress invariant I_1 and J_2 can be expressed in terms of principle stresses by equation (2.5) and (2.6).

$$I_1 = \sigma_1 + \sigma_2 + \sigma_3 \quad (2.5)$$

$$J_2 = \frac{1}{6} \left[(\sigma_1 - \sigma_2)^2 + (\sigma_2 - \sigma_3)^2 + (\sigma_3 - \sigma_1)^2 \right]$$

(2.6) Furthermore, similar to equation (2.4), the plastic potential function can be expressed as:

$$Q_s = \frac{I_1}{3} \sin \psi + \sqrt{J_2} \left[\cos \theta - \frac{1}{\sqrt{3}} \sin \theta \sin \psi \right] = \text{constant} \quad (2.7)$$

Where, ψ is the dilation angle. The dilation angle can be less than or equal to residual friction angle (ϕ_r) based on non-associated or associated flow rule respectively (PLAXIS 2D (2019)). The residual friction angle (ϕ_r) is the friction angle of the rock after failure.

2.2.2 Hoek-Brown and generalised Hoek-Brown failure criterion

The Hoek-Brown (HB) failure criterion is the most commonly used failure criterion to demonstrate failure of rock masses. It was introduced by Hoek and Brown (1980). The HB criterion is based on the intact rock properties, which are scaled-down by geological strength index (GSI) and disturbance factor (D) to cope up with the presence of discontinuities in the rock mass. The HB failure criterion is expressed in terms of principle stress in equation (2.8).

$$F_s = \sigma_1 - \sigma_3 - \sigma_{ci} \left(m_b \frac{-\sigma_1}{\sigma_{ci}} + s \right)^{0.5} = 0 \quad (2.8)$$

Where, σ_{ci} is the uniaxial compressive strength of the intact rock, m_b is reduced value of material constant for intact rock m_i and s is also a material constant.

The generalised HB failure criterion is same as HB failure criterion except the power of 0.5 in equation (2.8) is replaced by a new parameter a as evident from equation (2.9). In order to calculate reduced values of material constant m_b , s and a , the geological strength index (GSI) and disturbance factor (D) are used. The GSI is further discussed in Section 2.3.3 (iv) of this report.

In drill and blast method, the rock mass surrounding the excavation gets damaged and therefore become weaker than rock mass away from the excavation. Although, it is difficult to precisely assess the degree of disturbance due to blasting. However, based on experience gained from many different underground constructions around the world, the authors introduced a unit-less parameter called the disturbance factor (D). D depends on the quality of blasting and estimated from Figure 2.2. It is important to note that the disturbance due to blasting extends only 2 to 3 away from the excavation. Therefore, a non-zero disturbance factor shall only be applied to the rock mass surrounding the excavation and for the rest of rock mass disturbance factor shall be zero.




Appearance of rock mass	Description of rock mass	Suggested value of D
	Excellent quality controlled blasting or excavation by Tunnel Boring Machine results in minimal disturbance to the confined rock mass surrounding a tunnel.	$D = 0$
	Mechanical or hand excavation in poor quality rock masses (no blasting) results in minimal disturbance to the surrounding rock mass. Where squeezing problems result in significant floor heave, disturbance can be severe unless a temporary invert, as shown in the photograph, is placed.	$D = 0$ $D = 0.5$ No invert
	Very poor quality blasting in a hard rock tunnel results in severe local damage, extending 2 or 3 m, in the surrounding rock mass.	$D = 0.8$

Figure 2.3: Disturbance factor based on different quality of blasting for tunnels (Hoek et al. (2002))

The reduced value of material constants can be calculated through GSI and D from equations (2.10) to (2.12).

$$F_s = \sigma_1 - \sigma_3 - \sigma_{ci} \left(m_b \frac{-\sigma_1}{\sigma_{ci}} + s \right)^a = 0 \quad (2.9)$$

$$m_b = m_i \exp \left(\frac{GSI - 100}{28 - 14D} \right) \quad (2.10)$$

$$s = \exp \left(\frac{GSI - 100}{9 - 3D} \right) \quad (2.11)$$

$$a = \frac{1}{2} + \frac{1}{6} \left(\exp \left(\frac{-GSI}{15} \right) - \exp \left(\frac{-20}{3} \right) \right) \quad (2.12)$$

The generalised HB criterion can be expressed in terms of Lode angle (θ), first stress invariant (I_1) and second deviatoric stress invariant (J_2) as presented in equation (2.13).

$$F_s = 2 \cos \theta \sqrt{J_2} - \sigma_{ci} \left(\frac{m_b}{\sigma_{ci}} \left(\frac{-I_1}{3} + \sqrt{\frac{J_2}{3}} (\sin \theta - \sqrt{3} \cos \theta) \right) + s \right)^a = 0 \quad (2.13)$$

Similar to equation (2.13), the plastic potential function can be expressed as:

$$Q_s = 2 \cos \theta \sqrt{J_2} - \sigma_{ci} \left(\frac{m_\psi}{\sigma_{ci}} \left(\frac{-I_1}{3} + \sqrt{\frac{J_2}{3}} (\sin \theta - \sqrt{3} \cos \theta) \right) \right)^a = \text{Constant} \quad (2.14)$$

Where, m_ψ is dilation parameter. m_ψ can be less than or equal to m_b based on nonassociated or associated flow rule respectively (PLAXIS 2D (2019)).

2.2.3 Drucker-Prager failure criterion

The Drucker-Prager (DP) failure criterion is another failure criterion used for rocks. It's similar to MC failure criterion except in 3-dimensional stress space the DP failure criterion creates a cone instead of six-sided pyramid in case of MC failure criterion.

The DP failure criterion can be expressed in terms of first stress invariant (I_1) and second deviatoric stress invariant (J_2) as in equation (2.15).

$$F_s = \sqrt{J_2} + q \frac{I_1}{3} - k = 0 \quad (2.15)$$

Where, q and k are material properties. The plastic potential function can be expressed as:

$$Q_s = \sqrt{J_2} + q_\psi \frac{I_1}{3} = \text{Constant} \quad (2.16)$$

Where, q_ψ is dilation parameter. The dilation parameter (q_ψ) can be less than or equal to q based on non-associated or associated flow rule respectively.

2.3 Design methods

There are many different design methods being used to design the rock supports for tunnels around the world. The most frequently used methods are summarized below as elaborated by Wittke (2014):

- Methods based on the rock mechanical model
- Methods based on assessment of the rock mass behavior
- Methods based on rock classification system

2.3.1 The design methods based on the rock mechanical model

The methods based on rock mechanical model to design the tunnels are being used for many years in the industry. The method involves to create 2D or 3D model to analyze the rock mass behavior as a result of excavation. The rock mass type is defined by appropriate rock mass parameters that define deformability, strength, permeability and in-situ stress state of the rock mass. There are many analysis methods being used to analyses the rock mass such as finite element method (FEM), distinct element method (DEM), finite difference method (FDM) and boundary element method (BEM) etc. The most frequently used method for analysis is the finite element method (FEM). However, other methods are used based on the type of rock mass, as some methods are more accurate to assess the rock behavior than others. For instance, FEM and FDM are recommended to use for a very blocky rock mass with a presence of many joint sets and DEM and BEM are recommended to use for a better quality of rock mass with a presence of very few joint sets. The rock mechanical models are also used in this report to assess the rock support, therefore required input parameters are discussed in detail in Section 4.1.

2.3.2 The methods based on the rock mass behavior

The methods based on rock mass behavior are probably the oldest method being used to design rock support. These methods are mainly in use in Austria and Switzerland Wittke (2014). In these methods, the rock mass behavior type is defined based on the intact rock properties, in-situ stress state, groundwater conditions and orientation and number of discontinuity sets. In a study by Andreas Goricki in Goricki (2003), the detailed description of these behavior types is presented. Thereafter, the support measures are recommended based on the rock behavior type.

2.3.3 The methods based on rock classification system

The methods based on rock classification system are initially developed to design rock support system for tunnels. The basis of these methods is to obtain a numerical value using an empirical formula consisting predefined parameters based on the intact rock properties and deformation properties, groundwater condition, in-situ stress state and orientation of discontinuities as a input. Based on the calculated numerical value, the support classes are defined. The most frequently used classifications systems are briefly described.

(i) Rock quality designation (RQD)

The RQD is one of the oldest classification systems available to rate rock mass. The RQD was defined by Deere (1963) and defined as “the sum of the lengths (between natural joints) of all core pieces more than 10 cm long (or core diameter x 2) as a percentage of total core length”. RQD value of 100% refers to an excellent quality of rock and a value below 25% refers to a very poor quality (soil-like) rock. The RQD is not a design method but it is used in other design methods as input developed later.

(ii) Rock mass rating (RMR)

The RMR is a design method to estimate rock supports for tunnels based on rock mass classification. It was introduced by Bieniawski (1974) specifically to design a rock support system of tunnels. Later, in Bieniawski (1976) and Bieniawski (1989) it was further developed for the application on other areas of construction in rock mass such as foundations and slopes. The basis of the method is to calculate rock mass rating index RMR by summing up the six parameters. The parameters are defined by positive parameters from R_1 to R_5 representing unconfined compressive strength of the rock, RQD, spacing of discontinuities, the appearance of discontinuities and ground/joint water respectively. There is one more negative parameter R_6 defined to account for the orientation of discontinuities. The value of R_6 is different depending upon area of application. Eventually, RMR can be calculated from equation (2.17).

$$RMR = R_1 + R_2 + R_3 + R_4 + R_5 + R_6 \quad (2.17)$$

The RMR can range from 0 to 100. Where a higher value of RMR represents better quality of rock mass and lower value represents poor quality of rock mass. Based on RMR value the support classes are defined.

(iii) Q-system

The Q-system is the most used method to design rock supports based on rock mass classification system. It was introduced by Barton et al. (1974) and adopted for the design of tunnels in the industry especially in Norway. The Q-system is later published in an internal report of the Norwegian geotechnical institute (NGI) NGI (2015).

The objective of this thesis is to optimise rock supports recommended by Q-system using numerical methods for poor quality rock masses. Therefore, Q-system is further discussed in detail in Section 2.5 of this report.

(iv) Geological strength index (GSI)

The GSI was introduced by Hoek et al. (1992) and further developed to use for Hoek and Brown (HB) failure criteria in Hoek (1994). The HB failure criteria is discussed earlier in Section 2.2.2 of this report. The purpose of developing GSI was to relate the HB failure criterion with geological observation. Unlike RMR and Q-system GSI is not a design method it is rather a rock mass classification scheme. As discussed earlier in this section, the RMR and Q-system heavily depends upon RQD to design rock support. The GSI replaces the need of RQD in the HB failure criterion. Unlike the RQD, GSI also includes information about material, its structure (blockiness of the mass), surface condition of discontinuities and geological history. The GSI chart from an article by Marinos et al. (2005) is presented in the Figure 2.4. In the chart, vertical axis provides information about the structure of rock mass and horizontal axis about the surface quality of the discontinuities in the rock mass.

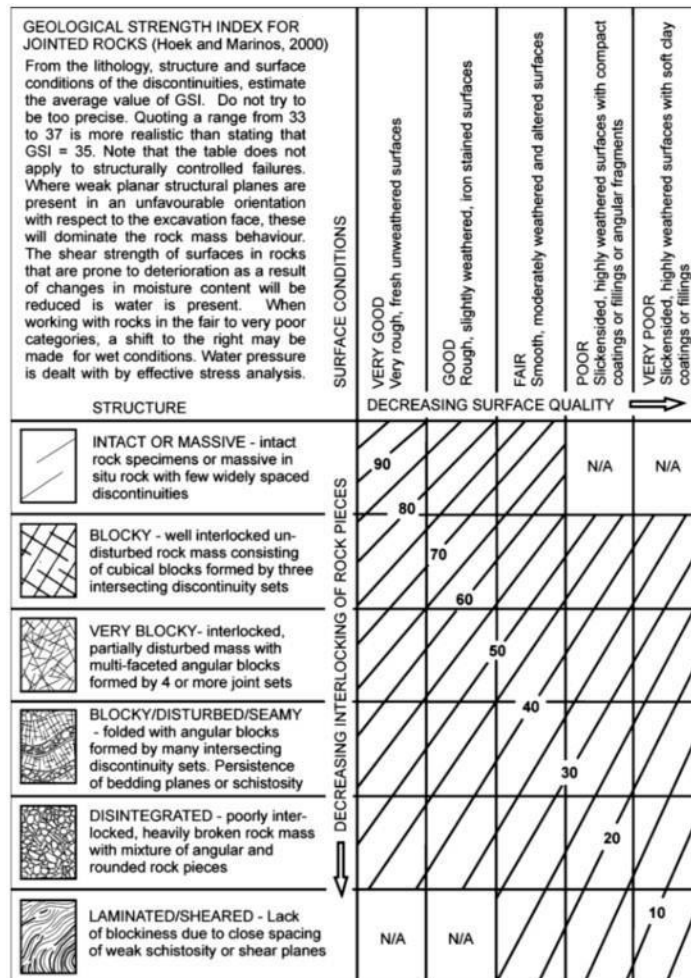


Figure 2.4: Geological strength index (GSI) chart from Marinos et al. (2005)

The GSI can be easily estimated by visual examination of borehole cores, surface excavation for road cuts or tunnel faces. Once the GSI number is obtained, it can be used to calculate rock mass properties as explained in Section 2.2.2 as an input for numerical analysis.

(v) Rock mass index (RMI)

The RMI is another design method based on rock mass classification. It was introduced by Palmstrøm (1995) in his doctoral thesis at the University of Oslo and further modified in Palmstrøm (2000). Similar to RMR method, RMI is a numerical

value calculated by an empirical formula. The formula consists of unconfined compressive strength of intact rock (σ_{ci}), joint roughness (j_R), degree of weathering (j_A), persistence of discontinuities (j_L) and number of joint sets (block volume (V_b)) as input. The empirical formula are presented in equations (2.18) to (2.20).

$$j_c = \left(\frac{j_R}{j_A} \right) j_L$$

$$J_p = 0.2 \cdot j_c \cdot V_n \quad (2.19)$$

$$RMi = \sigma_{ci} \cdot J_p \quad (2.20)$$

Where J_p is jointing parameter and j_c joint condition factor. The parameter j and j_A to calculate RMi value are based on parameter J_r and J_a of Q-system, discuss in Section 2.5. A RMi value < 0.00 represents an extremely weak rock mass, whereas a RMi value of > 100 represents an extremely strong rock mass. The purpose of introduction of RMi method in Palmström (1995) is to use RMi as input in other engineering methods as RMR and Q-system. Later study in Palmström (2000) include a support chart to estimate rock supports.

2.4 Numerical modelling approaches

The rock mass behaviour in response to excavation of a tunnel is although a complex engineering problem, however realistic results may be achieved by proper finite element modelling (FEM). There are other computational methods such as finite difference method (FDM) and Distinct element method (DEM) as mentioned in Section 2.3.1 to achieve realistic rock mass behavior (Barla and Barla (2000)). When it comes to choosing a numerical modelling approach for a tunnelling problem, there are mainly two approaches are available - continuum and discontinuum modelling approaches. A brief description of both approaches is provided as follows.

(i) Continuum modelling approach

In continuum modelling the rock mass is considered as an equivalent continuum with equal strength and deformation properties in all directions. The most common way to do so is to scale-down the intact rock properties to rock mass properties using imperial relationships given by Hoek and Brown in Hoek and Brown (1997) and explained in Section 2.2.2.

(ii) Discontinuum modelling approach

The presence of joints and discontinuities play as an important role in response of rock masses, such as joints can create loose blocks at the tunnel roof and cause local failure; the presence of joints can alter water flow near excavation; joints can also weaken the rock and enlarge the displacement zones caused by excavation (Barla and Barla (2000)). Therefore, the discontinuum modelling approach shall be adopted to study the mentioned effects of joints or discontinuities in the rock mass. The discontinuum modelling can be done mainly by the use of universal distinct element code (UDEC) and 3-dimensional distinct element code (3DEC). In the distinct element method (DEM), the rock mass is represented as a collection of discrete blocks which may be considered either "deformable" or "non-deformable". The joints and discontinuities are then behaves as interfaces between these distinct bodies. The DEM method is more appropriate to capture the mechanics between discrete bodies. For instance, it allows finite displacement detachment and it recognises new contacts automatically as the calculation proceeds (Barla and Barla (2000)).

In a study by Barton (1998), a range of application of continuum and discontinuum modelling is provided

based on Q-values. The Figure 2.5 from Barton (1998) shows that for an approximate range of Q-values between 0.1 to 100, discontinuum modelling approach is more appropriate than continuum modelling. Therefore, for poor rock masses having Q-values less than 0.1, FEM or FDM will provide more realistic results.

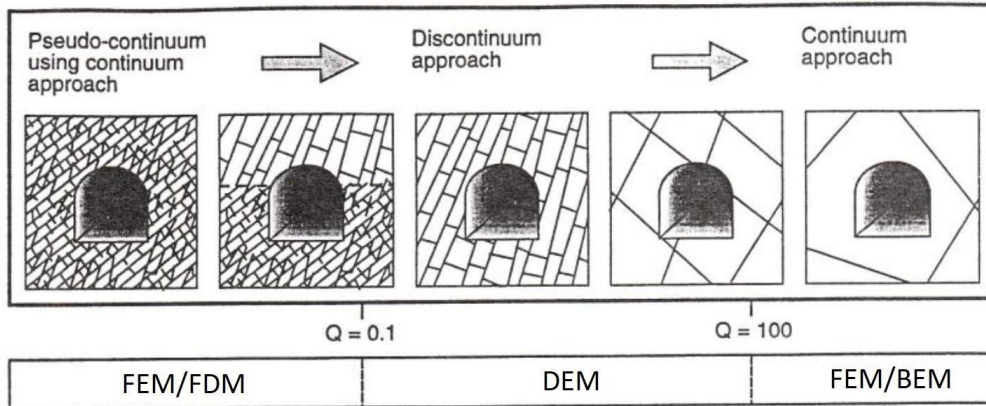


Figure 2.5: Application of continuum and discontinuum modelling approaches in relation to Q- values (Barton (1998))

2.5 Q-system

As mentioned several times earlier, the Q-system classifies the rock mass into 7 categories from A to G, where A represents the exceptionally good quality of rock mass and the G represents the exceptionally poor rock mass. The report focuses only on poor quality of rock masses, as the poor quality of rock mass requires heavier rock support. Therefore, only very poor quality (E), extremely poor (F) and exceptionally poor (G) quality of rock masses according to Q-system NGI(2015):p. 34 are assessed in this report. According to NGI (2015), 6 parameters of the rock shall be known to calculate a Q-value as presented in the equation (2.21).

$$Q = \frac{RQD}{J_n} \times \frac{J_r}{J_a} \times \frac{J_w}{SRF}$$

As evident from the equation (2.21), the Q-value is the multiplication of the three quotients. The first quotient (RQD/J_n) represents the structure of the rock mass and it is

also a measure of the block or particle size. The second quotient (J_r/J_a) represents the frictional characteristics of the joints or joint infills. The arctan of the second quotient is a good approximation of the friction angle (ϕ) of the rock mass. The third quotient (J_w/SRF) contains two stress parameters related to water pressure and stresses in the rock mass and represents stress condition in the rock mass. The rock parameters required to calculate the corresponding Q-values presented in the equation (2.21) are discussed in detail below.

(i) Rock Quality Designation (RQD)

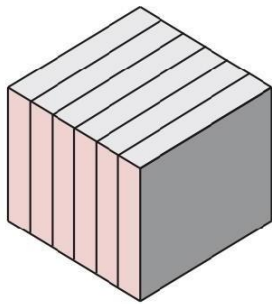
As discussed earlier in Section 2.3.3, the RQD refers to Rock Quality Designation. It was defined in 1963 by Deere in Deere (1963) to be used as a simple classification system for the stability of rock masses. The RQD can be calculated from a drilled core as follows:

“RQD is the sum of the lengths (between natural joints) of all core pieces more than 10 cm long (or core diameter x 2) as a percentage of total core length”

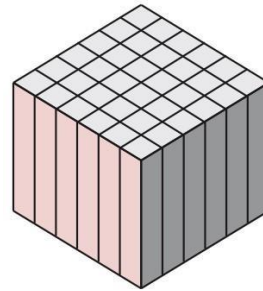
As per the Table 1 in handbook “Using the Q-system” NGI (2015):p. 12, the rocks having RQD values in the range of 0 - 25 and 25 - 50 are designated as very poor and poor quality of rock respectively. Whereas, a RQD value of 50 - 75, 75 - 90 and 90 - 100 represents fair, good and excellent quality of rock mass respectively.

Whenever, RQD lies in the range of 0 to 10, [NGI \(2015\)](#) recommends to use a minimum value RQD as 10 to calculate the Q-value.

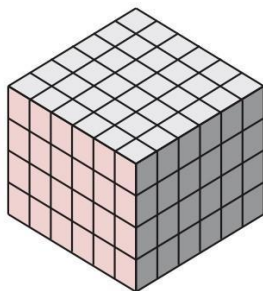
(ii) Joint set number (J_n)



(a) One joint set ($J_n = 2$)



(b) Two joint sets $J_n = 4$



(c) Three joint sets ($J_n = 9$)

(d) Three joint sets ($J_n = 12$)

Figure 2.6: Joint set numbers for different number of joint sets ([NGI \(2015\):p .17](#))

The joint set number is a number defined in the handbook “Using the Q-system” [NGI \(2015\)](#) based on the number of joint sets present in the rock mass. Usually, the joints in a joint set are nearly parallel to each other and reflect a representative spacing. However, the joints which do not occur systematically or do not follow a pattern in the rock mass are called “random joints”. In the Table 2 of handbook “Using the Q-system” [NGI \(2015\):p. 15](#), the joint set numbers are defined based on the number of joint sets present within a rock mass.

For a better understanding of joint set numbers rock masses consisting different joint sets along with respective joint set numbers are presented in the Figure 2.6. The Figure 2.6a shows a rock mass where only one joint set is present. Similarly, the Figure 2.6b, Figure 2.6c shows the rock mass with two and three joint sets respectively. The Figure 2.6d demonstrates a random joint set presented in red lines along with three other joint sets. It is evident from the Figure 2.6, the joint set number is not same as the number of joint sets present in the rock mass.

There is one more special case of joint sets when columnar jointing with three joint direction is present in the rock mass. The joint set number is 4 for this kind of rock mass.

(iii) Joint roughness number (J_r)

The joints in a rock mass may have some friction between the joint walls. The amount of friction depends upon the nature of joint wall surfaces if they are smooth, rough, planer or undulating. The joint roughness number describes the condition of joint wall surfaces whether it is filled or not (clean) and it depends on the nature of asperities present in the discontinuities. In the Table 3 of handbook “Using the Q-system” [NGI \(2015\):p .18](#), joint roughness numbers for different types of joints are presented.

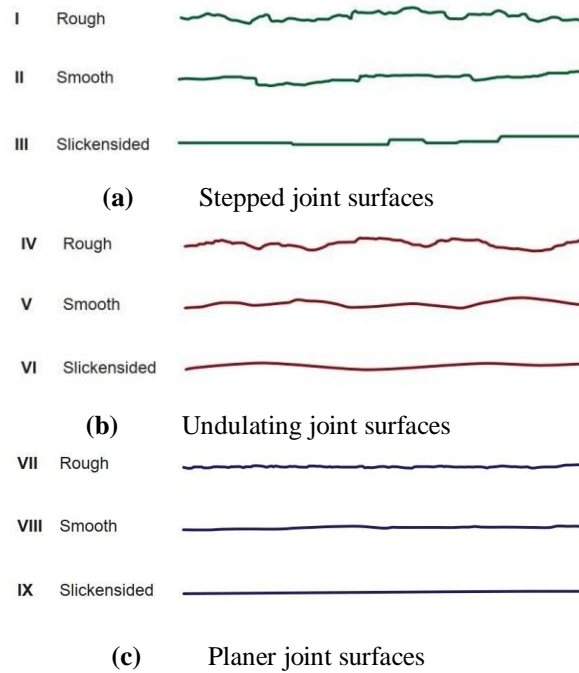


Figure 2.7: Different types of joint surfaces and joint roughnesses (NGI (2015):p .20)

(iv) Joint alteration number (J_a)

The joint alteration number corresponds to joint infill. The infill between the joints is an important factor while assessing joint friction as the joint fill may disrupt the rock wall contact and subsequently can affect the friction between the walls. Based on the type and thickness of infill between the joints, the joint infill is divided into three parts a, b and c. Where a category a means there is no infill in the joint, the b means there is a thin layer of infill and c means there is a thick layer of infill between the joint. While choosing a joint alteration number, it is recommended to assess all the joint sets present in a rock mass and the most unfavorable value shall be used to calculate the Q-value.

The type of mineral between the rock wall is also important while assessing this number. For instance, a sandy/silty fill may not be washed easily in presence of water whereas a clayey layer may wash or swell even with the presence of a very small quantity of water. In Table 4 of the handbook NGI (2015):p 22, joint alteration numbers for many different joint conditions are provided. A general trend can be seen that the number is higher when the infill between rock walls is thicker. As the J_a is in the denominator of the equation (2.21), the higher value of J_a will result into a lower Q-value and subsequently weaker rock mass.

(v) Joint water reduction factor (J_w)

The water in the rock mass may wash the infill between joints, subsequently reduce the friction on the joint plane. Therefore, the joint friction shall be reduced by joint water reduction factor based on the presence of water. The value of (J_w) depends upon the water pressure inside the rock mass. Moreover, the water pressure between rock wall reduces the normal stiffness of the joint and makes shear deformations easier to occur. Therefore, it is important to carefully observe water pressure while assessing the J_w . In table 5 of the handbook “Using the Q-system” NGI (2015):p 24, the J_w values are presented for different conditions. The maximum value of J_w is 1 for completely dry excavation or with very minor water inflow. A value of J_w lower than 0.2 indicates a very high water inflow in the excavation. According to the handbook NGI (2015), rock mass with $J_w < 0.2$ may have large stability problems.

(vi) Stress reduction factor (SRF)

The SRF is a factor that describes a relationship between stress and rock strength around a tunnel. In a massive rock it is rather easier to determine SRF than a weak rock. For the massive rock, SRF can be calculated from the relationship between uniaxial compressive strength (σ_{ci}) of the rock and the major principle stress (σ_1). The σ_{ci} and the σ_1 can be measured at site. The Q-system NGI (2015) recommends to determine the stress situations before determining SRF. The stress situations are categorised as follows:

- **Weakness zones** - A weakness zone is a zone that contains heavily jointed or chemically altered rock and therefore is weaker than surrounding rock. The width of the weakness zone may vary from one-tenth of a meter to hundreds of meters. If the zones are very weak, it can not take the stress from surrounding rock. Subsequently, a stress concentration can occur at one side of the zone while de-stressing can occur at other side of the zone. In case a weakness zone passing through the excavation, unexpected stress situations can occur. Generally, in a low-stress situation, a weakness zone may show unexpected stress conditions inside the zone itself or in a small area around the zone. If several weak zones are present, the larger area of the excavation may be affected. While evaluating SRF-value, the effect of weakness zone on the excavation shall be taken into account.

- **Competent rock** - For the competent rock, it may be difficult to assess SRF value due to different stress situations. The shallow tunnel has low-stress situations due to low overburden and subsequently poor stability. Therefore, a low SRF-values would be fine to use. Generally, moderate stresses are very appropriate for the stability of the tunnel and SRF-value 1 should be used. In case of high stresses, spalling or rock burst may occur in the excavation and a high SRF value for

instance 400 may be used. In high stress situations, it is also important to assess the time after excavation when the spalling or rock burst occurs while assessing SRF-values. For instance, when spalling in a short duration after excavation, a high values of SRF is recommended, whereas when it takes longer duration to show this problems, a lower value of SRF shall be used.

- **Squeezing rock** - The squeezing rock is where stresses in rock exceeds the rock mass strength, resulting in plastic deformation in the rock. Generally, squeezing rock problems happen in the weak/soft or heavily crushed rock. It may be really difficult to estimate rock parameters to calculate Q-value in case of very soft rock and Q-system may not be an appropriate classification system to be used for this case. Therefore, the numerical modelling method shall be chosen to design the supports.

- **Swelling rock** - Some mineral may swell (increase in volume) when comes in contact with water as a result of a chemical process. The rocks containing such mineral can swell and generate swelling pressure around the excavation. In this case, a laboratory test is necessary to determine the swelling pressure for correct estimation of SRF-value.

(vii) Excavation support ratio

In order to use the support chart provided in NGI (2015):p 34 to design the rock supports, span/ESR or height/ESR ratios must be determined beforehand. The span/ESR or height/ESR ratios are referred as the equivalent dimension of the tunnel as shown in equation (2.22) and the ESR refers to excavation support ratio. The span or height of the tunnel, whichever is higher shall be used to calculate the equivalent dimension. In general, the larger span or height of the tunnel will require an increase in need of support.

The ESR is a factor that indicates the required level of safety for an underground opening. The safety requirement for an underground opening depends upon its purpose or use. For instance, an underground nuclear power station will require higher level of safety than a temporary mine

opening. For important underground structures, the ESR values are lower as compared to other underground structures. A lower ESR-value implies the requirement of a high level of safety, whereas the high ESR value implies the requirement of a low level of safety. Practically, the lower ESR-value results into bigger equivalent dimension that means the tunnel will be designed for a

$$\frac{\text{Span or height in m}}{\text{ESR}} = \text{Equivalent dimension}$$

larger span of height than its actual span or height. The Table 7 in NGI (2015):p 33 shows different ESR value recommended for different types of construction based on required level of safety.

(viii) Support chart and rock supports

Once the Q-value of the rock mass and equivalent dimension of the tunnel is known, the rock supports can be estimated from the supports chart presented in the Figure 2.8.

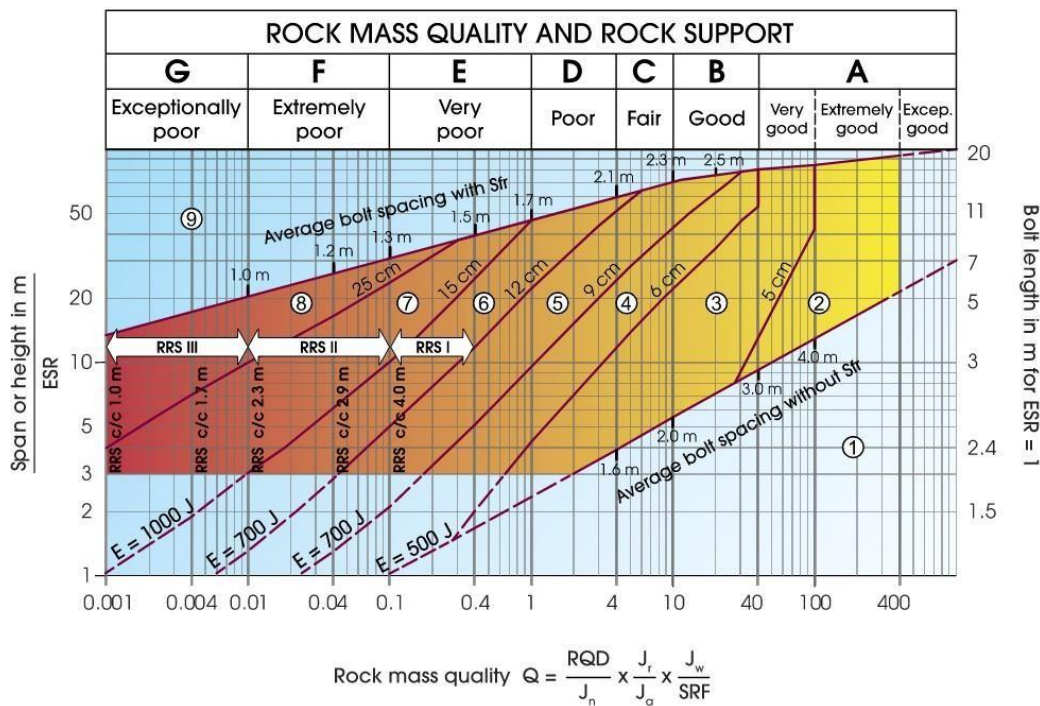


Figure 2.8: Support chart for estimating rock support for a tunnel using Q-system (NGI (2015):p 34)

The rock supports can be estimated in form of support categories, which are marked in the support chart from number 1 to 9. The support categories are defined in the Q-system handbook NGI (2015):p 35. The support category 1 means rock can be unsupported or few rock bolts need to be installed for stability, Whereas the support category 9 means that the special evaluations shall be made to estimate the rock supports. Support categories 2 to 4 require a layer of fibre reinforced concrete and rock bolts. The required thickness of fibre reinforced concrete, spacing and length of rock bolts are shown in the support chart based on the support category. Support categories 6 to 8 require reinforced ribs of sprayed concrete (RRS) along with fibre reinforced concrete and rock bolts. The spacing of RRS are also shown in the support chart for different support categories.

In addition to thickness of fibre reinforced concrete, the energy absorption class is also provided in the support chart. The energy absorption class defined by the energy dissipated to pull out the

fibres from the cracked concrete. The energy dissipated to crack plain concrete matrix is generally much lower than the fibre reinforced concrete, which makes it more favorable material to use in construction. According to Q-system handbook NGI (2015), three energy absorption classes E500, E700 and E1000 are defined as per the Norwegian Concrete Association publication number 7 (NB (2011)).

Support categories

- ① Unsupported or spot bolting
- ② Spot bolting, **SB**
- ③ Systematic bolting, fibre reinforced sprayed concrete, 5-6 cm, **B+Sfr**
- ④ Fibre reinforced sprayed concrete and bolting, 6-9 cm, **Sfr (E500)+B**
- ⑤ Fibre reinforced sprayed concrete and bolting, 9-12 cm, **Sfr (E700)+B**
- ⑥ Fibre reinforced sprayed concrete and bolting, 12-15 cm + reinforced ribs of sprayed concrete and bolting, **Sfr (E700)+RRS I +B**
- ⑦ Fibre reinforced sprayed concrete >15 cm + reinforced ribs of sprayed concrete and bolting, **Sfr (E1000)+RRS II+B**
- ⑧ Cast concrete lining, **CCA** or **Sfr (E1000)+RRS III+B**
- ⑨ Special evaluation

Bolts spacing is mainly based on $\varnothing 20$ mm

E = Energy absorption in fibre reinforced sprayed concrete

ESR = Excavation Support Ratio

Areas with dashed lines have no empirical data

RRS - spacing related to Q-value

I	Si30/6 $\varnothing 16$ - $\varnothing 20$ (span 10m) D40/6+2 $\varnothing 16$ -20 (span 20m)
II	Si35/6 $\varnothing 16$ -20 (span 5m) D45/6+2 $\varnothing 16$-20 (span 10m) D55/6+4 $\varnothing 20$ (span 20m)
III	D40/6+4 $\varnothing 16$ -20 (span 5m) D55/6+4 $\varnothing 20$ (span 10 m) Special evaluation (span 20 m)

Si30/6 = Single layer of 6 rebars,
30 cm thickness of sprayed concrete

D = Double layer of rebars

$\varnothing 16$ = Rebar diameter is 16 mm

c/c = RSS spacing, centre - centre

Figure 2.9: Rock support categories as per Q-system (NGI (2015))

When fibre reinforced shotcrete and rock bolts are not enough for the tunnel's stability, the reinforced ribs of sprayed concrete (RSS) need to be provided. RRS is similar to a reinforced concrete beam spaced at a specific distance in the tunnel. There are three type of RRS defined in the Q-system handbook - RRSI, RRSII and RRSIII. The RRSI contains lowest amount of reinforcement, whereas the RRSIII are thickest and contains the highest amount of reinforcement as shown in the Figure 2.9. The typical RRS construction is shown in the Figure 2.10. The RRS may contain single or double layers of reinforcement based on the span of underground opening. For instance, RRSII will require only one layer of reinforcement for 5 m span, whereas 2 layers of reinforcement in case of 10 or 20 m span as shown in the Figure 2.9.

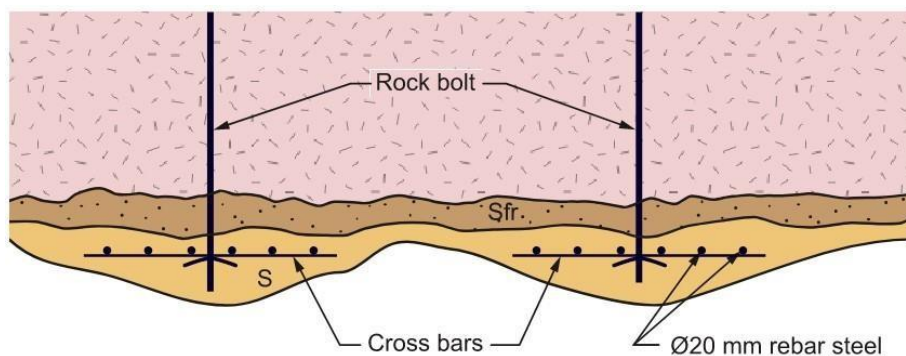


Figure 2.10: Typical layout of RRS construction (NGI (2015))

2.6 Strength parameters for joints in rock mass

For discontinuum model, the joint properties need to be assessed. The joint parameters depends upon the failure or slip criterion for joints being used. There are many slip criterion for joints such as Barton-Bandis, Mohr-Coulomb, Geosynthesis Hyperbolic etc. In this report, the Barton-Bandis failure criterion is adopted for joints. The criterion was

2.6. Strength parameters for joints in rock mass

introduced by Barton and Bandis (1982) for jointed rocks. According to Barton and Bandis (1982), the shear strength of the joint can be calculated from equation (2.23).

$$\tau = \sigma_n \tan \left(\phi_r + \text{JRC} \log_{10} \left(\frac{\text{JCS}}{\sigma_n} \right) \right) \quad (2.23)$$

Where, JRC is joint roughness coefficient, JCS is joint compressive strength, σ_n is normal stress and ϕ_r is residual friction angle of the joint surface.

The Joint roughness coefficient (JRC) is a coefficient that express roughness of the joint surface. The coefficient is similar to the joint roughness number J_r of the Q-system. The JRC can be estimated by comparing the roughness of the joint surface with the roughness profiles published by Barton and Choubey (1977). The roughness profiles are presented in the Figure 2.11.

Bandis (1993) provided an approximate relationship between JRC and J_r as shown in the Figure 2.11b. The Figure 2.11b provide approximate values of JRC_{20} and JRC_{100} . Where, JRC_{20} is for 20 cm long defects and JRC_{100} is for 100 cm long defects.

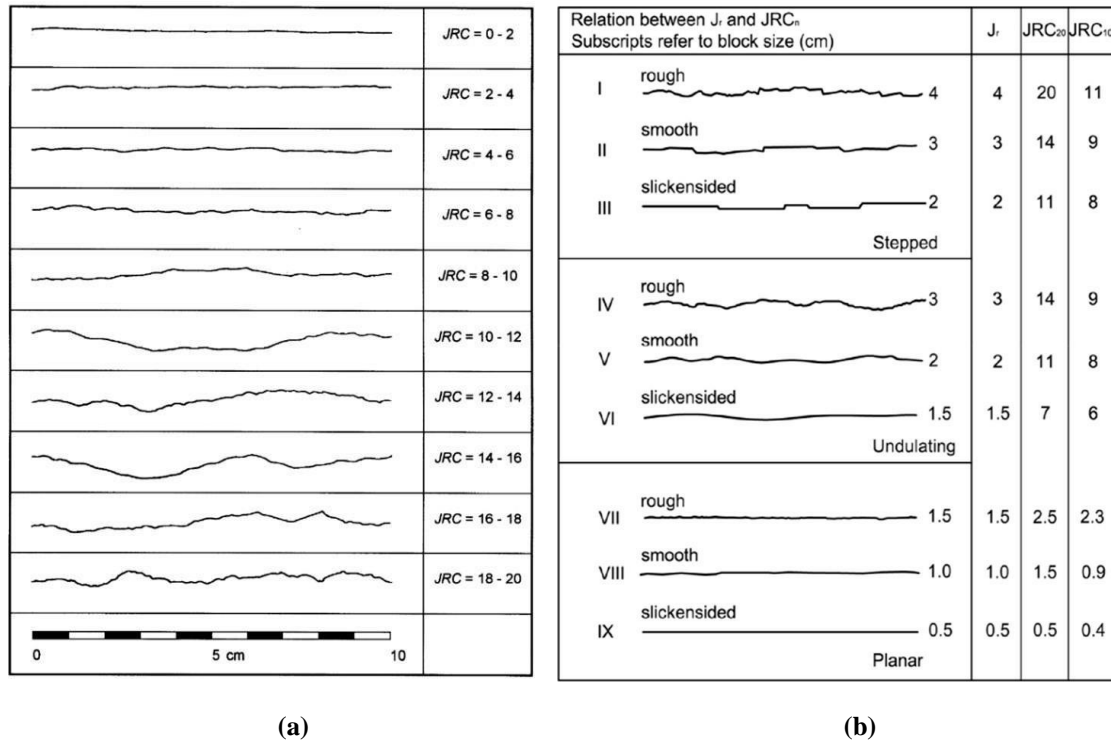


Figure 2.11: (a) Roughness profiles of joints and corresponding JRC values (Barton and Choubey (1977)) (b) Joint roughness numbers J_r for several roughness profiles and corresponding JRC values for 20 cm and 100 cm long defects (subscript of JRC represents the length of defects (Bandis (1993))). The compressive strength of the rock comprising joint wall can be expressed in terms of joint wall compressive strength (JCS). The JCS is a very important component of shear strength and deformability of the joint. The JCS can be estimated at the field by several methods described in ISRM (1978). The Schmidt rebound method is one of the easy and popular method to estimate JCS at field. However, the JRC and JCS both can be estimated in the laboratory from a smaller sample of rock. Thereafter, the in-

situ values of JRC_n and JCS_n can be calculated from laboratory values from equations (2.24) and (2.25) provided by Barton and Bandis (1982). Where, JRC_o , JCS_o and L_o are estimated values for 100 mm laboratory scaled sample and JRC_n , JCS_n and L_n are estimated values for in-situ block size. It can be noticed from the equations that the in-situ JRC_n and JCS_n depends upon the scale and likely to decrease with the increase in scale. Therefore, it is important to use scaled values in the analysis not the laboratory values.

In case the field or laboratory test data is not available, the range of JCS_n values is provided in the Plaxis 2D(2019) software for different types of rocks as presented in the following Table 2.1.

Table 2.1: Joint compressive strength (JCS) for different types of rocks (from RocData (2019))

Description	JCS [MPa]
Extremely weak rock	0.25 - 1.0
Very weak rock	1.0 - 5.0
Weak rock	5.0 - 25
Medium strong rock	25 - 50
Strong rock	50 - 100
Very strong rock	100 - 250
Extremely strong rock	> 250

The normal stiffness (k_n) of the joint is also an input parameter in a discontinuum model. It is defined as the maximum load that joint can cater per square meter of area before failure. Barton (1972) proposed equation (2.26) to calculate k_n from rock mass modulus (E_{rm}), intact rock modulus (E_i) and mean joint spacing (s_j).

$$k_n = \frac{E_{rm}E_i}{(E_i - E_{rm})s_j} \quad (2.26)$$

Similar to normal stiffness, the shear stiffness (k_s) of the joint is defined as the maximum shear force that joint can cater per square meter of area before failure. According to Barton and Choubey (1977), shear stiffness (k_s) of a joint can be obtained from the ratio of shear strength (τ) and the shear displacement (u_s) required to reach the shear strength. The shear displacement (u_s) can be expressed in terms of JRC and length of joint (L) as presented in equation (2.27). Therefore, from equation (2.23) and (2.27), the shear stiffness is shown in equation (2.28).

$$u_s = \frac{L}{500} \left(\frac{JRC}{L} \right)^{0.33} \quad (2.27)$$

$$k_s = \frac{\tau}{u_s} \Rightarrow \frac{\sigma_n \tan \left(\phi_r + JRC \log_{10} \left(\frac{JCS}{\sigma_n} \right) \right)}{\frac{L}{500} \left(\frac{JRC}{L} \right)^{0.33}} \quad (2.28)$$

2.7 Strength of young sprayed concrete

The strength of young sprayed concrete is an important factor while designing the rock support system. It takes 28 days for the concrete to achieve its full strength after installing. Thus, early age strength of concrete can be said to the strength gained from 0 to 28 days. However, in practice early age strength is generally referred as the strength gained from 0 to 7 days. In a study by Chang and Stille (1993), the empirical equations (2.29), (2.30) and (2.31) are provided to calculate the properties of young sprayed concrete.

$$\sigma = a \cdot \sigma_{28} \cdot e^{(c/t)0.7} \quad (2.29)$$

$$E = a \cdot E_{28} \cdot e^{(c/t)0.7} \quad (2.30)$$

$$E = 3.86 \cdot \sigma^{0.60} \quad (2.31)$$

Where, σ and E are the compressive strength and Young's modulus of concrete after 't' days respectively, E_{28} and σ_{28} are compressive strength and Young's modulus of concrete after 28 days respectively, a and c are constants.

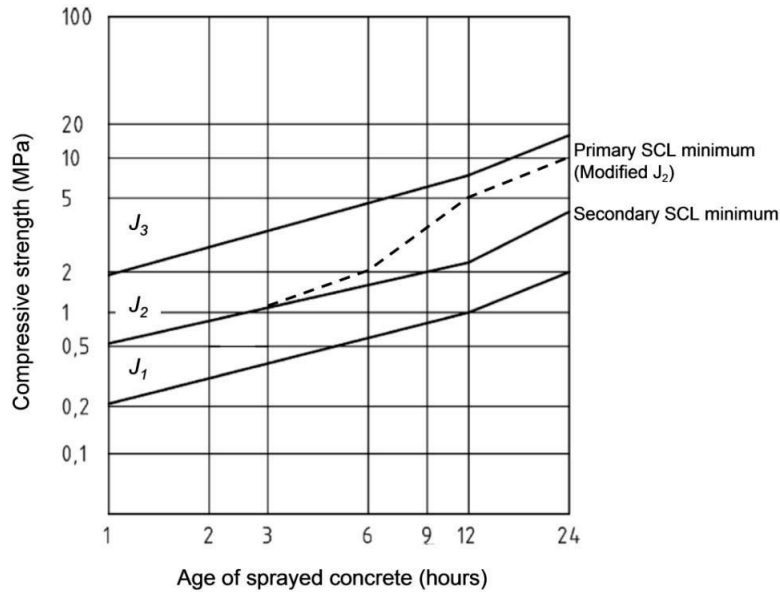


Figure 2.12: Early strength development of sprayed concrete - The modified J2 curve(based on DS/EN-14487-1 (2005))

According to DS/EN-14487-1 (2005), three early strength classes J1, J2 and J3 are defined for young concrete as presented in Figure 2.12. To fulfill its functional requirement, the strength of sprayed concrete shall exceed the strength defined in modified J2 curve in first 24 hours after installation. For this project, the J2 values for sprayed concrete obtained by penetration needle test (as recommended by DS/EN-14487-1 (2005)) are provided by COWI as presented in Table 2.2.

Table 2.2: J2 values obtained from tests for first 24 hours

t (time)	J2
[hours]	[MPa]
0.5	0.52
1	0.86
2	1.20
4	2.24
6	3.44
9	3.44
12	8.60
24	15.00

Subsequently, the compressive strength of young concrete is estimated from J2 values for first 24 hours and from equations (2.29) and (2.31) for 36 hours to 7 days. The compressive strength and Young's modulus between 24 hours to 26 hours are interpolated.

The compressive strength and Young's modulus for concrete grade C30/37 are calculated and plotted

with the time as presented in Figure 2.13 and Figure 2.14. The calculated values at each data point is presented in Appendix A. It is to be noted that the effect of creep on concrete is ignored for this analysis and creep coefficient ($\phi(\infty, t_0)$) is assumed

1.

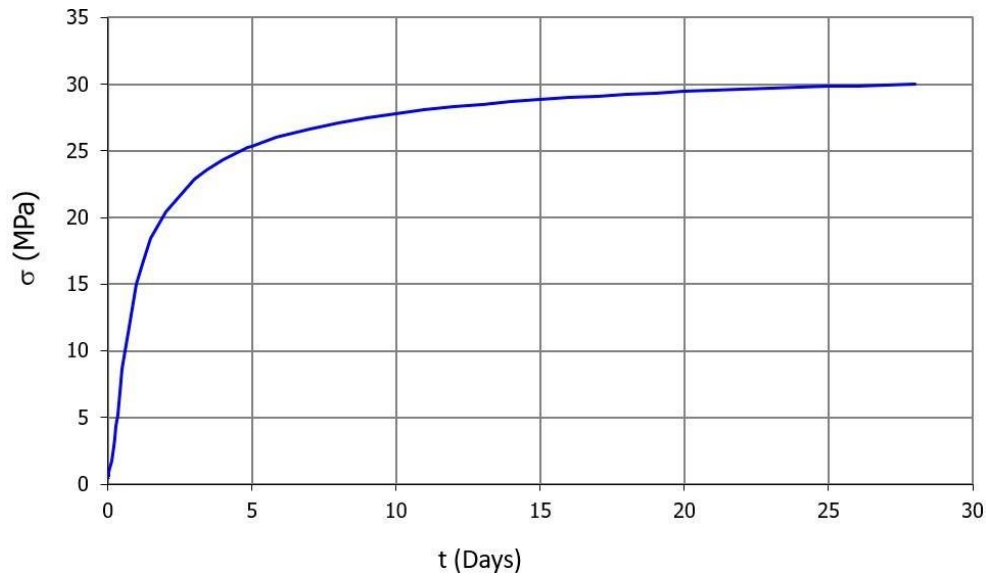


Figure 2.13: Compressive strength (σ) of sprayed concrete for 0 to 28 days after spraying

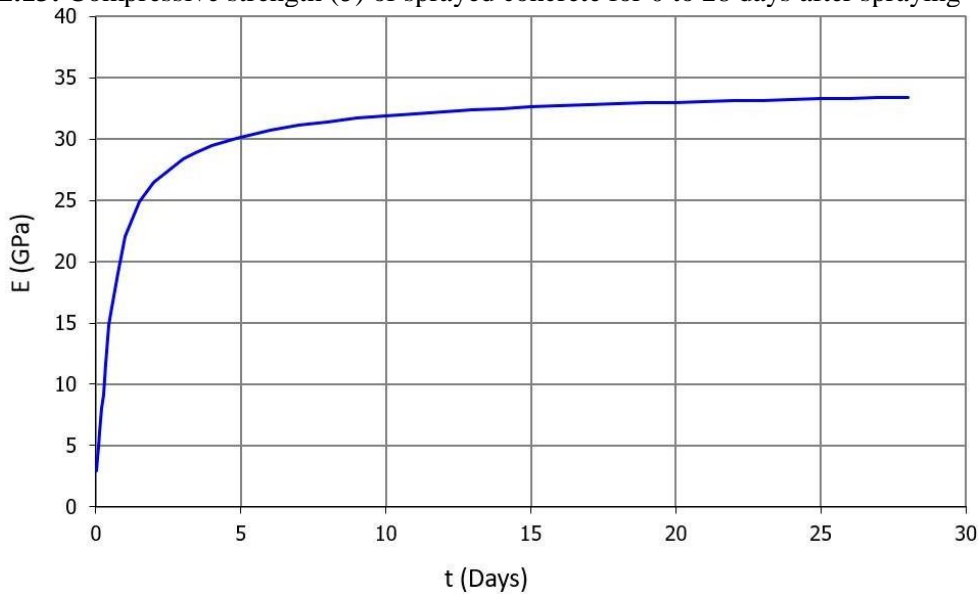


Figure 2.14: Young's modulus (E) of sprayed concrete for 0 to 28 days after spraying

2.8 M-N interaction curves

The acceptable combination of axial force and bending moment for axially loaded concrete element can be estimated through M-N interaction curve. The M-N curves are used to verify the RRS for the design forces further in Section 4.4, therefore the M-N curves for plain concrete (PC), steel fibre reinforced concrete (SFRC) and reinforced concrete (RC) are discussed in this section.

The plain concrete (PC) and steel fibre reinforced concrete (SFRC) are have very similar strength properties, when compressive forces are being applied. Due to added steel fibre, SFRC has better tensile strength than the PC. According to Fib (2013), when compressive forces are applied PC and SFRC exhibits similar parabolic stress-strain relationship, where after reaching the peak strength (top of parabola), concrete fails. However, after peak the drop of strength is more abrupt for PC.

Besides, when tensile forces are applied, PC fails after reaching its peak tensile strength, but SFRC shows strain-softening behaviour, where after reaching the peak, the strength drops to a residual value. Therefore, while calculating bending moment capacity of SFRC, residual strengths are taken into account.

2.8.1 For plain and reinforced concrete

The principle of calculating acceptable bending moment and axial force combination is based on the stress distribution diagram provided in DS/EN-1992-1-1 (2005) and presented in Figure 2.15.

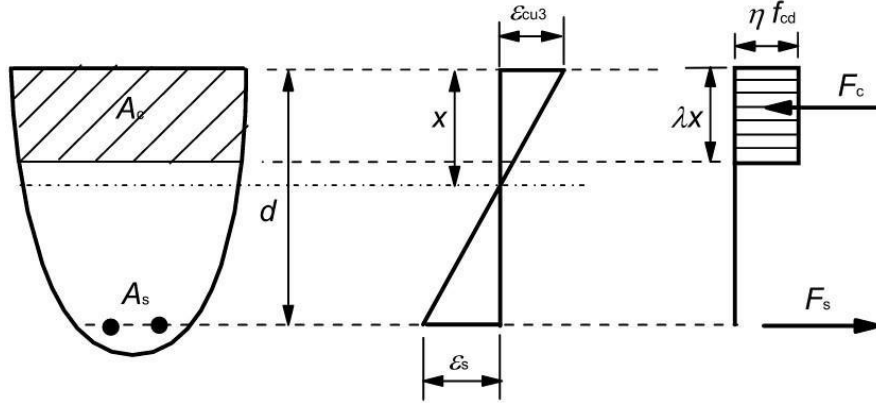


Figure 2.15: Rectangular stress distribution in reinforced concrete (from DS/EN-1992-11 (2005)), A_c is area of compression zone, A_s is cross-sectional area of reinforcement, λ and η are factors for defining effective height of compression zone (λx) and effective strength (ηf_{cd}), f_{cd} is design compressive strength of concrete, ϵ_s is maximum yield strain in reinforcement, ϵ_{cu3} is ultimate strain in concrete, F_c and F_s are total compressive and tensile forces respectively.

The factors λ and η are calculated based on the characteristic compressive strength of concrete (f_{ck}) from equations (2.32) and (2.33) respectively.

$$\begin{aligned} \lambda &= 0,8 && \text{for } f_{ck} \leq 50 \text{ MPa} && \text{for} && (2.32) \\ \lambda &= 0,8 - (f_{ck} - 50)/400 && 50 < f_{ck} \leq 90 \text{ MPa} && && \end{aligned}$$

$$\begin{aligned} \eta &= 1,0 && \text{for } f_{ck} \leq 50 \text{ MPa} && \text{for} && (2.33) \\ \eta &= 1,0 - (f_{ck} - 50)/200 && 50 < f_{ck} \leq 90 \text{ MPa} && && \end{aligned}$$

The design strength of concrete (f_{cd}) is calculated from equation (2.34).

$$f_{cd} = \alpha_{cc} f_{ck} / \gamma_c \quad (2.34)$$

Where, α_{cc} is a factor for considering long-term effects and load application on compressive strength of concrete and γ_c is partial safety factor for concrete. According to DS/EN1992-1-1 (2005), α_{cc} is assumed 0.8 for plain concrete and 1 for SFRC and reinforced concrete and γ_c is 1.5.

Similarly, design strength of steel (f_{yd}) is calculated from characteristic yield strength of steel (f_{yk}) by equation (2.35), assuming partial safety factor of steel $\gamma_s = 1.15$ as per DS/EN-1992-1-1 (2005).

$$f_{yd} = f_{yk} / \gamma_s \quad (2.35)$$

The Young's modulus of concrete (E_c) is obtained from DS/EN-1992-1-1 (2005) based on the grade of concrete and Young's modulus of steel (E_s) is assumed as 200000 MPa.

Thereafter, the maximum yield strain in steel is calculated as:

$$\varepsilon_s = E_s/f_{yd} \quad (2.36)$$

Furthermore, the strains in concrete ε_{c2} , ε_{c3} and ε_{cu} are calculated from following equation (2.37), (2.38) and (2.39) provided in DS/EN-1992-1-1 (2005).

$$\begin{aligned} \varepsilon_{c2} &= 0.002 && \text{for } f_{ck} < 50 \text{ MPa} \\ \varepsilon_{c2}(\%) &= 2.0 + 0.085(f_{ck} - 50)^{0.53} && \text{for } f_{ck} \geq 50 \text{ MPa} \end{aligned} \quad (2.37)$$

$$\begin{aligned} \varepsilon_{c3} &= 0.00175 && \text{for } f_{ck} < 50 \text{ MPa for} \\ \varepsilon_{c3}(\%) &= 1.75 + 0.55[(f_{ck} - 50)/40] && f_{ck} \geq 50 \text{ MPa} \end{aligned} \quad (2.38)$$

$$\begin{aligned} \varepsilon_{cu} &= 0.0035 && \text{for } f_{ck} < 50 \text{ MPa} \\ \varepsilon_{cu}(\%) &= 2.6 + 35[(90 - f_{ck})/100]^4 && \text{for } f_{ck} \geq 50 \text{ MPa} \end{aligned} \quad (2.39)$$

Where, ε_{c2} is stain in concrete at reaching maximum strength when stress-strain relationship for concrete is considered parabolic-rectangular, ε_{c2} is stain in concrete at reaching maximum strength when stress-strain relation for concrete is considered bi-linear and ε_{cu} in the ultimate strain. The parabolic-rectangular and bi-linear stress-strain diagrams are presented in DS/EN-1992-1-1 (2005). Thereafter, above mentioned stress-strain relationships are used to calculate the total compression force (F_c) in concrete and total tension force (F_s) is steel in accordance with Figure 2.15 from equations (2.40) and (2.41).

$$F_c = f_c \lambda x b \quad (2.40)$$

$$F_s = f_s A_s \quad (2.41)$$

Where, b is width of the section, f_c is compressive stress, f_s is tensile stress A_s is crosssectional area of reinforcement.

Lastly, F_c and F_s are used to calculate bending moment (M) and axial force (N) capacities of the section in accordance with Figure 2.15 as shown in the equation (2.42) and (2.43). Where, h_w is depth of the section.

$$M = F_c \left(\frac{h_w}{2} - \frac{\lambda x}{2} \right) - F_s \cdot \left(d - \frac{h_w}{2} \right) \quad (2.42)$$

$$N = F_c - F_s \quad (2.43)$$

2.8.2 For steel fibre reinforced concrete

The M-N curve for steel fibre reinforced concrete (SFRC) is developed in the same way as explained for reinforced concrete section in previous section by replacing the contribution of reinforcement by steel fibers. For the properties of SFRC, Fib model code for concrete structures 2010 Fib (2013) is referred. According to Fib (2013), the SFRC is classified based on the two parameters - the range of characteristic flexural residual strength (f_{R1k}) in serviceability condition and the ratio of flexural residual strength (f_{R3k}/f_{R1k}) in serviceability and ultimate conditions.

The range of f_{R1k} is defined by a strength value and the subsequent number in the series

1.0, 1.5, 2.0, 2.5, 3.0, 4.0, 5.0, 6.0, 7.0, 8.0. [Mpa], whereas the f_{R3k}/f_{R1k} is defined by a letter from a to e, as shown

below. a if $0.5 < f_{R3k}/f_{R1k} <$

0.7 b if

$0.7 \leq f_{R3k}/f_{R1k} < 0.9$ c if $0.9 \leq$

$f_{R3k}/f_{R1k} < 1.1$ d if 1.1

$$\leq f_{R3k}/f_{R1k} < 1.3 \text{ e if } 1.3$$

$$\leq f_{R3k}/f_{R1k}$$

In this report, the SFRC of class 4c is used in accordance with COWI (2019a), which means $4.0 \text{ MPa} < f_{R1k} < 5.0 \text{ MPa}$ and $0.9 \leq f_{R3k}/f_{R1k} < 1.1$.

In further calculation, lower limits of the provided range is used as a conservative approach i.e. $f_{R1k} = 4$ and $f_{R3k}/f_{R1k} = 0.9$.

Therefore, the characteristic flexural residual strength (f_{R3k}) in ultimate condition is obtained from equation (2.44).

$$f_{R3k} = \frac{f_{R3k}}{f_{R1k}} \cdot f_{R1k} \quad (2.44)$$

The design axial strengths in serviceability (f_{Ftsd}) and ultimate (f_{Ftud}) conditions are calculated from equation (2.46).

$$f_{Ftsd} = f_{Ftsk} / \gamma_F K \quad (2.46)$$

$$f_{Ftud} = f_{Ftuk} / \gamma_F K$$

Where, γ_F is partial safety factor and K is a factor for fibre orientation, considered as 1.5 and 1 respectively as per Fib (2013).

Lastly, the bending moment (M) and axial force (N) capacities of the section in accordance with Figure 2.15 can be calculated as:

$$M = F_c \left(\frac{h_w}{2} - \frac{\lambda x}{2} \right) - f_{Ftud} (h_w - \lambda x) (\lambda x + (h_w - \lambda x)/2) b \quad (2.47)$$

$$N = F_c - f_{Ftud} (h_w - \lambda x) b \quad (2.48)$$

The calculated bending moment capacities and corresponding axial force capacities are plotted to obtain the M-N interaction curve as presented in Figure 2.16 for plain concrete of grade C30/37 and SFRC class 4c for a $0.5 \text{ m} \times 0.55 \text{ m}$ section as an example, and the calculations are presented in Appendix B.

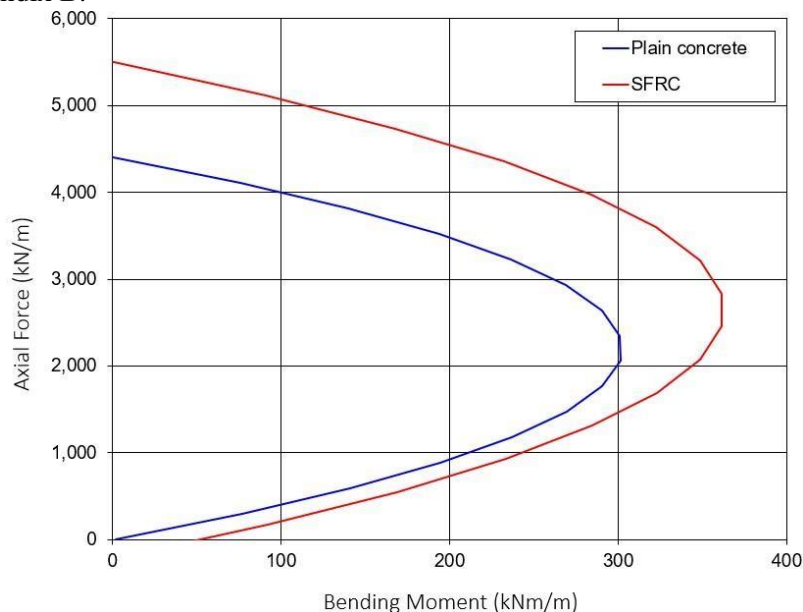


Figure 2.16: M-N interaction curve of C30/37 concrete grade for plain concrete and SFRC class

Chapter 3

ROCK MASS CLASSIFICATION AND ROCKSUPPORT ASSESSMENT

Primarily, the mechanical behaviour or properties of the rock mass are determined by the laboratory tests and number, arrangement and intersection of the sets of discontinuities present within the rock mass, but the geological properties of the rock mass also have a relevant impact on the development of these discontinuities [Palmström and Stille \(2010\)](#). Thus, geological lithologies in the alignment of Rohtang Tunnel provide in [BRO](#) are discussed in this chapter followed by the input parameters for Q-system.

3.1 Geological Lithologies

For the Rohtang Tunnel project, several Geological lithologies have been mapped along the route. The geological lithologies are briefly described below.

3.1.1 Quartz with Mica Minerals (Biotite and Muscovite) defining the schistosity in schistose quartzite)

Most of the tunnel alignment lies in the rhombus-porphry which is a volcanic rock and form as a results of cooling down of magma. According to classification of igneous rocks it is trachyte rock. It has a fine-grained red-brown matrix (aphanitic texture) and consists of tightly closed phenocrysts of feldspar (rhombus shaped), usually bigger than 1 cm.

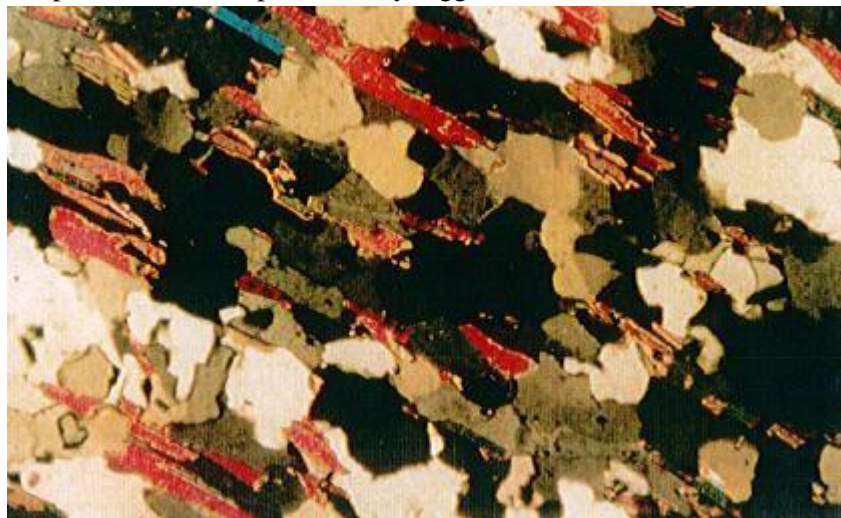


Figure 3.1: Quartz with Mica mineral

According to the logging of the geotechnical cores, at least 8 different types of rhombus porphyries are found. The different types of rhombus porphyries are distinguished based on color, shape, distribution and sizes of the rhombus along the length of the tunnel. In some areas, the porphyries consist several millimeters big cavities, filled with Calcite. A picture of rhombus-porphry from Rohtang Tunnel project site is presented in Figure 3.1. The picture is taken from a report by [Jakobsen \(2018\)](#), uploaded at Bane Nor's website .

3.1.2 Porphyroblasts of Biotite and muscovite in schistose quartzite

As evident from the name latite lava is a fine-grained igneous rock. It usually occurs in compact layers and is mainly has distinct pink color due to its mineral composition which consists of alkali feldspar and plagioclase in approximately equal amount. The latite lava is seen at several place along the tunnel alignment. A picture of latite lava found at Rohtang Tunnel site is presented in the Figure 3.2.

3.1.3 Quartz II Porphyroblast in Quartz – Biotite Schist

Basalt rock is fine-grained, compact rock, usually has black or greyish-black color. At the high slopes, basalt is mapped together with latite lava. On the border between the rocks, a very loose, almost gravely layer of pink rock was recorded in a dark grey matrix. The gravely mass has been mapped to have orientation almost parallel to the axis of planned new railway line. It has a very close inclination dip of approximately 80° towards west. The basalt found at the site shown in the Figure 3.2.

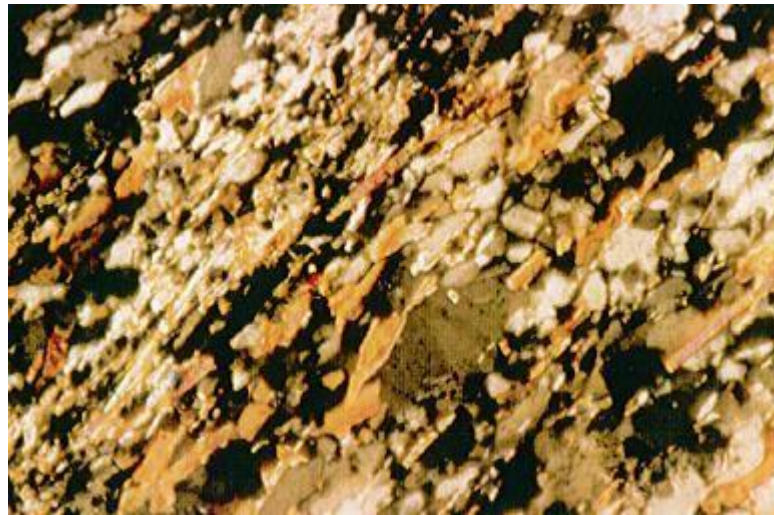


Figure 3.2: Basalt (black rock at top) and latite lava (pink rock at bottom) mapped at Rohtang Tunnel site (Jakobsen (2018))

3.2 Structural geology

From available information, it has been noticed that there is a relatively large spread of strikes and dips of the joints along the tunnel alignment. Mainly, three joint sets are mapped at along with a few random joints. The main joint set has strike in the North South direction with a steep dip towards East. Other joint set has strike in Northeast Southwest to East-West direction with a dip towards South. The last joint set has strike in a Northwest-Southeast direction and dip towards North-East. Thus, the dominating strike is in North-South direction, with most of the joints having dip towards East. These joints can have an adverse effect on stability of the tunnel.

3.3 Rock parameters for Q-system

As explained earlier in Chapter 1, required rock supports for 3 quality of rock masses namely exceptionally poor (G), extremely poor (F) and very poor (E) are assessed in the support. In order to do so, the parameters for calculating Q-values are estimated based on the observation carried out on available borehole loggings. The estimation of six rock mass parameters to calculate Q-values is based on the description of the Q-system presented in Section 2.5.

While assessing the values of the parameters which give shape to the Q system, sometimes it could be really difficult to select a single rating for a particular parameter therefore, a range of the rating has been adopted. In such cases, a sort of geometrical mean could be obtained from the minimum

and maximum values or an upper and lower bound values as a representative value of the parameter.

However, it is suggested in [Barton and Grimstad \(2014\)](#) to adopt a unique value for certain rock parameters, especially J_w and SFR. Therefore, the ratings for some parameters are estimates as a range of values and for other a single value.

3.3.1 Rock Quality Designation

Rock quality designation (RQD) is assessed from the boreholes loggings according to the definition provided in [Deere \(1963\)](#). The observed RQD values from boreholes is described as follows:

SKBH-01

The RQD values in borehole SKBH-01 mainly varies between 60 to 100 %, which correspond to slightly joined, good quality rock mass. However, in some other areas of the borehole, the rock mass consists of one to three joint sets and reflects a RQD value of 40 to 80 %. The average value for the entire core length may be estimated to vary between 50 to 100 %.

SKBH-02

The main rock type found in the borehole SKBH-02 is porphyry. The borehole indicates a large variation in RQD values along the core length. Almost 80% of the core length represents an RQD value of 50 to 100 % which correspond to slightly joined, good quality of rock. Whereas, the rest 20% of the core length significantly lower value of RQD ranging from 10 to 25% in some localised areas and 25 to 50 % in rest, which corresponds to more disturbed and jointed rock mass.

It is evident from the above borehole data that the rock condition along most of the tunnel length could be considered satisfactory. However, the boreholes indicate the presence of several weak zones. These weak zones could impose challenging conditions while excavating and supporting the tunnels. Therefore, these zones are considered as areas of particular interest in the present work.

As mentioned earlier, only 3 quality is aimed to be analysed in this report. Therefore, keeping the borehole data in mind the three sets of RQD values are assumed. The upper limit of the RQD is obtained from borehole data as 40 to 50 %. In [Barton et al. \(1974\)](#), it is recommended to use a minimum value of RQD as 10 % for rock mass, as the 0 to 10% of RQD corresponds to soils. Therefore, a value between 20 to 25 % is considered as the lower limit. The estimated RQD values for the three sets are presented in the Table 3.1.

Table 3.1: Three different sets of RQD values estimated from available boreholes loggings

Parameter	Set 1	Set 2	Set 3
Estimated RQD [%]	20 to 25	30 to 35	40 to 45

3.3.2 Joint set numbers

As mentioned earlier in this report, the number of discontinuities present in the rock mass affects the mechanical behaviour of the rock mass. The number of joint sets may be defined by choosing an appropriate joint set number (J_n) from the Q-system handbook [NGI \(2015\)](#):p 15 based on the presence of discontinuities in the rock mass. In general, the number of joint sets in a rock mass is affected by foliations, schistosity, slaty cleavages or beddings etc. From Section 3.1, the rock type along the tunnel is mostly volcanic. The volcanic rocks usually delimit joints related to decompressional volume change, whereas joints mostly occur due to thermal contraction while cooling and propagate perpendicularly to isotherms and with a spacing controlled by the rate of cooling.

From the borehole data and site observations, 2 to 3 joint sets are observed to be present in the rock mass. Additionally, some random joints are also present in the rock mass due to local flaws. Therefore, three joints sets and one random joint set is assumed to be present in the rock mass. However, at several locations four or more joint sets are also observed. Therefore, corresponding joint set numbers (J_n) shall vary from 6 to 15 for most of the core length. The most of the rock mass is have three joint sets and one random joint sets, and in some cases two joint sets and one random joint sets. The values of J_n are estimated keeping in mind the [NGI \(2015\)](#) recommendation of choosing the least favorable value as a representative value for the rock domain. The estimated values of J_n are presented in the Table 3.2 for the three sets.

Table 3.2: Three different sets of joint set numbers estimated from available boreholes loggings

Parameter	Set 1	Set 2	Set 3
Description	Three joint sets plus one random to four or more joints	Three joint sets and sometimes plus one random joint	Two joint sets plus one random and sometimes three joint sets
Assigned J_n rating	12 to 15	9 to 12	6 to 9

3.3.3 Joint roughness numbers

The joint roughness number (J_r) can be estimated visually by comparing the nature of asperities with the chart presented in Figure 2.7. In case of very fine asperities, physical touch of joint surface may provide better understanding of the nature of asperities. For this study, the joint roughness numbers are estimated by analysing available boreholes and assigning a J_r value to joint surfaces according to the Table 3 in Q-system handbook [NGI \(2015\)](#):p .18. The assessment of boreholes is summarised as follows:

- SKBH-01

The logged data in borehole SKBH-01 indicates that the majority (nearly 80 %) of joint surfaces are rough and uneven. This corresponds to a J_r equal to 3.

- SKBH-02

In borehole SKBH-02, the rock condition shows that around 40% of the joint planes have rough surfaces, therefore J_r equal to 3 and the remaining 60% have rough and planar surfaces correspond to J_r equal to 1 - 1.5.

The surface conditions identified from the boreholes have been arranged within the previously mentioned three sets and presented in the Table 3.3.

Table 3.3: Three different sets of joint roughness numbers estimated from available boreholes loggings

Parameter	Set 1	Set 2	Set 3
Description	Smooth, planer	Rough, irregular, planer	Rough or irregular, undulating

Assigned J_r rating	1	1.5	3
-----------------------	---	-----	---

3.3.4 Joint alteration numbers

The joint alteration numbers (J_a) are estimated from available boreholes by observing the joint surfaces for the presence of stains or filling. Subsequently, a rating is assigned to joint surface according to the J_a Table 4 from [NGI \(2015\)](#):p 22.

The recorded loggings show that majority of the joints are in relatively good condition, having tight joints with stains or thin filling comprising sandy particles or clay minerals. The value of J_a is therefore ranging from 1 to 3 corresponds to unaltered joints and thin sandy or silty clay coating, respectively. However, in several joints relatively thick clay fillings is observed that corresponds to a Joint alteration number of 8. As the objective of this study are those ground conditions with the lowest performances, it is assumed that a certain weathering would always be present. This assumption is also in line with [NGI \(2015\)](#) recommendations, that the least favorable of these conditions should be chosen as the representative of the rock domain. The assigned J_a values are presented in the Table 3.4.

Table 3.4: Three different sets of joint alteration numbers estimated from available boreholes loggings

Parameter	Set 1	Set 2	Set 3
Description	Medium or low over-consolidation, softening, clay mineral fillings (continuous, but <5 mm thickness)	Sandy particles, clay-free disintegrated rock, etc	Silty or sandy clay coatings, small clay fraction (nonsoftening).
Assigned J_a rating	8	4	3

3.3.5 Joint water reduction factors

The rating for the water inflow which might cause washing of the discontinuities or relevant inflow in the underground excavation is usually assessed by mean of is-situ permeability test. In the absence of permeability test, the joint water reduction factor J_w is approximately estimated based on rock condition.

From RQD values estimated in Table 3.1, it is evident that the degree of jointing is poor. Therefore, it can be expected that the severe groundwater conditions may occur for the tunnel section with the lowest RQD values and severe to moderate for the tunnel section with slightly higher RQD values. From the Figure 1.1, the average depth of tunnel section (h) is 15 m below ground level from Table 1.1. It is expected that the natural ground water level lies above the tunnel section. Subsequently, a seepage may develop leading a certain ground water inflow towards the excavation. For this study, considering the worst-case scenario, it is assumed that the gradient developed by the seepage is sufficient to wash all the discontinuities. The estimated ratings of J_w are summarised in the Table 3.5.

Table 3.5: Three different sets of joint water reduction factors estimated from available boreholes loggings

Parameter	Set 1	Set 2	Set 3
Description	Jet inflow or high pressure in competent rock with un-filled joints	Medium inflow, occasional out wash of joint fillings (many drips/"rain")	Medium inflow, occasional out wash of joint fillings (many drips/"rain")
Assigned J_w rating	0.5	0.66	0.66

3.3.6 Stress reduction factors

As already mentioned in Section 1.2, the stress reduction factor (SRF) is one of the most difficult parameter to address properly. For this study, it is assumed that this factor is governed by the presence of several weak zones intersecting the underground opening rather than problems related to stresses or squeezing with plastic deformation.

In order to be consistent with all the previous estimations, which indicate presence of weak zones with clay and disintegrated rock, the [NGI \(2015\)](#) recommendations are adopted to estimate SRF value. As per [NGI \(2015\)](#), a unique value for the rock domain is assumed, considering the worst-case scenario for all the rock masses. The estimated SRF rating is presented in the Table 3.6.

Table 3.6: Three different sets of stress reduction factors (SRF) estimated from available boreholes loggings

Parameter	Set 1, 2 and 3
Description	Multiple occurrences of weak zones within a short section containing clay or chemically disintegrated, very loose surrounding rock (any depth), or long sections with incompetent (weak) rock (any depth)
Assigned SRF rating	10

3.4 Q-values

The input parameters for Q-system are already estimated in previous section. Subsequently, the corresponding Q-values are calculated from equation (2.21) and summarized in the Table 3.7. From the table, it can be seen that the ranges of Q-values for set 1 to 3 correspond to rock mass qualities exceptionally poor (G), extremely poor (F) and very poor (E) from the support chart from [NGI \(2015\)](#):p 34 as aimed in the start of this study.

Table 3.7: Summary of estimated rock parameters (Q-parameters), corresponding Q values and rock mass qualities

Rock parameters	Units	Set 1	Set 2	Set 3
RQD	[%]	20 - 25	30 - 35	40 - 45
J_n	[-]	15 - 12	12 - 9	9 - 6
J_r	[-]	1	1.5	3
J_a	[-]	8	4	3
J_w	[-]	0.5	0.66	0.66
SRF	[-]	10	10	10
Q-values		0.008 - 0.01	0.06 - 0.1	0.3 - 0.5
Rock mass quality		Exceptionally poor	Extremely poor	Very poor

Rock mass quality according to Q-system ¹	G	F	E
--	---	---	---

Hereinafter, set 1, set 2 and set 3 are referred as exceptionally poor, extremely poor and very poor quality rock mass in this report.

3.5 Assessment of rock supports for the tunnel

The rock supports for the tunnel are evaluated in this section for the calculated Q-values in Table 3.7. In order to assess the supports, the support chart from the handbook “Using the Q-system” NGI (2015) is referred. The support chart is presented in the Figure 3.4. As mentioned in the Section 2.5, the span/ESR or height/ESR ratio shall be evaluated using equation (2.22) beforehand assessing the supports.

The ESR-values for different uses are provided in the Q-system handbook NGI (2015):p 33. Rohtang Tunnel is a twin-track railway tunnel. The ESR value of 1 is recommended to use for the railway tunnels according to the Q-system handbook. From Table 1.1, the span of the tunnel (S_t) is 14.5 m, while the height (H_t) is 10.5 m. Therefore, span of the tunnel is used to calculate equivalent dimension, as presented in the equation (3.1).

The equivalent dimension and the Q-values from Table 3.7 are marked on the support chart to determine the support category. In the Figure 3.4, the horizontal blue line represents the equivalent dimension, whereas the vertical green, yellow and pink shaded areas represent the Q-values for exceptionally poor, extremely poor and very poor quality of rock mass respectively.

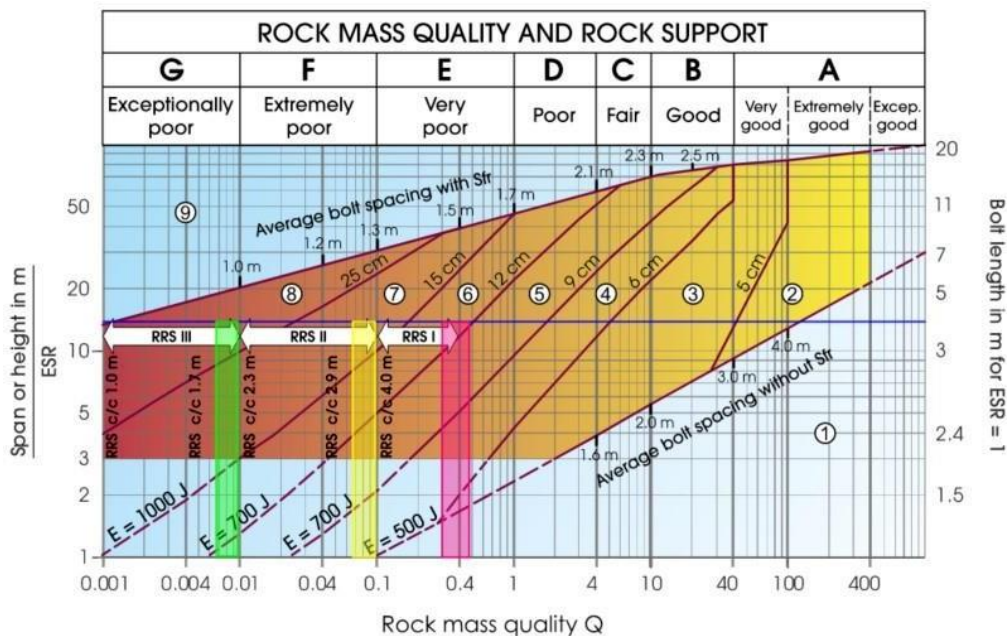


Figure 3.4: Support chart from Q-system handbook NGI (2015):p 34, horizontal blue line represents equivalent dimension of the tunnel and vertical green, yellow and pink boxes represent Q-values for exceptionally poor, extremely poor and very poor rock masses respectively, presented in Table 3.7

¹ The rock mass qualities (E, F and G) are as per support chart (Figure 7) in handbook “Using the Qsystem” NGI (2015):p 34. The support chart is presented in Figure 3.4

From Figure 3.4, support category 8 is recommended for exceptionally poor-quality rock mass. From Table 3.7, the Q-values for exceptionally poor-quality rock mass are 0.008 to 0.01. Considering worst-case scenario, only lower bound Q-value i.e., 0.008 is used. The rock support recommendation for support category 8 includes cast concrete lining (CCA) or more than 25 cm thick steel fibre reinforced shotcrete layer, rock bolts spaced at 1 to 1.2 m and reinforced ribs of sprayed concrete (RRS III) spaced at 1.7 to 2.3 m. The support recommendation from Figure 3.4 are summarized in the Table 3.8.

Table 3.8: Rock support recommendations from Q-system’s support chart for exceptionally poor quality rock mass

Rock mass quality	Q-value	Support category	Rock supports
Exceptionally poor	0.008	8	Cast concrete lining (CCA) or > 25 cm thick steel fibre reinforced sprayed concrete (SFRC) of energy absorption class E1000 Rock bolts spaced at 1.0 - 1.2 m Reinforced ribs of sprayed concrete (RRS III) spaced at 1.7 - 2.3 m c/c

Similarly, from Figure 3.4, support category 7 is recommended for extremely poor quality rock mass. From Table 3.7, the Q-values for extremely poor quality rock mass are 0.06 to 0.1. Considering worst-case scenario, only lower bound Q-value i.e. 0.06 is used. The rock support recommendation for support category 7 includes more than 15 cm thick steel fibre reinforced shotcrete (SFRC) layer, rock bolts spaced at 1.2 to 1.3 m and reinforced ribs of sprayed concrete (RRS II) spaced at 2.9 to 4.0 m. The support recommendation from Figure 3.4 are summarised in the Table 3.9.

Table 3.9: Rock support recommendations from Q-system’s support chart for extremely poor quality rock mass

Rock mass quality	Q-value	Support category	Rock supports
Extremely poor	0.06	7	> 15 cm thick steel fibre reinforced sprayed concrete (SFRC) of energy absorption class E1000 Rock bolts spaced at 1.2 - 1.3 m Reinforced ribs of sprayed concrete (RRS II) spaced at 2.9 - 4.0 m c/c

Lastly, from Figure 3.4, support category 6 is recommended for very poor quality rock mass. From Table 3.7, the Q-values for very poor quality rock mass are 0.3 to 0.5. Considering worst-case scenario, only lower bound Q-value i.e. 0.3 is used.

Table 3.10: Rock support recommendations from Q-system’s support chart for very poor quality rock mass

Rock mass quality	Q-value	Support category	Rock supports
Very poor	0.3	6	12 - 15 cm thick steel fibre reinforced sprayed concrete (SFRC) of energy absorption class E700 Rock bolts spaced at 1.7 - 2.1 m Reinforced ribs of sprayed concrete (RRS I) spaced at 4.0 m c/c

The rock support recommendation for support category 6 includes 12 - 15 cm thick steel fibre reinforced shotcrete (SFRC) layer, rock bolts spaced at 1.7 to 2.1 m and reinforced ribs of sprayed concrete (RRS I) spaced at 4.0 m. The support recommendation from Figure 3.4 are summarized in the Table 3.10.

Chapter 4

NUMERICAL ANALYSIS

The rock supports estimated in Tables 3.8 to 3.10 are applied in the rock mechanical models to observe the response of rock mass and supports. There are two types of rock mechanical model which can be prepared to observe the response - a 2D plane strain model or a 3D model. In 2D plane strain model, the out of plane strains and displacements are assumed to be zero. Therefore, it is acknowledged that a 3D model would be far better for analyzing a tunnel section compared with a 2D model. However, it should be recognized that the 3D modelling is a very time-consuming task and shall be used when a significant improvement in results is expected. Thus, an easier and less time consuming approach is adopted to analyze out-of-plane behavior of sprayed concrete lining (SCL - RRS and SFRC). A 2D rock mechanical model is prepared and the response of SCL is calibrated in 3D full-scale structural model. In this way, the supports are also analyzed for out-of-plane stresses without creating a heavy 3D rock mechanical model. Furthermore, the structural model is better to present distribution of stresses in the SCL.

The finite element software, **PLAXIS 2D**, developed by Bentley Inc. is used for the rock mechanical models and **STAAD PRO V8i**, developed by Bentley Inc. is used for structural models. The input parameters for the 2D rock mechanical models are presented in Section 4.1 and input parameters for structural models are presented in the Section 4.2. Subsequently, the outputs from both 2D and 3D model are shown in Section 4.3. Lastly, the structural verification of RRS are provided in Section 4.4.

4.1 Rock mechanical models

The post-peak behavior of material and modelling approach is adopted based on rock mass qualities and Q-values prior to modelling. The post-peak behavior of different rock masses, suggested by **Hoek and Brown (1997)** is presented in Figure 2.1. The rock mass qualities assessed in Table 3.7 show that the assessed rock masses are very poor in general and should exhibit elastic-perfectly plastic post-peak behavior.

From Figure 2.5, one of the modelling approach from continuum and discontinuum can be adopted based on the calculated Q-value as proposed by **Barton (1998)**. The Figure 2.5 suggests that for a Q-value approximately between 0.1 to 100, the continuum modelling approach is more appropriate than the discontinuum modelling. From Tables 3.8 to 3.10, exceptionally poor and extremely poor-quality rock mass have Q-values 0.08 and 0.06, therefore continuum model is considered. Whereas, for very poor-quality rock mass, q-value is 0.3, hence a continuum and discontinuum both models are prepared. Thereafter, the outputs of continuum and discontinuum models are compared and the model with worse rock mass response is chosen for further analysis. The adopted post-peak behaviour, modelling approach and Q-values are summarised in the Table 4.1.

Table 4.1: Adopted modelling approach and post-peak material behaviour for rock mechanical models

Parameters	Rock mass quality		
	Exceptionally poor	Extremely poor	Very poor
Post-peak behavior	Elastic perfectly plastic		
Q-values	0.008	0.06	0.3
Modelling approaches	Continuum	Continuum	Continuum and Discontinuum

4.1.1 Geometry

The geometry of a rock mechanical model includes modelling assumption (2D or 3D), model boundaries, fixities at boundaries, and finite element (FE) mesh. As mentioned earlier in this section, the rock mechanical models are prepared as 2D plane strain model. In a 2D plane strain model, a plane or a vertical section through the tunnel is analyzed. The displacements and strains in third direction (longitudinal direction) are assumed to be zero. Furthermore, the area of interest and model boundaries are defined. The horseshoe shape tunnel section is the area of interest in this case. The model boundaries refer to height and width of rock mass modelled along with area of interest. The model boundaries shall be chosen such that the boundary should not be very close to area of interest. Boundaries too close to area of interest would introduce boundary effects in output, meaning the fixities imposed at boundaries may significantly influence output results. However, the model boundaries should not also be very large, as large boundaries will require longer calculation time. Therefore, a test model is analyzed with different model boundaries to check the effects of fixities on the area of interest. It is concluded to have a model boundary of 100 m (width) x 50 m (height) for all the models.

In order to establish equilibrium and solve the global stiffness equation, the fixities at model boundaries shall be define. The model boundaries can be free, fixed for horizontal or vertical movement or fixed in all direction and rotation. If the boundary is located sufficiently far away from the area of interest, nature of fixities does not cause any significant change in the output. In this report for all the models, the vertical boundaries are fixed for any horizontal movements and free for vertical movements. The top boundary represents ground level as presented in Figure 1.2 therefore is free for movement in any direction. The bottom boundary is fixed for movement in both horizontal and vertical direction.

In a finite element model (FEM), the geometry is divided in to smaller element to create the finite element (FE) mesh. These elements are connected to each other at their nodes. The nodes are discrete points where primary unknowns such as displacements are calculated. The nodal displacements are then interpolation to obtain the secondary unknowns. The sizes of the elements define precision of the results. The smaller elements will provide more precise results as compared to the large elements. However, a finer mesh (having small elements) will increase the calculation time. Therefore, the element size should be moderate to avoid unnecessary calculation time and provide sufficiently precise result. As per [PLAXIS 2D](#) user manual either 3, 6-noded triangular or 4, 8-noded quadrilateral elements can be chosen. In this report, 6-noded triangular elements are used in all the models.

A typical geometry including model boundaries, fixities at boundaries, and mesh is presented in the following Figure 4.1. It applies to all the rock mechanical model in this report.

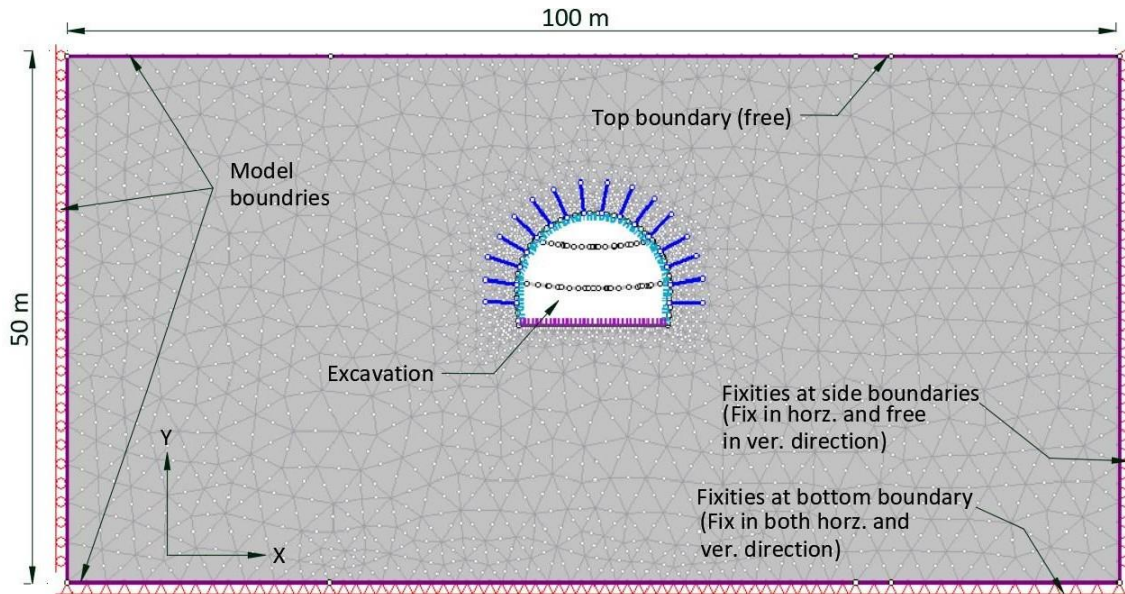


Figure 4.1: Modal boundaries, fixities at boundaries and finite element mesh for the rock mechanical models

4.1.2 Initial element loading

The initial element loading defines the stress condition in the rock mass before excavation in the finite element model (FEM). As per PLAXIS 2D (2019), a finite element (FE) can have two initial loadings, body force and field stress. The body force is the self-weight of the material, whereas the field stress is defined as the locked stress in the element due to confinement. The field stress can be better understood by thinking of an elastic material that is compressed in all directions. If the material is released at one of its edges, it will expand in that direction. In the same way, the rock masses have some initial stress due to confinement and as a result of excavation it will try to expand.

The body force and field stress balance each other in a rock mass and therefore cause no initial displacement in the model. The PLAXIS 2D software allows to choose an option from field stress only, field stress and body force, body force only and none as an initial element loading..

In the PLAXIS 2D software, the body force is calculated using the unit weight of material and field stress can be calculated in two ways. First one is to input directly the field stresses in form of σ_1 , σ_3 and σ_z . Where σ_1 is major in-plane principle field stress, σ_3 is minor in-plane principle field stress and σ_z is out-of-plane field stress. The angle between the direction of σ_1 and positive horizontal axis (x-axis) shall also be input along with field stresses. This way of defining field stresses is called 'constant field stresses', where the stress does not vary with the depth. Another way of defining field stresses is the 'gravity field stresses', where the stresses are calculated based on provided stress ratio (horizontal stress/vertical stress) and surface elevation. The gravity field stresses varies along with the depth and typically used for surface or near surface excavation.

The Rohtang Tunnel is around 15 m below ground surface from Table 1.1, therefore is considered as a shallow excavation. Thus, gravity field stresses are chosen to define field stresses. The surface elevation is defined as the ground level and the stress ratio is assumed as 0.5. The initial element loading is defined as 'field stress and body force' in all rock mechanical models.

4.1.3 Strength and deformation properties of rock masses

The strength and deformation properties of the material (rock mass) shall be calculated to input in PLAXIS 2D software for the analysis. The input parameters depends upon which failure criterion is chosen in the

software. Any of the available failure criterion i.e. MohrCoulomb (MC), Hoek-Brown (HB) or Drucker-prager (DP) etc. can be chosen in PLAXIS 2D software for the analysis.

In a study by Saiang and Marshall (2013), it is explained that the response of rock mass is different when results from HB and MC failure criteria are compared. The authors concluded that use of HB failure criterion results into an overestimation of displacements and strains, whereas use of MB failure criterion shows concentrations of displacements and strains as they expected. In another study by Barla and Barla (2000), the HB failure criterion is used in continuum model and MC failure criterion in discontinuum model. However, Barla and Barla (2000) do not provide any justification for the choice of failure criterion for continuum and discontinuum model. Azami et al. (2013) developed a constitutive model for jointed rock and used HB failure criterion in their discontinuum model. In the light of studied by Saiang and Marshall (2013); Barla and Barla (2000); Azami et al. (2013), anticipating to obtain optimum output, the MC failure criterion is adopted for both continuum and discontinuum models in this report.

The MC parameters can be easily obtained from laboratory tests for the given rock. For this study, no field or laboratory test data is available, therefore MC parameters could not be obtained directly from the tests. Hence, the geological strength index (GSI) is estimated and used to calculate HB-parameters. Thereafter, the MC parameters are obtained from HB parameters.

As mentioned in Section 3.5, considering worst case scenario, only lower bound Q-value is used to estimate the rock support. Similarly, strength and deformation properties of rock masses are also calculated corresponding to lower bound Q-values as presented in Table 3.7. However, the whole range of properties corresponding to lower and upper bound Q-values is presented in Appendix B for reference.

4.1.3.1 Geological strength index (GSI)

As explained in Section 2.3.3(iv), the GSI can be estimated from the GSI chart if the structure of the rock mass (block sizes) and surface quality of discontinuities are known. Moreover, GSI-values can also be calculated by empirical equations provided in Hoek et al. (2013). The GSI is calculated by both methods and compared further in the report to obtain the most appropriate values.

GSI from chart

The two main input for GSI i.e. block size and surface quality are in line with the first two quotients of the Q-system. As explained earlier in the Section 2.5, the equation (2.21) to calculate Q-values, consists of three quotients. The first quotient RQD/J_n of the equation is a rough estimate of block size of the rock mass. That means lower value of RQD/J_n represents smaller block sizes in the rock mass. The second quotient J_r/J_a of the equation represents the frictional characteristics of the joints or joint infills based on their roughness and alteration. A lower value of the second quotient represents the smoother surface quality of discontinuity.

Therefore, the RQD and J_n values estimated in Section 3.4 are used to calculate the block sizes i.e. quotient RQD/J_n . Subsequently, the structure of rock mass is judged based on the block sizes using the GSI-chart presented in Figure 4.2. The estimated structure of the rock mass is summarised in the Table 4.2.

Table 4.2: Structure of the rock mass based on RQD and J_n for GSI estimation

Parameters	Rock mass quality		
	Exceptionally poor	Extremely poor	Very poor
RQD	20	30	40
J_n	15	12	9
RQD/ J_n	1.3	2.5	4.4
Structure of the rock mass as per GSI chart	DISINTEGRATED -Poorly interlocked, heavily broken rock mass with mixture of angular and rounded rock pieces	BLOCKY/DISTURBED/SEAMY - Folded with angular blocks formed by many intersecting discontinuity sets. Persistence of bedding planes or schistosity	BLOCKY - Well interlocked undisturbed rock mass consisting of cubical blocks formed by three intersecting discontinuity sets

Similarly, the values of J_r and J_a estimated in Section 3.4 are used to calculate the surface quality of the discontinuities i.e., quotient J_r/J_a . Subsequently, the surface quality of discontinuities in the rock mass is judged from the Figure 4.2 and presented in Table 4.3.

Table 4.3: Structure of the rock mass based on J_r and J_a for GSI estimation

Parameters	Rock mass quality		
	Exceptionally poor	Extremely poor	Very poor
J_r	1	1.5	3
J_a	8	4	3
J_r/J_a	0.1	0.4	1.0
Structure of the rock mass as per GSI chart	POOR Slickensided or highly weathered surfaces or compact coatings with fillings of angular fragments	- FAIR - Smooth and moderately weathered and altered surfaces.	FAIR - Smooth and moderately weathered and altered surfaces.

After combining the results from both Table 4.2 and Table 4.3, the GSI-values of the rock masses are estimated and presented in the Table 4.4 and Figure 4.2. The estimated GSI values are highlighted in the GSI chart and presented in the Figure 4.2.

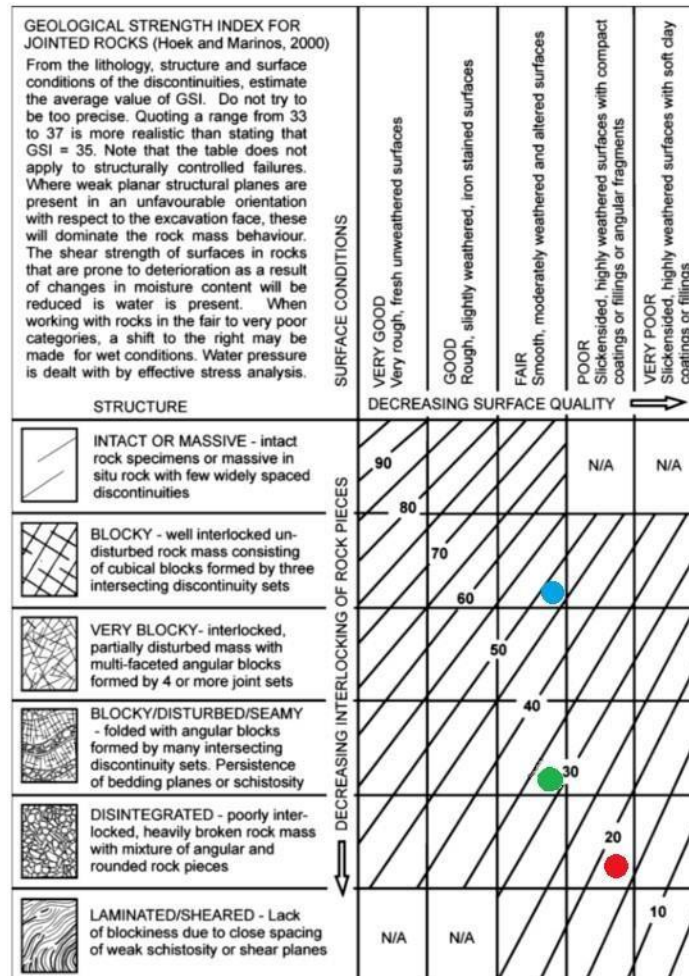


Figure 4.2: Estimated GSI values presented in GSI chart (Marinos et al. (2005)) for exceptionally poor (red), extremely poor (green) and Very poor (blue) rock masses

GSI from empirical equations

In an article by Hoek et al. (2013), the quantification of GSI chart is proposed based on two rock parameters - joint condition and RQD. According to authors, the GSI can be calculated from the equation (4.1). Where, $J_{Cond_{89}}$ is a rating for rock joints introduced by Bieniawski (1989).

$$GSI = 1.5 \cdot J_{Cond_{89}} + RQD/2 \quad (4.1)$$

The authors compared the rating $J_{Cond_{89}}$ with Q-system's rating J_r and J_a and establish a relationship as presented in equation (4.2).

$$J_{Cond_{89}} = 35 \frac{J_r}{1 + J_a} \quad (4.2)$$

Combining the equation (4.1) and (4.2) gives the equation (4.3) to calculate GSI directly from the Q-parameters, J_r and J_a and RQD.

$$GSI = \frac{52 \cdot Jr/Ja}{(1 + Jr/Ja)} + RQD/2 \quad (4.3)$$

Table 4.4: GSI estimated from GSI chart (Figure 4.2) and equation (4.3)

Parameters	Rock mass quality		
	Exceptionally poor	Extremely poor	Very poor
GSI (from chart)	15	30	45
GSI (from equations)	16	29	46

It is evident from Table 4.4, the GSI values estimated from both methods are very similar. However, the values from empirical equations are directly related to Q-system therefore, used to calculate HB-parameters further in this report. **4.1.3.2 Disturbance factor**




Appearance of rock mass	Description of rock mass	Suggested value of <i>D</i>
	Excellent quality controlled blasting or excavation by Tunnel Boring Machine results in minimal disturbance to the confined rock mass surrounding a tunnel.	<i>D</i> = 0
	Mechanical or hand excavation in poor quality rock masses (no blasting) results in minimal disturbance to the surrounding rock mass. Where squeezing problems result in significant floor heave, disturbance can be severe unless a temporary invert, as shown in the photograph, is placed.	<i>D</i> = 0 <i>D</i> = 0.5 No invert
	Very poor quality blasting in a hard rock tunnel results in severe local damage, extending 2 or 3 m, in the surrounding rock mass.	<i>D</i> = 0.8

Figure 4.3: Estimated disturbance factors according to quality of blasting (Hoek et al. (2002))

The disturbance factor (*D*) is discussed in Section 2.2.2. The table for estimating disturbance factor from Hoek et al. (2002) is reproduced in Figure 4.3. As recommended by the authors, the disturbance factor should only be applied only for the 2 to 3 m wide rock mass surrounding the excavation. As mentioned earlier, in this thesis only exceptionally poor, extremely poor and very poor quality of rock mass are analysed. Assuming that the quality controlled blasting will be done at site, the *D* = 0 is considered for all rock masses.

Besides, in further sections it is explained that a forepole umbrella is provided for exceptionally and extremely poor rock masses, which will improve the strength of rock mass surrounding excavation. Therefore, the damage due to blasting would be lesser and justifies the assumption of *D* = 0.

Further, in Section 4.1.3.3 and Section 4.1.3.4 the input parameters for rock mechanical models are calculated for $D = 0$, however, the parameters with $D = 0.8$ also presented in Appendix C to demonstrate the effect of disturbance factor on the strength of rock mass as a reference.

4.1.3.3 Generalized Hoek-Brown parameters

The Hoek-Brown failure criterion is discussed earlier in Section 2.2.2 The Hoek-Brown parameters are calculated in this section. First of all, the material parameters for intact rock m_i , s , a uniaxial compressive strength σ_{ci} of intact rock are estimated. According to Hoek and Brown (2018), the values of material constants s and a for intact rock are fixed to 1 and 0.5 respectively and m_i , σ_{ci} depends upon the type of rock and should be determined from a triaxial test in the laboratory. As mentioned before, the laboratory tests are not available for this work, therefore values of m_i and σ_{ci} are taken from literature.

In Section 3.1, the geological lithologies of the field are presented. Most of the tunnel alignment lies in rhombus-porphyrries. In the book *Practical Rock Engineering* by Hoek (2006), field estimates of m_i for different volcanic rocks are provided as presented in the Figure 4.4.

From Figure 4.4, the m_i for most of the rocks from lava group, including basalt varies from 20 to 30 with an average of 25. Thus, the value of material parameters for intact rock m_i is considered 25 for the further analysis in this report.

Rock type	Class	Group	Texture			
			Coarse	Medium	Fine	Very fine
IGNEOUS	Plutonic	Light	Granite 32 ± 3	Diorite 25 ± 5	Granodiorite (29 ± 3)	
		Dark	Gabbro 27 ± 3	Norite 20 ± 5	Dolerite (16 ± 5)	
	Hypabyssal		Porphyries (20 ± 5)		Diabase (15 ± 5)	Peridotite (25 ± 5)
	Volcanic	Lava	Rhyolite (25 ± 5)		Dacite (25 ± 3)	Obsidian (19 ± 3)
			Andesite 25 ± 5		Basalt (25 ± 5)	
	Pyroclastic	Agglomerate (19 ± 3)	Breccia (19 ± 5)	Tuff (13 ± 5)		

Figure 4.4: Field estimates of Hoek-Brown material parameter for intact rock (m_i) for different igneous rocks (Hoek (2006))

Furthermore, the field estimated of σ_{ci} are provided in the book *Practical Rock Engineering* by Hoek (2006) as presented in the Figure 4.5. From the figure, the σ_{ci} for the igneous rocks, for instance, basalt is very high and varies from 100 MPa to more than 250 MPa.

However, as explained in the Section 3.3, the rock mass considered in this study is highly weathered and heavily jointed. Therefore, a lower value of $\sigma_{ci} = 50$ MPa is adopted.

Grade*	Term	Uniaxial Comp. Strength (MPa)	Point Load Index (MPa)	Field estimate of strength	Examples
R6	Extremely Strong	> 250	>10	Specimen can only be chipped with a geological hammer	Fresh basalt, chert, diabase, gneiss, granite, quartzite
R5	Very strong	100 - 250	4 - 10	Specimen requires many blows of a geological hammer to fracture it	Amphibolite, sandstone, basalt, gabbro, gneiss, granodiorite, limestone, marble, rhyolite, tuff
R4	Strong	50 - 100	2 - 4	Specimen requires more than one blow of a geological hammer to fracture it	Limestone, marble, phyllite, sandstone, schist, shale
R3	Medium strong	25 - 50	1 - 2	Cannot be scraped or peeled with a pocket knife, specimen can be fractured with a single blow from a geological hammer	Claystone, coal, concrete, schist, shale, siltstone
R2	Weak	5 - 25	**	Can be peeled with a pocket knife with difficulty, shallow indentation made by firm blow with point of a geological hammer	Chalk, rocksalt, potash
R1	Very weak	1 - 5	**	Crumbles under firm blows with point of a geological hammer, can be peeled by a pocket knife	Highly weathered or altered rock
R0	Extremely weak	0.25 - 1	**	Indented by thumbnail	Stiff fault gouge

Figure 4.5: Field estimates of uniaxial compressive strength (σ_{ci}) for several rock types (Hoek (2006))

The material parameters for intact rock m_i , s , a and σ_{ci} are summarised in the following Table 4.5.

Table 4.5: Hoek-Brown material parameters for intact rock m_i , s , a and σ_{ci}

Parameters	Rock mass quality Units		
	Exceptionally poor	Extremely poor	Very poor
m_i	[-]	25	
s	[-]	1	
a	[-]	0.5	
σ_{ci}	[Mpa]	50	

Thereafter, the material parameters for the rock mass m_b , s , a are calculated using equations (2.10), (2.11) and (2.12). The GSI-values calculated from equation 4.3 presented in Table 4.4 and disturbance factor $D = 0$ are used to calculate the parameters.

Table 4.6: Material parameters for rock mass m_b , s and a for $D = 0$

Parameters	Rock mass quality		
	Exceptionally poor	Extremely poor	Very poor
m_b	1.235	1.993	3.634
s	9×10^{-5}	3.8×10^{-4}	2.48×10^{-3}
a	0.558	0.524	0.508

As suggested in PLAXIS 2D (2019) and explained in Section 2.1, the dilation parameter, $m_\psi = 0$ in the software, as the rock masses are very poor in general.

4.1.3.4 Mohr-Coulomb parameters

In order to obtain equivalent Mohr-Coulomb (MC) parameters corresponding to HoekBrown (HB) parameters, the method suggested by Hoek et al. (2002) is used. In the method, the linear equation of MC failure criterion is adjusted to the non-linear equation of HB failure criterion for a minor principle stress range $\sigma_t < \sigma_3 < \sigma_{3max}$. Where, σ_t is tensile strength and σ_{3max} is maximum value of minor principle stress (maximum confining stress). Hoek et al. (2002) provided equations (4.4) and (4.5) to calculate equivalent angle of internal friction (ϕ) and cohesion (c) respectively.

$$\phi = \sin^{-1} \left[\frac{6am_b (s + m_b \sigma_{3n})^{a-1}}{2(1+a)(2+a) + 6am_b (s + m_b \sigma_{3n})^{a-1}} \right] \quad (4.4)$$

$$c = \frac{\sigma_{ci} [(1+2a)s + (1-a)m_b \sigma_{3n}] (s + m_b \sigma_{3n})^{a-1}}{(1+a)(2+a) \sqrt{1 + \left(6am_b (s + m_b \sigma_{3n})^{a-1} \right) / ((1+a)(2+a))}} \quad (4.5)$$

Where, σ_{3n} is the ratio of maximum confining stress (σ_{3max}) and uniaxial compressive strength of the intact rock (σ_{ci}) as shown in the equation (4.6).

$$\sigma_{3n} = \frac{\sigma_{3max}}{\sigma_{ci}} \quad (4.6)$$

The maximum confining stress (σ_{3max}) depends on the type of excavation, for instance, tunnels and slopes. In order to determine σ_{3max} for tunnels, the authors distinguished between deep and shallow tunnels. The shallow tunnels are described, where the tunnel depth from ground level is less than the 3 times of tunnel diameters.

For deep tunnels, Hoek et al. (2002) analyzed many closed-form solution from generalized HB and MC criteria to determine the σ_{3max} . They have plotted the results and determined the equation (4.7) to calculate σ_{3max} . For shallow tunnels, the authors suggested to use same equation (4.7) to calculate σ_{3max} with a condition that the surface caving (deformation at ground surface) is avoided.

$$\frac{\sigma_{3max}}{\sigma_{cm}} = 0.47 \left(\frac{\sigma_{cm}}{\gamma h_t} \right)^{-0.94} \quad (4.7)$$

Where, γ is the unit weight of the rock mass, h_t is depth of the tunnel below ground surface and σ_{cm} is rock mass strength.

The unit weight of the rock is taken from the literature. The ranges of unit weights for the rock type considered in this report are presented in Table 4.7 from several literature. From the table, the unit weight for basalt varies from 22 - 30 kN/m³. As mentioned in the Section 3.1, the rocks at field are found to be highly weathered. The unit-weight value of 27 kN/m³ is considered. From Table 1.1, the depth of the tunnel below ground (h_t) is 15 m and σ_{cm} is calculated from HB-parameters using equation (4.8).

Table 4.7: Unit weight (γ) of igneous rocks from literature

Unit weight (γ) [kN/m ³]	Rock types	References
25 - 30	Basalt and Porphyry	Hoek and Bray (1977)
22 - 27	Basalt	Read and Stacey (2010)
27 - 29	Basalt	Vallejo and Ferrer (2011)

$$\sigma_{cm} = \sigma_{ci} \cdot \frac{(m_b + 4s - a(m_b - 8s))(m_b/4 + s)^{a-1}}{2(1+a)(2+a)} \quad (4.8)$$

Table 4.8: Equivalent Mohr-Coulomb parameters calculated from Hoek-Brown parameters for exceptionally poor, extremely poor and very poor rock mass for $D = 0$

Parameters	Units	Rock mass quality		
		Exceptionally poor	Extremely poor	Very poor
σ_{cm}	[MPa]	5.8	8.6	12.5
σ_{3max}	[MPa]	0.223	0.229	0.234
ϕ	[°]	57	62	66
c	[MPa]	0.10	0.15	0.29

From Table 4.8, equivalent friction angles (ϕ) for the rock masses seems very high. Therefore, the field estimated of friction angles of the rock types used in report are searched in the literature. As described in the Section 3.1, the tunnel alignment is passing through igneous rocks. Basalt is taken as a reference for searching in the literature. The friction angles (ϕ) and cohesion (c) from several different literature are summarized in the following Table 4.9.

The literature values presented in the Table 4.9 suggest that the friction angle (ϕ) for the rock types considered in this report shall be between 30 to 45 °. However, the calculated values are much higher than the literature values.

Table 4.9: Friction angles (ϕ) and cohesion (c) for several igneous rock from literature

parameters	Description	47	Reference
------------	-------------	----	-----------

MC			
ϕ [°]	c [MPa]		
35 - 45	30 - 55	For Basalt	Hoek and Bray (1977)
42	0.24	For Basalt rock filled with clayey and basalt content	Hoek (2006)
-	40 - 42	For Basalt without infill material	Read and Stacey (2010)
30	-	For RQD range of 0 to 70 %	Kulhawy and Goodman (2010)
34 - 40	-	For Basalt	Wyllie and Mah (2006)

The possible reason for non-realistic friction angles could be the depth of tunnel from ground level (h_t). The Rohtang Tunnel tunnel is only 15 m below ground level and the maximum diameter of the tunnel (S_t) is 14.5 m from Table 1.1. Therefore, the depth of the tunnel from ground level is less than the 3 times of diameter i.e. 43.5 m and the tunnel is considered as a shallow tunnel. According to Hoek et al. (2002), the equation (4.7) is developed for deep tunnel and it is valid for shallow tunnels if the surface caving does not occur. However, for the tunnel designed in this report, the surfacing caving is occurring, that can be seen in the Section 4.3.1, where the outputs are presented. Thus, the calculated σ_{3max} values as presented in Table 4.8 may not be correct and hence result in unrealistic friction angles.

Saiang and Marshall (2013) explained, using HB failure criterion may provide misleading results over MC failure criterion, when large plastic strains are expected. However, authors realised when small strains are expected HB failure criterion produce sensible results similar to MC failure criterion. They have mentioned that the PLAXIS 2D software is a small strain program, therefore produce meaningful results when HB or Mc parameters are used. In addition, Azami et al. (2013) developed a constitutive model for jointed rock mass for PLAXIS 2D software and used HB failure criterion to demonstrate the model. It is also described in PLAXIS 2D (2019) user manual that any of MC or HB failure criteria can be used to analyse a jointed rock mass (discontinuum model). Therefore, the HB-parameters are used in all rock mechanical models in this report.

4.1.3.5 Rock mass modulus

The rock mass modulus (E_{rm}) is calculated using the equations provide in an article by Hoek and Diederichs (2006). The authors used an unit-less parameter modulus ratio

(MR), introduced by Deere (1968) to calculate E_{rm} . The modulus ratio depends upon the rock type and presented in the Figure 4.6 for several igneous rocks from Hoek (2006). The product of MR and uniaxial compresses strength of intact rock (σ_{ci}) gives the intact rock modulus (E_i) as shown in equation (4.9). Thereafter, E_{rm} is calculated by equation (4.10).

$$E_i = MR \cdot \sigma_{ci} \quad (4.9)$$

$$E_{rm} = E_i \left(0.02 + \frac{1 - D/2}{1 + e^{((60+15D-GSI)/11)}} \right) \quad (4.10)$$

	Class	Group	Texture				
			Coarse	Medium	Fine	Very fine	
IGNEOUS	Plutonic	Light	Granite+	Diorite+			
			300-550	300-350			
				Granodiorite+			
				400-450			
	Dark	Gabbro	Dolerite				
		400-500	300-400				
		Norite					
		350-400					
	Hypabyssal	Porphyries (400)**		Diabase 300-350	Peridotite 250-300		
Volcanic	Lava		Rhyolite 300-500	Dacite 350-450			
			Andesite 300-500	Basalt 250-450			
	Pyroclastic	Agglomerate 400-600	Volcanic breccia (500)**	Tuff 200-400			

Figure 4.6: Modulus ratios (MR) for different igneous rocks (Hoek (2006))

From the Figure 4.6, the modulus ratio for basalt varies from 250 to 450. Therefore, an average value of MR = 350 is used to calculate rock mass modulus (E_{rm}).

Table 4.10: Rock mass moduli (E_{rm}) for exceptionally poor, extremely poor and very poor rock mass for $D = 0$

Parameters	Units	Rock mass quality		
		Exceptionally poor	Extremely poor	Very poor
MR	[-]	350		
σ_{ci}	[MPa]	50		
E_i	[MPa]	17500		
E_{rm}	[MPa]	659	1352	4179

4.1.4 Strength properties of joints in rock mass

From Table 4.1, it is evident that the discontinuum modelling approach is adopted only for very poor quality of rock mass. In discontinuum model, the joints shall be modelled and therefore the joint properties are estimated in this section.

As explained in the Section 2.6, the Barton-Bandis failure criterion introduced by Barton and Bandis (1982) is used for the joints. The shear strength of the joints (τ) can be calculated using equation (2.23) according to the failure criterion, which requires normal stress (σ_n), joint roughness coefficient (JRC), joint compressive strength (JCS) and residual friction angle (ϕ_r) as input. Subsequently, the shear stiffness of the joints (k_s) can be calculated from equation (2.28).

The JRC is estimated from Figure 2.11b considering the length of joints $L = 1$ m. The $J_r = 3$ rating for very poor quality rock mass from Table 3.7 corresponds to rough, undulating surface condition as shown in Figure 2.7. Thus, the JRC from Figure 2.11b is estimated as 9. From the Table 4.9, the friction angle of Basalt varies between 30 - 45 °. The Table 4.1 shows that the elastic-perfectly plastic material behaviour is assumed for the rock masses, where the peak strength is equal to residual strength, as evident from the Figure 2.1c. Thus, the residual friction angle (ϕ_r) for the very poor quality rock mass is

considered as the lowest value provided in the literature i.e. 30° . In general, the igneous rocks are strong rocks, however, as explained in Section 3.3 rocks in the tunnel alignment are highly weathered. Therefore, considering weathered rock, lower bound JCS value for 'medium-strong rock' i.e. 25 MPa is assumed for the very poor rock mass, as presented in the Table 2.1.

Subsequently, the normal stiffness (k_n) is calculated from equation (2.26). The intact rock modulus (E_i) and rock mass modulus (E_{rm}) for very poor rock mass is used from Table 4.10. The joint spacing (s_j) is assumed to be 1 m. The calculated joint parameters are summarized in the Table 4.11.

Table 4.11: Estimated strength parameters of joints for very poor rock mass

Parameters	Units	Values
Rock mass quality	[-]	Very poor
L	[m]	1
s	[m]	1
J_r	[-]	3
JRC	[-]	9
JCS	[MPa]	25
ϕ_r	[$^\circ$]	30
E_i	[MPa]	17500
E_{rm}	[MPa]	4179
k_s	[MPa]	102
k_n	[MPa]	5490

4.1.5 Rock Supports

The rock supports include SFRC layer, rock bolts, reinforced ribs of sprayed concrete (RRS) and forepoles according to Q-system handbook NGI (2015). From Tables 3.8 to 3.10, all three rock masses i.e. exceptionally poor, extremely poor and very poor require SFRC layer, rock bolts and RRS. Moreover, from NGI (2015):p 38, for the rock masses with Q-values below 0.1 (or 0.6, depends upon span of underground opening) generally require forepoling aspre-excavation support. The supports applied in the rock mechanical models are discussed further in this chapter.

4.1.5.1 SFRC

The steel fibre reinforced concrete (SFRC) is used for the analysis. The grade of concrete is assumed as C30/37 according to Eurocode 2 DS/EN-1992-1-1 (2005). The Fib (2013) is referred for the properties of SFRC as explained in Section 2.8. The thicknesses of SFRC layer from Tables 3.8 to 3.10, grade of concrete, properties of concrete and energy absorption classes are summarized in Table 4.12. Where, f_{ck} is characteristic compressive strength of cylindrical specimen, f_{ctm} is mean tensile strength and E_c is Young's modulus of concrete grade C30/37 according to Eurocode 2 DS/EN-1992-1-1 (2005).

Table 4.12: Thickness and properties of concrete used for the analysis

Parameters	Units	Rock mass quality		
		Exceptionally poor	Extremely poor	Very poor
Thickness	[mm]	300	200	150
Energy absorption class	[-]	E1000	E1000	E700
Concrete grade	[-]		C30/37	

f_{ck}	[MPa]	30
f_{ctm}	[MPa]	2.9
E_c	[MPa]	33000

4.1.5.2 Rock bolts

In PLAXIS 2D software a rock bolt can be defined as an end anchored or fully bonded bolt. The end anchored bolts behave as a single element and interact with the finite element mesh only through the endpoints, whereas the fully bonded rock bolts are divided into smaller bolt elements wherever they cross the finiteelement mesh. The bolt elements in fully bonded bolt acts independently, that means one element do not directly affect the neighboring bolt element, however they may influence the neighboring bolts through their effect on the rock mass.

Moreover, due to the way of interaction with finite element mesh, end anchored bolts shows constant tensile force throughout the length of the bolt. However, in a fully bonded bolt, the tensile force may vary along the length of the bolt.

The end anchored bolts are used in all the rock mechanical models in this report. The axial stiffness (K_b) of an end anchored bolt can be expressed in terms of bolt modulus (E_b), its cross-sectional area (A_b) and bolt length (L_b) as presented in equation (4.11).

$$K_b = \frac{E_b A_b}{L_b} \quad (4.11)$$

The bolt parameters used in the rock mechanical models are summarized in the Table 4.13. The in-planespacing of bolts are taken from Tables 3.8 to 3.9 and out-of-plane spacing considered same as in-plane.

Table 4.13: Properties of rock-bolts defined in rock mechanical models

Parameters	Units	Rock mass quality		
		Exceptionally poor	Extremely poor	Very poor
Diameter	[mm]		20	
In-plane spacing	[m]	1	1.2	1.7
Out-of-plane spacing	[m]	1	1.2	1.7
E_b	[MPa]		200000	
L_b	[m]		3	
A_b	[mm ²]		314	
Tensile capacity	[MN]		0.1	

Subsequently, the equivalent strength of 'reinforced rock' is calculated from the method provided by Hoek (2004). The calculated cross-section area and equivalent force for each element in 'reinforced rock' i.e. rock mass, fore pole and grout are summarized in the Table 4.16.

Table 4.16: Material quantities for calculating equivalent strength of 'reinforced rock' for exceptionally poor rock mass

Component	Cross-sectional area [m ²]	Strength [MPa]	Equivalent force [MPa]
Rock mass	0.6	5.8^2	3.46

Forepoles	0.015	250	3.67
Grout	0.04	40	1.77
Sum	0.66		8.89

From Table 4.16, the equivalent strength of 'reinforced rock' for exceptionally poor rock mass is obtained as:

$$\text{Equivalent strength} = \frac{8.89}{0.66} \Rightarrow 13.5 \text{ MPa} \quad (4.12)$$

The equivalent rock mass properties corresponding to rock mass strength of 13.5 MPa are estimated from the Hoek-Brown failure criterion [Hoek et al. \(2002\)](#) as presented in the Table 4.17.

Table 4.17: Equivalent rock mass properties for 'reinforced rock' for exceptionally poor rock mass

Rock parameters	Units	Value
GSI	[-]	16
m_i	[-]	25
σ_{ci}	[MPa]	115
σ_{cm}	[MPa]	13.5
E_{rm}	[MPa]	1541

Extremely poor quality rock mass

Similar to exceptionally poor rock mass, the equivalent HB-parameters for forepole umbrella are obtained for extremely poor rock mass. The design parameters of forepole umbrella are summarised in the Table 4.18. The strength of forepole elements and grout are considered as 200 MPa and 30 MPa respectively for the calculation.

Afterwards, the equivalent strength of 'reinforced rock' is calculated from the method provided by [Hoek \(2004\)](#). The calculated cross-section area and equivalent force for each element in 'reinforced rock' i.e. rock mass, forepole and grout are summarised in the Table 4.19.

Table 4.18: Design parameters of forepole umbrella for extremely poor rock mass

Parameters	Units	values
L_{fp}	[m]	12
ϕ_{fp}	[mm]	80
t_{fp}	[mm]	6
Sc_{fp}	[m]	0.6
L_{fpo}	[m]	6
α_{fp}	[°]	5
α_{fpa}	[°]	160

Table 4.19: Material quantities for calculating equivalent strength of 'reinforced rock' for extremely poor rock mass

Component	Area [m ²]	Strength [MPa]	Equivalent force [MPa]
Rock	0.6	8.6 ³	5.18
Forepoles	0.002	200	0.46
Grout	0.01	30	0.18

Sum	0.61	5.82
-----	------	------

From Table 4.19, the equivalent strength of 'reinforced rock' for extremely poor rock mass is obtained as:

$$\text{Equivalent strength} = \frac{5.82}{0.61} \Rightarrow 9.6 \text{ MPa} \quad (4.13)$$

The equivalent rock mass properties corresponding to rock mass strength of 9.6 MPa are estimated from the Hoek-Brown failure criterion [Hoek et al. \(2002\)](#) and presented in the Table 4.20.

Table 4.20: Equivalent rock mass properties of 'reinforced rock' for extremely poor rock mass

Rock parameters	Unit	Value
GSI	[-]	29
m_i	[-]	25
σ_{ci}	[MPa]	56
σ_{cm}	[MPa]	9.6
E_{rm}	[MPa]	1514

4.1.5.4 Reinforced ribs of sprayed concrete (RRS)

From Tables 3.8 to 3.10, the RRS are required for all three rock masses. As mentioned in Section 2.5, the required reinforcement and thickness of the RRS depends upon the span of the underground opening. The maximum span of Rohtang Tunnel (S_t) is 14.5 m as per Table 1.1. From Figure 2.9, the reinforcement and thicknesses of RRS are only provided for 5, 10 and 20 m span. In Section 4.1.5.5, it is explained that the equivalent thickness for SFRC layer and RRS is modeled in PLAXIS 2D models. Therefore, the higher reinforcement in RRS will provide a thicker layer of SFRC and subsequently lesser deformation of tunnel roof.

Table 4.21: Properties of reinforced ribs of sprayed concrete (RRS) and required reinforcement for exceptionally poor, extremely poor and very poor rock mass

Parameters	Units	Rock mass quality		
		Exceptionally poor	Extremely poor	Very poor
RRS Type		RRSIII	RRSII	RRSI
Thickness	[mm]	550	450	300
No. of layers		2	2	1
Number of bars:				
First layer		6	6	6
Second layer		4	2	-
Dia. of bar	[mm]	20		

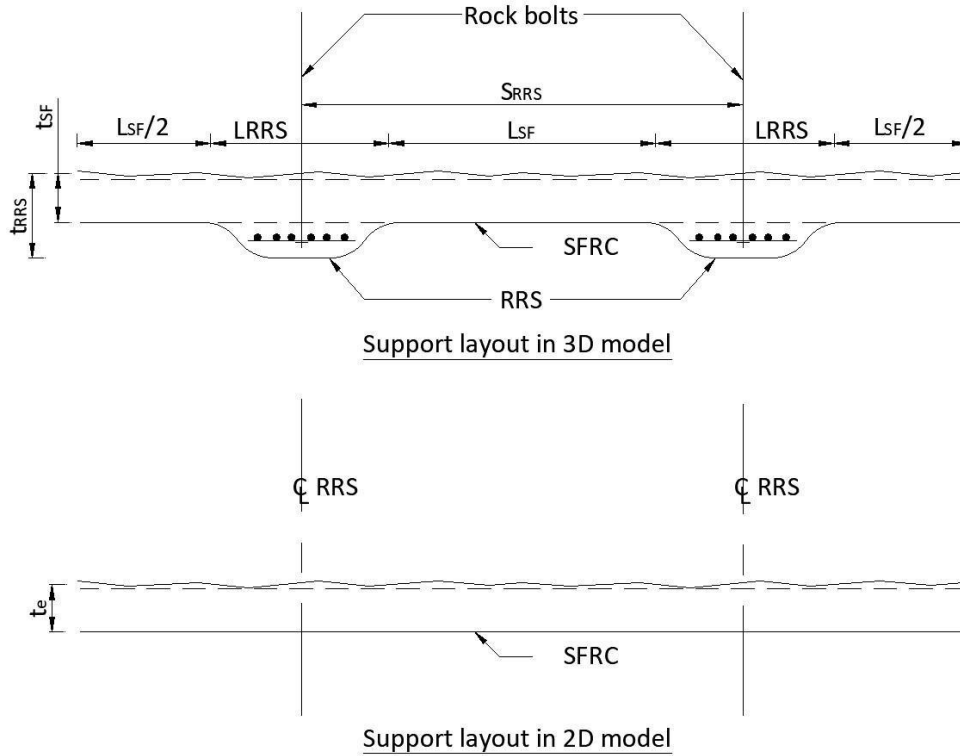
Center to center spacing of RRS [m]	1.7	2.9	4
-------------------------------------	-----	-----	---

As the structural models are prepared based on the response of SFRC in the rock mechanical model. Therefore, the reinforcement in RRS is taken for 10 m span from Figure 2.9 in spite of actual span being 14.5 m, as a conservative approach. Required thicknesses, reinforcement and spacing of RRS from Figures 2.8 and 2.9 are presented in the Table 4.21.

Tables 3.8 to 3.10 provide a range of center to center spacing between RRS. For the design of supports in numerical model, an only lower value is considered and presented in the Table 4.21.

4.1.5.5 Equivalent rock supports in PLAXIS 2D

As mentioned earlier in this chapter, the equivalent thickness of SFRC representing SFRC and RRS is calculated in this section in order to apply in the 2D plane strain rock mechanical model. In order to calculate the equivalent stiffness, the bending stiffness of each element i.e. RRS and SFRC are calculated. The total bending stiffness in 3D model is termed as '3D stiffness' and equivalent stiffness in 2D model termed as '2D stiffness'. It is assumed that the deformation in bending in both the models



will be the same. In Figure 4.8, a longitudinal cross-section of tunnel roof is presented. It shows the support layout in 3D model (consisting of RRS and SFRC) and 2D (equivalent thickness of SFRC).

Figure 4.8: Longitudinal section of tunnel roof showing supports layout in 3D model and equivalent support in 2D model. Where, S_{RRS} is center to center spacing between RRS, L_{RRS} is length of RRS in longitudinal direction, t_{RRS} is thickness of RRS, t_{SF} is thickness of SFRC layer, L_{SF} is length of SFRC layer in longitudinal direction excluding RRS length, t_e is equivalent thickness of SFRC in 2D model (Not to scale)

The 3D stiffness is the sum of bending stiffnesses of SFRC and RRS as shown in the equation (4.14).

$$3D \text{ stiffness} = [(E_c I_{RRS}) L_{RRS} + (E_c I_{SF}) L_{SF}] d_{3d} \quad (4.14)$$

Where, E_c is the elastic modulus of concrete, I_{RRS} is ideal moment of inertia of RRS, I_{SF} is moment of inertia of SFRC layer which is calculated from equation (4.15) and d_{3d} is the deformation in bending in 3D model.

$$I_{SF} = \frac{L_{SF} \cdot t_{SF}^3}{12} \quad (4.15)$$

Similarly, the 2D stiffness can be calculated as shown in the following equation (4.16).

$$\text{2D stiffness} = [(E_c I_e) L_e] d_{2d} \quad (4.16)$$

Where, I_e moment of inertia of equivalent thickness of SFRC and L_e is equivalent length in 2D model in longitudinal direction and d_{2d} deformation in bending in 2D model.

The deformation in bending in 2D and 3D model is assumed to be equal, aiming to obtain equivalent thickness in 2D model. The equivalent length (L_e) in 2D model is considered 1 m. Therefore, from equations (4.14) and (4.16):

$$I_e L_e = I_{RRS} L_{RRS} + I_{SF} L_{SF} \quad (4.17)$$

The moment of inertia of equivalent thickness is calculated from the equation (4.18).

$$I_e = \frac{L_e t_e^3}{12} \quad \xrightarrow{L_e = 1} \quad \frac{t_e^3}{12} \quad (4.18)$$

Where, t_e is the equivalent thickness of the SFRC layer in 2D model. Thus, from equations (4.17) and (4.18),

$$t_e = \sqrt[3]{\frac{12 (I_{RRS} L_{RRS} + I_{SF} L_{SF})}{L_e^2}} \quad (4.19)$$

Similar to a reinforced beam, the ideal center of gravity in the RRS will lie lower than the middle point due to presence of reinforcement. In order to calculate ideal moment of inertia of RRS, several geometric parameters are defined as presented in the following Figure 4.9.

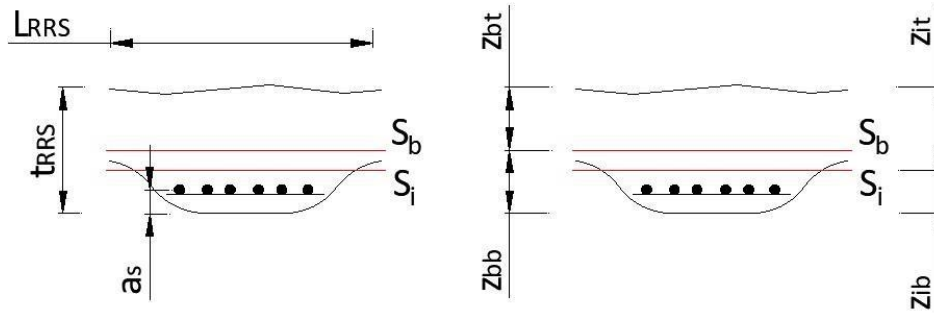


Figure 4.9: Typical sketch of RRS showing following geometric parameters: L_{RRS} is length of RRS, t_{RRS} is thickness of RRS, S_b center of gravity of RRS, S_i ideal center of gravity of the RRS, z_{bt} is distance of center of gravity from top of RRS, z_{bb} is distance of center of gravity from bottom of RRS, z_{it} is distance of ideal center of gravity from top of RRS, z_{ib} is distance of ideal center of gravity from bottom of RRS, a_s is distance of center of gravity of steel from bottom of RRS.

The moment of inertia of RRS (I_b) is calculated from the following equation (4.20).

$$I_b = \frac{L_{RRS} t_{SC}^3}{12} \quad (4.20).$$

The cross-sectional area of RRS (A_b) is calculated using equation (4.21).

$$A_b = L_{RRS} t_{RRS} \quad (4.21)$$

Thereafter, the net area (A_n) can be calculated from equation (4.22).

$$A_n = A_b - A_s \quad (4.22)$$

Where, A_s is total cross-sectional area of reinforcement. Furthermore, the ideal crosssectional area of RRS is calculated from equation (4.23).

$$A_i = A_n + n \cdot A_s = A_b + (n - 1) \cdot A_s \quad (4.23)$$

Where, n is modular ratio, defined as the ration of Young modulus of steel and concrete as shown in equation (4.24).

$$n = \frac{E_s}{E_c} \quad (4.24)$$

Besides, the geometric distances z_{ib} , z_{it} and z_{is} are calculated from equations (4.25), (4.26) and (4.27).

$$z_{ib} = \frac{A_b \cdot z_{bb} + (n - 1) \cdot A_s \cdot a_s}{A_i}$$

$$z_{it} = t_{RRS} - z_{ib} \quad (4.27)$$

$$z_{is} = z_{ib} - a_s$$

Finally, the ideal moment of inertia of RRS (I_{RRS}) is calculated from the equation (4.28) and the equivalent thickness of SFRC to apply in 2D model is calculated from equation (4.19).

$$I_{RRS} = I_b + A_b \cdot (z_{bb} - z_{ib})^2 + (n - 1) \cdot A_s \cdot z_{is}^2 \quad (4.28)$$

The equivalent thicknesses along with all the parameters are summarised in the following Table 4.22.

Table 4.22: Thicknesses of SFRC layer equivalent to SFRC and RRS to use in 2D models for exceptionally poor, extremely poor and very poor rock masses

Parameters	Units	Rock mass quality		
		Exceptionally poor	Extremely poor	Very poor
f_{ck}	[MPa]		30	
f_y	[MPa]		500	
E_c	[MPa]		33000	
E_s	[MPa]		200000	
n	[-]		6.1	
S_{RRS}	[mm]	1700	2900	4000
t_{RRS}	[mm]	550	450	300
L_{RRS}	[mm]	500	500	500
t_{SF}	[mm]	300	200	150
L_{SF}	[mm]	1200	2400	3500
L_e	[mm]	1000	1000	1000
A_b	[mm ²]	275000	225000	150000
A_s	[mm ²]	3142	2513	1885
a_s	[mm]	120	120	110
A_n	[mm ²]	271858	222487	148115
A_i	[mm ²]	290898	237719	159539
z_{bb}	[mm]	275	225	150
z_{ib}	[mm]	267	219	148
z_{it}	[mm]	283	231	152
z_{is}	[mm]	147	99	38
I_{sF}	[mm ⁴]	2.700×10^9	1.600×10^9	9.844×10^8
I_b	[mm ⁴]	6.932×10^9	3.797×10^9	1.125×10^9
I_{RRS}	[mm ⁴]	7.293×10^9	3.930×10^{10}	1.139×10^9
t_e	[mm]	436	411	364

4.1.6 Hydraulic properties

The hydraulic properties of the material need to be input in the PLAXIS 2D software. The hydraulic properties include material behaviour, porosity and static water mode. The material behaviour can be drained or undrained based on the presence of water in the rock mass. The rock masses considered in the study are very poor in general. That means rock mass consists of many joint sets and consists small blocks. It is also evident from RQD and J_n values presented in Table 4.2. Therefore, water can not stay longer in the rock mass and have a high probability of being drained off. Thus, the drained material behaviour is assumed for all the rock masses.

The porosity of a material is the ratio of pore volume and the rock volume. The porosity of igneous rocks is usually low due to their nature of having interlocking crystals. However, the basalt may have a bit higher porosity compared to other volcanic rock, as it is formed when lava is cooled down and consist of many pores due to the formation of bubbles. Nonetheless, the rock masses may have higher porosity due to presence of fracture, joints. It is also called as secondary porosity of rocks. The porosity of a rock can be determined in the laboratory. However, no laboratory test data is available for this study. Thus, keeping in mind the RQD values of the rock masses as discussed in the previous paragraph, a porosity value of 50 % is assumed.

As the material behaviour is assumed to be drained, the static water mode is considered dry in the PLAXIS 2D software.

4.1.7 Sign convention in rock mechanical models

In order to understand the output of rock mechanical models, the sign convention need to defined in advance. The horizontal direction from left to right is defined as the positive x-axis and the vertical

direction from bottom to top is defined as the positive y-axis. Moreover, the signs of axial force and bending moments in supports (rock bolts and lining) and their natures are presented in the Table 4.23.

Table 4.23: Sign convention in PLAXIS 2D software

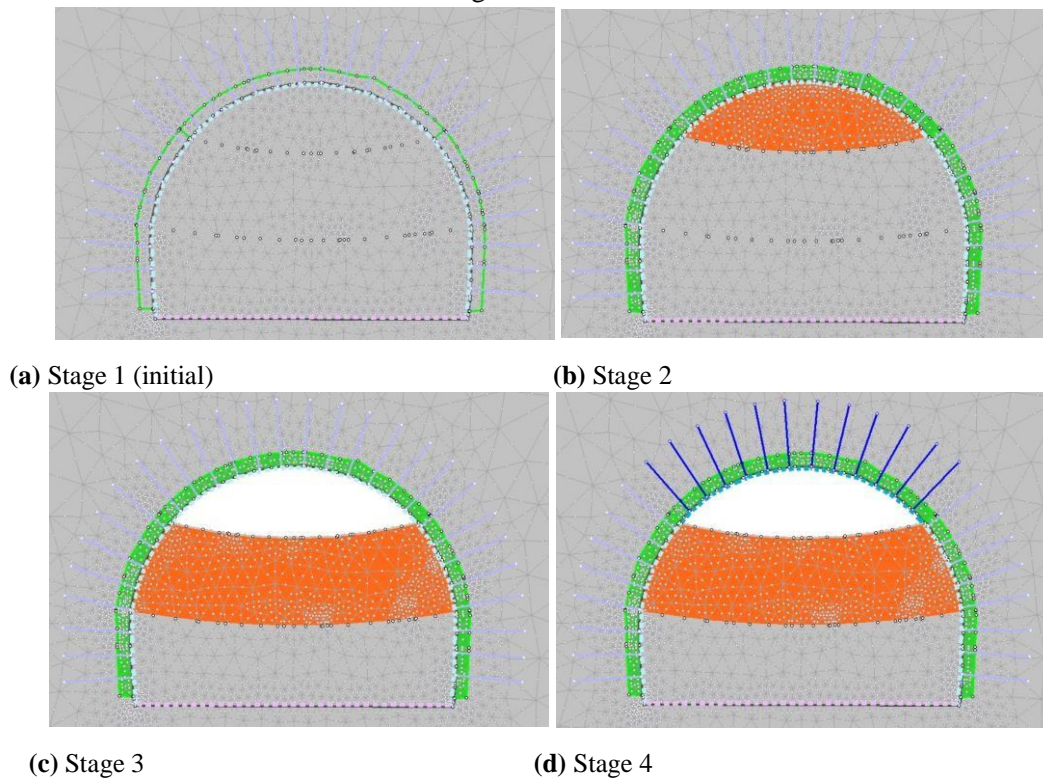
Parameters	Signs	
	Negative	Positive
Stresses	Tensile	Compressive
Bending moment	Hogging	Sagging
Axial force (bolts)	Compression	Tension
Axial force (SCL)	Tension	Compression

4.1.8 Construction stages

In poor rock masses, it is generally difficult to excavate the whole tunnel face in one go due to stability problems. Therefore, partial face excavation method should be adopted as explained in Hoek (2006). In this method, a partial face of tunnel (reduced area of tunnel face) is excavation first. Ensuring the stability of partial face, subsequent faces are excavated. This method is slow and expensive, however it may be necessary to adopt it in poor rock masses.

For all rock mechanical models, this method is adopted by dividing the tunnel face into three partial faces. Additionally, the estimated supports in Section 4.1.5 (forepoles, rock bolts and SCL) are also installed as the excavation proceeds. As a consequence of forepole installation, the rock mass in top heading (excavation stage 1) become softer as defined in Hoek (2006). It is defined in models by reducing the deformation modulus of the rock mass by 50% (shown in orange color in Figure 4.10). Similarly, as the top heading is excavated, the middle heading (excavation stage 2) is softened along with the installation of supports at top heading and similarly for the bench (excavation stage 3). The construction stages are presented in the

Figure 4.10.



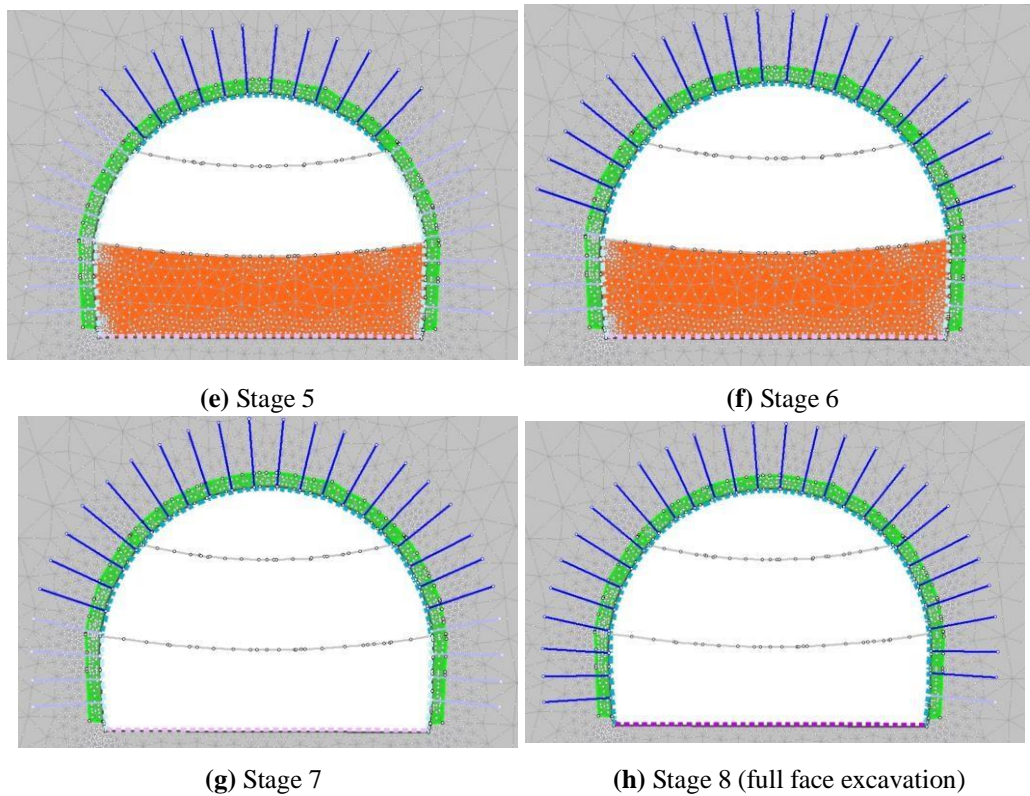
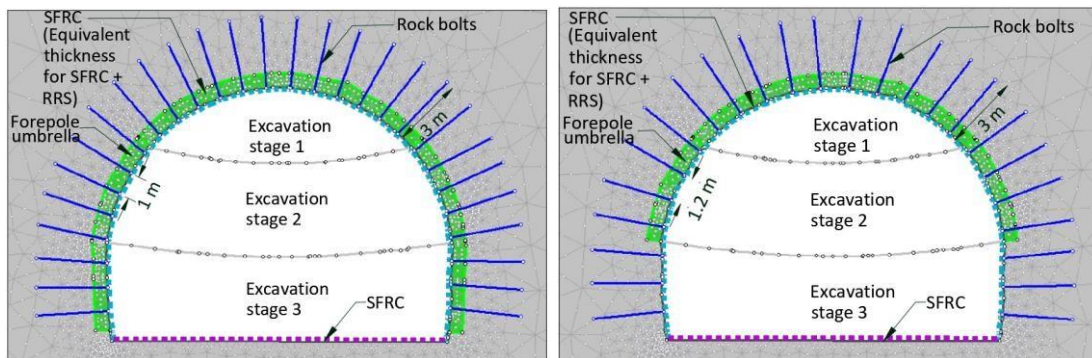


Figure 4.10: Typical construction stages defined in rock mechanical models

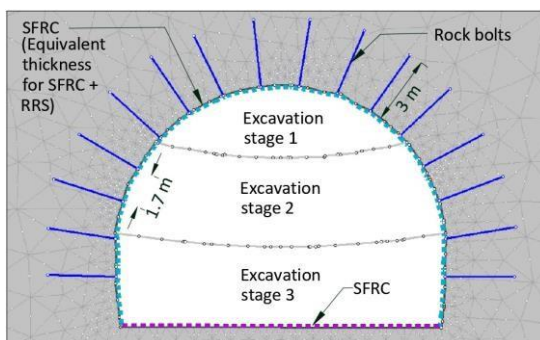
4.1.9 Summary of supports and excavation stages

Lastly, the summary of geometry and installed supports in all four rock mechanical models are presented

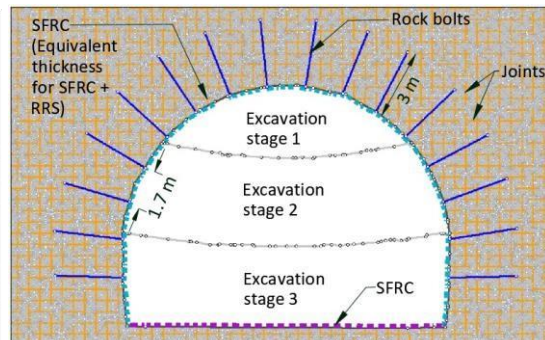


in the Figure 4.11.

(a) Exceptionally poor rock mass (Continuum



(b) Extremely poor rock mass (Continuum model) model)



(c) Very poor rock mass (Continuum model) **(d)** Very poor rock mass (Discontinuum model) **Figure 4.11:** Geometry and supports defined in rock mechanical models

4.2 Structural models

As explained in Chapter 4, the structural models are prepared for exceptionally poor, exceptionally poor and very poor rock masses. In the structural models, the out-of-plane behaviour of shotcrete and RRS is analysed. The geometry, loads and supports applied in structural models are discussed in this section.

4.2.1 Geometry

In a structural model, geometry include structure type, finite element type, section properties (thicknesses) and FE mesh. The Autodesk ROBOT has several predefined structure type such as building design, truss design, shell design, plate design etc. The structure type is the first parameter to choose in the model and shall be carefully chosen, else it may provide false results. The most suitable structure type is shell design to create 3D finite element model, therefore it has been used in the analysis.

Furthermore, the finite element type is defined in the model. Based on different degree of freedom, mainly three finite element types shell, membrane and slab are defined in the software. The finite element type dictates the stress distribution in the finite element, therefore it is an important parameter. A shell element allows transfer of loads in both direction i.e. transverse and longitudinal, therefore chosen for this analysis. The thickness of shell elements (shotcrete or RRS) are defined as presented in the Table 4.22.

In the software, there are several different methods for meshing are provided based on the complexity of the geometry for instance Coon method, Delaunay method etc. The Coon method is recommended for simple geometry. In the method, 4-node quadrilaterals elements of user- defined size can be created. The mesh is generated automatically in the software and the mesh sizes are decided based on the spacing of rock bolts to keep application of springs supports easier. The chosen mesh sizes are presented in the Table 4.24.

Table 4.24: Chosen finite element mesh size in structural models

Parameters	Units	Rock mass quality		
		Exceptionally poor	Extremely poor	Very poor
Mesh size	[m x m]	0.5 x 0.5	0.6 x 0.6	0.85 x 0.85

4.2.2 Material and sectional properties

Furthermore, the material properties are defined to shell elements in the models. Similar to rock mechanical models. The concrete grade of C30/37 according to Eurocode 2 [DS/EN1992-1-1 \(2005\)](#) is used. The material properties are defined as provided in the Table 4.12.

As structural models are 3D models, the actual supports are defined, meaning the original thicknesses RRS and SFRC are modelled as presented in Table 4.12 and Table 4.21.

4.2.3 Calibration

As mentioned earlier in this chapter, a 3D rock mechanical model could be the best choice to analyses a tunnel in rock mass. However, it is very time-consuming process to make a 3D rock mechanical model. Therefore, the 2D rock mechanical models are created and to observe the out-of-plane behavior of rock mass, the 3D structural models are created. The 3D structural models are calibrated to obtain the similar results as rock mechanical models. In this way, the modelling time is significantly reduced. Besides, the 3D structural model is no doubt better in present the

more realistic stress distribution in SCL than rock mechanical models.

Before calibrating the models, it should be acknowledged that the response of SCL will be different in structural models compared to rock mechanical models, due to its 3-dimensional geometry. The rock mechanical models are 2D plane strain models, meaning that the strains in out-of-plane direction are considered zero. Thus, the SCL is free to move in 2 dimension and have no restraint from continues tunnel section. On the other hand, a continues SCL along with RRS are modelled in the structural models and therefore restrained in out-of-plane (longitudinal) direction. Due to different geometrical assumptions, a 2D model will show higher deformation and bending moment in the SCL than a 3D model given that the same load is applied in both models.

The rock mechanical models show the response of SCL in terms of axial force, bending moment, shear force and displacement. Considering worst possible case, the bending moment from the rock mechanical models are calibrated with structural models. In order to do this, a uniformly distributed load (UDL) of arbitrary magnitude and extent is applied in structural model aiming to obtain the similar bending moment as in rock mechanical model. The extent of applied load is presented in Figure 4.12.

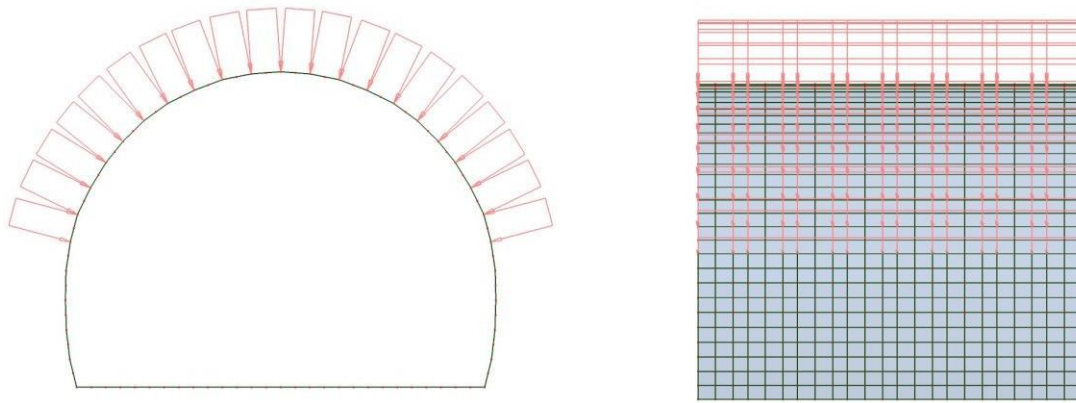


Figure 4.12: Applied load in the structural models - cross-section view (left) and side view (right)

4.2.4 Loads and load combinations

As per previous section, two load cases are defined in structural models, dead load (selfweight) and rock pressure. It should be noted the combination of dead load and rock pressure produces same bending moment in rock mechanical models. Both the loads are permanent in nature, meaning that they will be acting on the structure throughout its service life. As mentioned in the previous section the material type is considered as drained, therefore no water pressure applied on the structure.

Besides, the load combinations are defined as per recommendations provided in Eurocode 0 DS/EN-1990 (2007). The Eurocode 0 recommends to use a partial safety factor $\gamma_G = 1$ for serviceability limit state (SLS) and $\gamma_G = 1.35$ for ultimate or collapse limit state (ULS) for permanent action. In the light of Eurocode 0 recommendations, the load cases are presented in the Table 4.25.

Table 4.25: Load cases used in structural models

No.	Load case	Description
1	DL	Dead load (Self-weight) of the structure $\gamma_G = 1$ (SLS), $\gamma_G = 1.35$ (ULS)

2	RP	Rock pressure $\gamma_G = 1$ (SLS), $\gamma_G = 1.35$ (ULS)
---	----	--

Based on the load cases and partial safety factors presented in the Table 4.25, the load combinations are created to use in the structural model as shown in the Table 4.26.

Table 4.26: Load combinations used in structural models

No.	Load Combination	Description
101	SLS	1.0 x DL + 1.0 x RP
102	ULS	1.35 x DL + 1.35 x RP

4.2.5 Boundary conditions

The boundary conditions must be defined prior to proceeding with analysis in a structural model. The boundary conditions imply that either external force or displacement is known at the boundary. The external force or displacement could be zero or may have some value. For instance, if it is known that some specific point at the boundary has zero displacement, it means the structure is held on a place and no displacement allowed at the point. There are many boundary conditions which can be defined based in the structural model such as - pinned support where the displacement is known and is zero in all three direction x, y and z, whereas the rotation is not known and structure is allowed to rotate according to applied external force. Similarly, fixed support where displacement and rotation are known and kept zero in all direction, spring supports where an external force is known and displacements are not known, can be applied in the model.

The SFRC and RRS interact with surrounding rock mass and installed rock bolts. Consequently, the rock mass experience some external force that governs the displacements in these elements. The external force from surrounding rock mass and rock bolts are called as spring stiffness, which governs the displacement in the structure. The spring stiffness depends on the strength of the material, weaker material will provide more flexible support and stronger material will provide more rigid support. The spring stiffnesses of rock mass and rock bolts are calculated further in this section.

4.2.5.1 Spring stiffnesses due to rock mass

The structural elements will experience the resistance from rock mass if it tends to move towards rock mass, whereas it will not experience any resistance if moving away from the rock mass. Therefore, the springs shall act only in one direction, or in other word springs shall be compression only.

The springs are applied radially spaced at a certain distance therefore termed as radial springs. The spring stiffness (K_i) at a node "i" is calculated using following equation (4.29).

$$K_i = \left(\frac{E_{rm}}{R_i} \right) l_i \quad (4.29)$$

Where, E_{rm} is the rock mass modulus of surrounding rock, R_i is the radius of the tunnel lining (shotcrete or RRS) and l_i is the contributory distance of that particular node "i"

where the spring is acting. The parameters are better explained in the fig. 4.13 from Mayta et al. (2018).

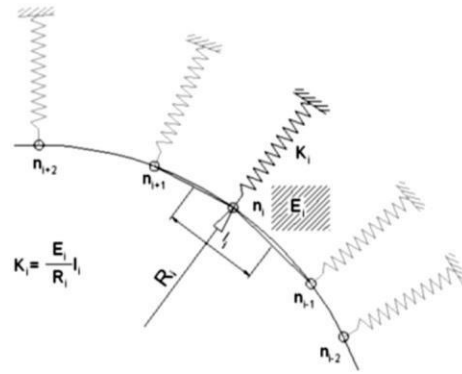


Figure 4.13: Typical spring beam model (Mayta et al. (2018))

Eventually, the spring stiffnesses are calculated from equation (4.29) for all three rock masses and presented in the following Table 4.27.

Table 4.27: Spring stiffnesses for exceptionally poor, extremely poor and very poor rock masses

Parameters	Units	Rock mass quality		
		Exceptionally poor	Extremely poor	Very poor
R_i	[m]	7.25		
l_i	[m]	1		
E_{rm}	[MPa]	659	1352	4179
K_i	[KN/m/m]	90838	186429	576391

It should be noted that the SCL will experience some resistance from rock mass in tangential direction also due to friction. However, for this analysis the tangential spring stiffness are ignored.

4.2.5.2 Rock bolts

Unlike the rock mass, the rock bolts provide resistance to structural elements while moving away from the rock mass and allows movement towards the rock mass. The spring stiffness of rock bolts (K_b) is calculated from equation (4.30).

$$K_b = \frac{E_b A_b}{L_b l_i}$$

Where, E_b is elastic modulus of bolts, A_b is cross-sectional area, L_b is length of the bolt and l_i is the contributory distance of the node "i" as explained in previous section. The calculated bolt stiffnesses are presented in Table 4.28.

Table 4.28: Spring stiffnesses of rock bolts for exceptionally poor, extremely poor and very poor rock mass

Parameters	Units	Rock mass quality		
		Exceptionally poor	Extremely poor	Very poor
L_b	[m]	3		
A_b	[mm ²]	314		
K_b	[kN/m/m]	20944	17453	12320

4.2.6 Sign convention in structural models

The sign convention in structural models is presented in the Figure 4.14. From the figure, the x-axis and y-axis are horizontal and z-axis is vertical. To distinguish the forces in x and y direction, the direction along the y-axis is considered as transverse direction and along the x-axis as longitudinal direction. Therefore, M_{yy} and N_{yy} are transverse bending moment and axial force respectively and M_{xx} and N_{xx} longitudinal bending moment and axial force respectively.

Positive moment in any direction represents hogging and negative represents sagging. Besides, positive axial force represents tension and negative represents compression.

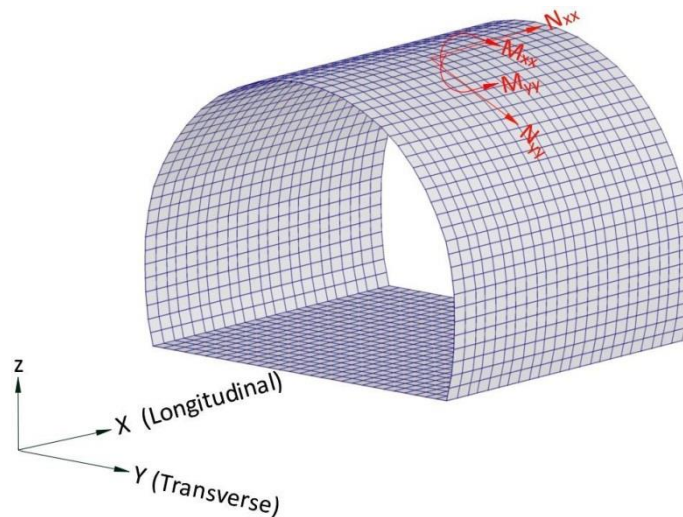


Figure 4.14: Transverse and longitudinal direction in structural models

4.2.6.1 Summary of geometry and supports in structural models

Finally, the summary of geometry and installed supports in all three structural models are presented in Figure 4.15.

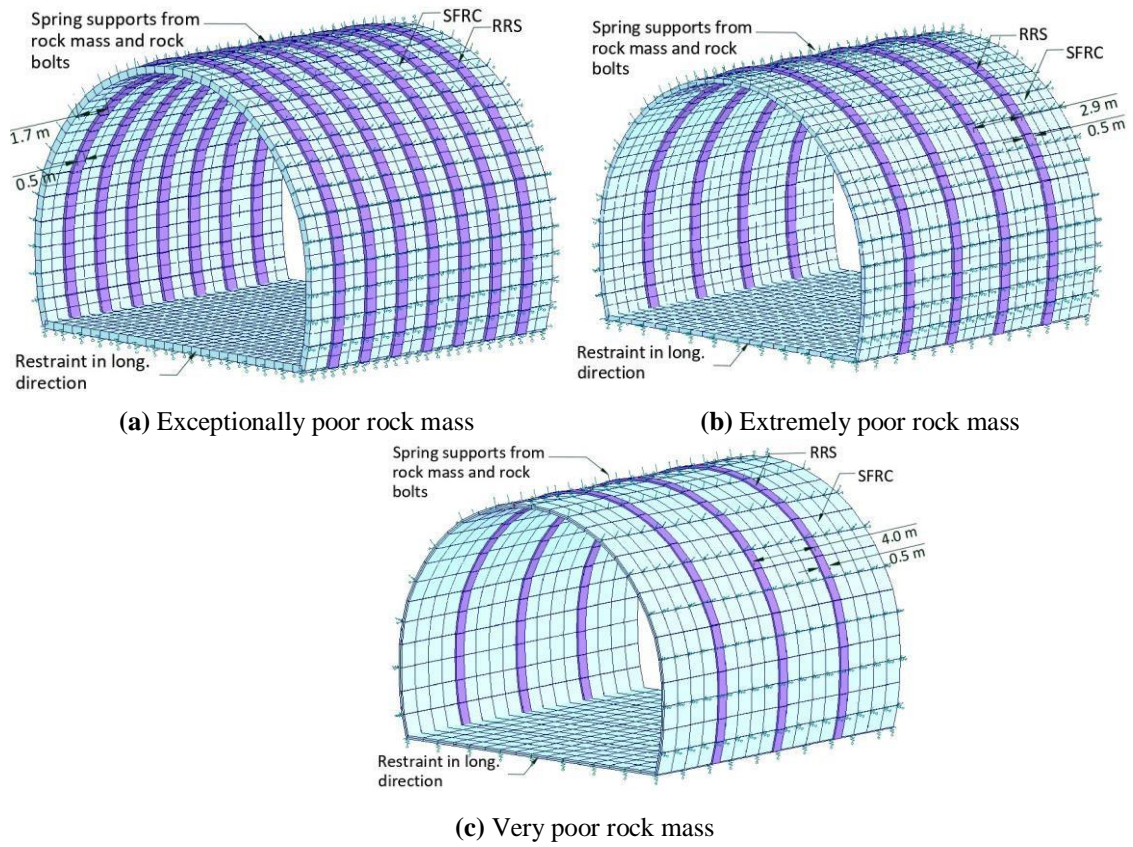


Figure 4.15: Description of geometry and supports elements in structural models

4.3 Output of numerical analysis

Three continuum rock mechanical model for exceptionally poor, extremely poor and very poor rock masses are prepared. One discontinuum model for very poor rock masses are prepared and outputs of all rock mechanical models are presented in Section 4.3.1.

Three structural models, corresponding to three continuum rock mechanical models are prepared and the outputs are presented in Section 4.3.2.

4.3.1 Output of rock mechanical models

The vertical, horizontal displacements, principle stresses, out-of-plane stresses and strength factors from rock mechanical models are presented in this section.

4.3.1.1 Vertical displacement

The vertical displacements in rock masses along with maximum displacement of crown (tunnel roof) and invert (tunnel base) are presented in Figure 4.16 to Figure 4.19.

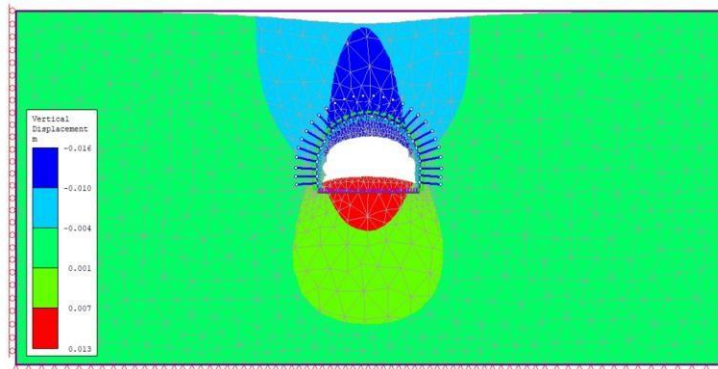


Figure 4.16: Vertical displacements in exceptionally poor rock mass form continuum model (Crown: 16 mm, Invert: 13 mm)

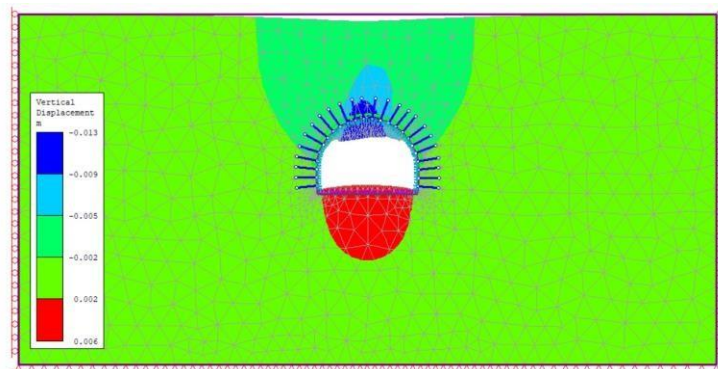


Figure 4.17: Vertical displacements in extremely poor rock mass form continuum model (Crown: 13 mm, Invert: 6 mm)

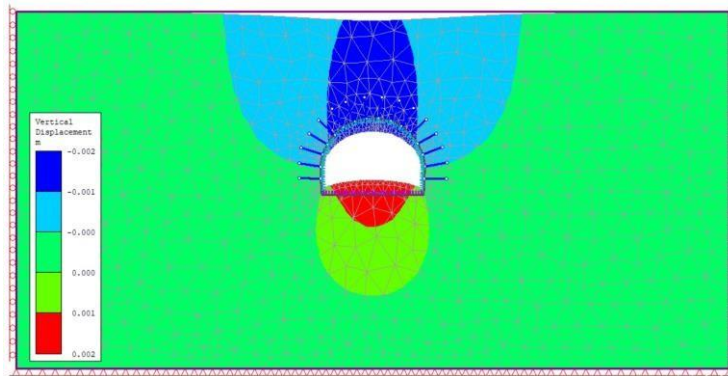


Figure 4.18: Vertical displacements in very poor rock mass form continuum model (Crown: 2 mm, Invert: 2 mm)

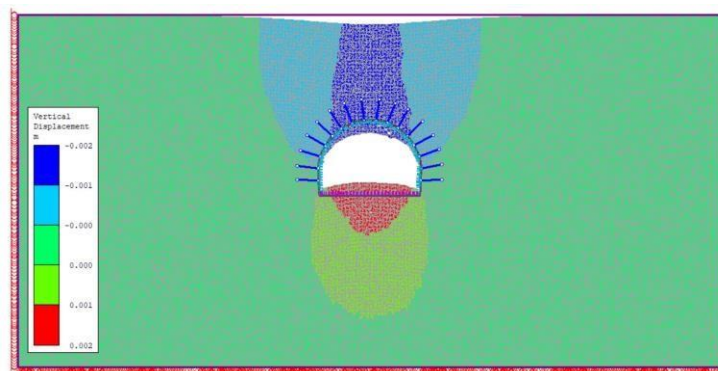


Figure 4.19: Vertical displacements in very poor rock mass form discontinuum model (Crown: 2 mm, Invert: 2 mm)

4.3.1.2 Horizontal displacement

The horizontal displacements in rock masses along with maximum displacement of tunnel side wall is presented in Figure 4.20 to Figure 4.23.

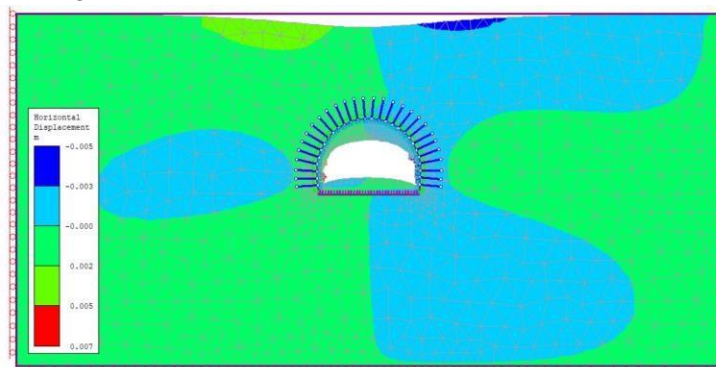


Figure 4.20: Horizontal displacements in exceptionally poor rock mass from continuum model (Max. at side wall: 7 mm)

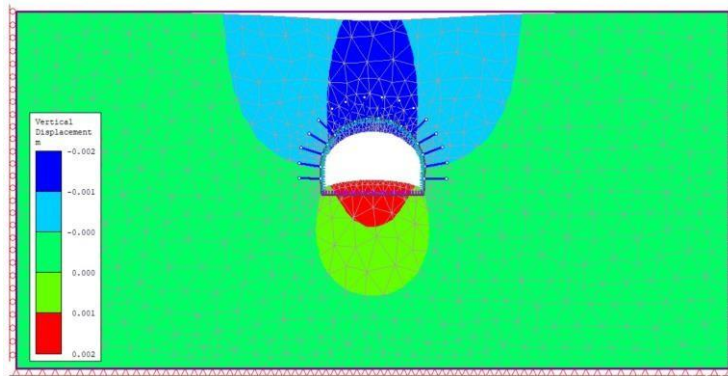


Figure 4.21: Horizontal displacements in extremely poor rock mass from continuum model (Max. at side wall: 2 mm)

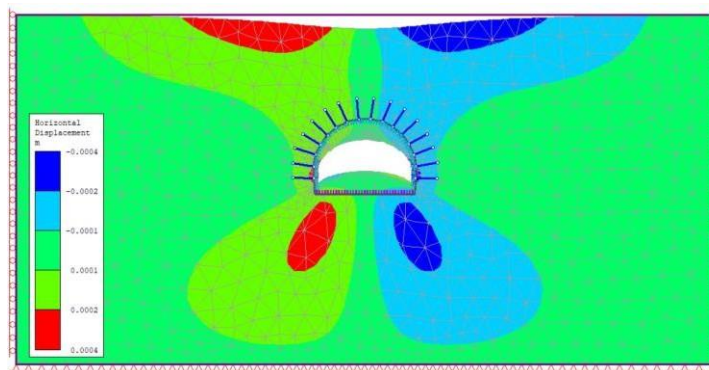


Figure 4.22: Horizontal displacements in very poor rock mass from continuum model (Max. at side wall: 0.4 mm)

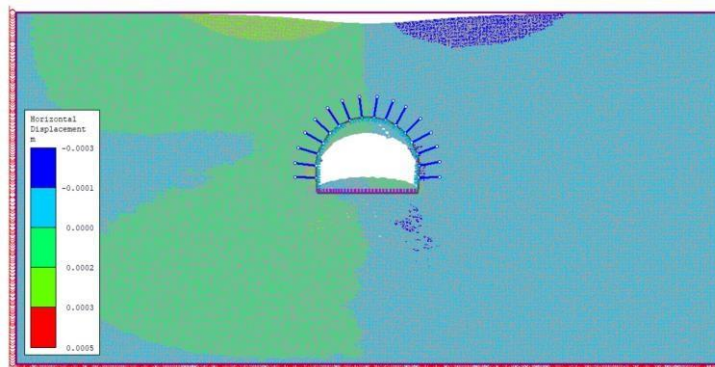


Figure 4.23: Horizontal displacements in very poor rock mass from discontinuum model (Max at side wall: 0.5 mm)

Chapter 5

DISCUSSION

The exercises of optimization of rock supports recommended by Q-system using numerical methods is partially successful. The reinforcement in RRS for extremely poor rock mass can be completely avoided, whereas for exceptionally and very poor rock mass, the reinforcement is needed for short-term verification, as mentioned in Section 4.4.1. The results of the assessment and possible measures to improve the outcome along with current measures are discussed.

From Section 4.3.1.1, it can be seen that the displacement at the crown of the tunnel (tunnel roof) is extending up to ground level. Nevertheless, the magnitude of displacement is less than 2 cm in all rock masses, it is a very difficult problem to deal with during construction of tunnels, especially when tunnel is being built in an urban environment. This problem is very common in shallow tunnels in poor rock masses and could increase the requirement of supports to limit the ground deformation. Moreover, as discussed in Section 4.1.3.4, the displacement at ground surface also affect the calculation of equivalent MC-parameters from HB-parameters, as the equation (4.7) from Hoek et al. (2002) is only valid for the cases when deformation at ground surface is not occurring. However, this problem is encountered by using HB-parameters in all models for the analysis.

In the Section 4.3.1.1, it can also be seen that there is upward displacement at tunnel invert (tunnel base). This phenomenon is called as 'invert heaving'. Usually, invert heaving occurs during construction or after the construction (application of supports). There could be many reasons of invert heaving, such as weak rock, water pressure, large spans or over-stressing around excavation (typically happens in very poor/disintegrated rock mass with large overburden Marinos (2012)). The invert heaving can be avoided or reduced by making some geometrical changes during design phase before excavation starts. For instance, instead of having a flat invert, it can be made curved downwards, thereby reducing the displacement due to heave. Another method for reducing heaving is the partial face excavation. As explained in Section 4.1.8, the tunnel face is already divided into 3 excavation stages for stability reason. Further dividing the existing excavation stages into two part, could reduce invert heaving. In extreme case, where large deformations occur, ground improvement or additional supports such as steel sets, may help to control the invert heaving. However, the displacement due to heaving are not very large in the present study, making a downward curved invert will be sufficient.

As explained in Chapter 4, only for very poor rock mass, continuum and discontinuum both modelling approaches are adopted to compare the results. Barla and Barla (2000) stated that the continuum and discontinuum model for the same rock mass properties may or may not provide similar results, although the rock failing modes such as block falling, joint sliding and joint opening can be visualised in discontinuum model. Consequently, a discontinuum model shows more realistic rock mass behaviour compared to a continuum model. The results in this thesis tend to agree with the findings of Barla and Barla (2000). Both continuum and discontinuum model shows more or less similar displacements, but the discontinuum model shows detached rock block at crown as shown in Figure 4.19. A larger picture of cross-section to closely observe these failure modes is presented in Figure D.1 in Appendix D. The Figures 4.38 and 4.39 show that the yielded elements are farther away from the excavation in continuum model, meaning that the rock mass failure is worse in continuum model. Hence, only continuum model is chosen for analysing supports in this thesis.

From Section 4.1.8, it can be seen that the sprayed concrete lining (SCL) and rock bolts are installed according to construction stages in the rock mechanical models. For instance, the top heading is excavated in stage 3 and SCL and rock bolts are installed in stage 4. Similarly, the last part of tunnel face is excavated in stage 7 and final supports are installed in stage 8. From the output of rock mechanical models, the tunnel wall shows negligible displacement and forces in the supports installed in the last stage (stage 8) as evident in Figures 4.40 to 4.43. According to PLAXIS 2D (2019), after excavating a tunnel, the tunnel wall usually deforms 30 - 45 % of final tunnel wall deformation before the supports can be installed. It means that the supports in PLAXIS 2D shall be installed in such a way that it can take the actual wall displacement into account, not the final displacement. It can either be done by a 3D finite element, asymmetric model or empirical equation provided by Vlachopoulos and Diederichs (2009), which is based on the convergence-confining method. In this thesis, due to time restrictions, this analysis is not performed and supports are only analysed from structural models, aiming to achieve more realistic distribution forces in SCL compared to 2D rock mechanical models.

From Section 4.2.3, the 2D models do not consider any out-of-plane strain and therefore do not take restraints in longitudinal direction into account, as it will be in reality. It is evident from the deformed shapes from structural models presented in Figure 4.44. From the figure, the SCL shows lesser displacement compared to rock mechanical models, while calibrated for the same bending moment. It justifies that the 3D model is better in producing more realistic results compared 2D models.

The structural models are showing higher compressive axial forces in transverse direction in the SCL than rock mechanical models, as shown in Figures 4.41 and 4.45. It can also be seen from the figures, the axial forces are more concentrated on RRS than SFRC between two consecutive RRS. It is happening because the RRS are stiffer than the SFRC layer, hence attracting more forces. In rock mechanical models, the SCL and rock bolts are installed in stages unlike the structural models. Therefore, the SCL is converging differently in both models. In rock mechanical models, the SCL installed in stage 4 and stage 6 (see Figures 4.10d and 4.10f) is supported only by rock bolts. After completion of SCL installation in stage 8 (see Figure 4.10h), the SCL behaves as a whole similar to structural model, whereas in structural model, it behaves as a whole when the full load is applied and thereby showing higher compressive axial forces. Moreover, the SCL will experience some resistance from soil in tangential direction in rock mechanical models due to friction, which is ignored in this analysis as mentioned in Section 4.2.5.1. Therefore, more sophisticated calibration of structural models with rock mechanical models by applying realistic tangential spring stiffness due to rock mass and realistic spring stiffnesses of rock bolts based on construction stages may provide similar distribution of axial forces. Along with high axial forces, high bending moments are also seen in the SCL in structural models compared with rock mechanical models, as presented in Figures 4.42 and 4.46. The high bending moments can also be explained by the justification provided for high axial forces in this paragraph. Besides, the spring stiffnesses due to rock masses in the structural models, kept same along the perimeter of SCL. However, the spring stiffnesses will not be same everywhere in the SCL, for instance the spring stiffness at invert would be higher than at the side wall. Hence, updating the spring stiffness would provide better distribution of bending moments

Besides, a very high axial force concentrations can be seen at the corners in Figure 4.45, it is due to meshing of structural elements. The spring stiffnesses of rock mass and rock bolts calculated in Section 4.2.5 are applied at nodes of finite element nodes. Therefore, ROBOT calculated a concentrated values at these nodes. However, in reality the support due to rock mass is linear, not concentrated on a point (node). Thus, these concentrated areas should be ignored in the analysis, and forces shall be looked at a distance away from corner, where more realistic distribution can be seen.

The structural verification presented in Section 4.4 shows the bending moments and corresponding axial force are higher than the respective capacities of RRS sections without reinforcement in exceptionally poor and very poor rock masses after 12 hours of construction as shown in Figure 4.52a and Figure

4.54a. However, it shall be noted that the structural model is producing results for the completely mobilized rock pressure, which is very unlikely to occur in reality. For a stable excavation, the rock pressure mobilizes with time after installing the supports. Both the cases, where design of RRS could not be verified, are after 12 hours of excavation. Therefore, assuming that the full rock pressure Will not be mobilized after 12 hours, the actual rock pressure shall be determined to apply in the structural model. Although, it may be very difficult to determine the mobilisation of rock pressure with time, detailed study of rock-linear interaction by analytical methods may provide a good estimation.

It is to be noted that the in current assessment only considers structure's self-weight and rock pressure acting on the SCL. Howbeit, the long-term effects such as creep and shrinkage, effect of change in ambient temperature should also be included, while designing a structure for its service life. The wind loads due to movement of trains (wind pressure of suction) may also have adverse effect on the stability, thus shall be included in detailed design.

Chapter 6

CONCLUSION

In this thesis, the rock parameters for establishing Q-system are estimated from the available borehole loggings in three sets, followed by the calculation of Q-values. From the calculated Q-values, the data sets are defined as exceptionally poor, extremely poor and very poor quality rock masses. Thereafter, the rock supports recommendations from Qsystem handbook NGI (2015) are assessed. The strength and deformation properties of rock mass are estimated for Hoek-Brown and Mohr-Coulomb failure criteria, from available borehole loggings and parameters for Q-system to input in numerical analysis. For the present case, the estimated Mohr-Coulomb parameters are found to be unrealistically high, and thus Hoek-Brown parameters are used.

The numerical analysis divided into two part in order to avoid the need of a 3D rock mechanical model. The 2D rock mechanical models are prepared and the bending moments in sprayed concrete lining (SCL) are calibrated with structural models to observe the behaviour of SCL in 3D. In is observed, the structural models cope with the initial assumption of obtaining the 3D distribution of forces in SCL. However, some uncertainties are observed in analysis, as discussed in previous chapter. Thereby, a detailed analytical rock-linear interaction analysis can help to cope with present uncertainties in structural models.

Lastly, the design of RRS are verified from M-N interaction curves for plain concrete, SFRC and reinforced concrete for short-term and long-term cases. It is observed that the RRS for exceptionally poor, extremely poor and very poor rock masses do not need any reinforcement in long-term case, as recommended by Q-system to cater the design forces. However, short-term verification does not providesatisfactory results and reinforcement in RRS is required for exceptionally and very poor rock masses. Albeit, the design forces are not much higher than the capacities, slight increase in the thickness of RRS can completely remove the requirement of reinforcement for exceptionally poor and very rock masses inshort-term condition.

From the analysis, it can be concluded that the present analysis successfully proves that the recommended rock supports from Q-system are conservative for exceptionally poor to very poor rock masses ($Q < 1$) and can be optimized by using numerical analysis. However, the numerical analysis is not easy to use as Q-system, but can improve the safety at site and the pace of construction by optimizing the rock supports.

6.1 Future work

In this thesis, a complicated analysis in carried out in relatively short time (6 months), thus, the assumptions and simplifications were necessary in absence of proper laboratory tests. The following recommendations could significantly improve the outcome of future work.

- (i) The geological mapping must be carried out to obtain rock parameters for Q-system and GSI. The rock parameters for intact rock m_i and σ_{ci} shall be obtained from the laboratory tests to calculate HB-parameters.
- (ii) In case MC failure criterion is used for the analysis, friction angle (ϕ) and cohesion (c) shall be obtained from laboratory tests.

- (iii) For calculating spring stiffnesses from rock mass and rock bolts to use in structural models, the analytical rock-linear interaction analysis must be carried out. The convergence-confinement analysis shall be included in rock mechanical models to obtain realistic forces in SCL from rock mechanical models.
- (iv) The non-linear time dependent strength of SFRC should be studied to analyse the behaviour of SFRC in both short-term and long-term, especially when tensile forces are being applied.
- (v) The structural model shall be calibration for the mobilised rock pressure at the time, when the analysis is being carried out, not the full rock pressure.
- (vi) For ease in modelling, the FE mesh in structural models are divided according to rock bolts spacing. However, when time is not a constraint, the finer mesh shall be created and the spring stiffness shall be applied to reflect the real case scenario.

REFERENCES

- Azami, A., T. Yacoub, J. Curran, and D. Wai (2013). "A Constitutive Model for Jointed Rock Mass". In: *International Society for Rock Mechanics and Rock Engineering*.
- Bandis (1993). "Engineering properties and characterization of rock discontinuities". In: *Comprehensive Rock Engineering: Principles, Practice & Projects*, Pergamon Press, Oxford, pp. 18–155.
- Barla, G. and M. Barla (2000). "Continuum and discontinuum modelling in tunnel engineering". In: *Rudarsko-Geološko-Naftni Zbornik 52*, pp. 45–57.
- Barton, N., R. Lien, and J. Lunde (Dec. 1974). "Engineering classification of rock masses for the design of tunnel support". In: *Rock Mechanics Felsmechanik Mecanique des Roches 6*, pp. 189–236.
- Barton, N. (1972). "A model study of rock-joint deformation". In: *Int. J. Rock Mech. Min. Sci., Vol. 9*, pp. 579–602.
- Barton, N. (1998). "Quantitative description of rock masses for the design of NMT reinforcement". In: *International conference on hydro power development in Himalayas, Shimla, India*.
- Barton, N. and S. Bandis (1982). "Effect of block size on the shear behavior of jointed rocks". In: *Proceedings - Symposium on Rock Mechanics*, pp. 739–760.
- Barton, N. and V. Choubey (1977). "The shear strength of rock joints in theory and practice". In: *Rock Mechanics Felsmechanik Mecanique des Roches 10*, pp. 1–54.
- Barton, N. and E. Grimstad (2014). *Q-system - an illustrated guide following forty years in tunneling*.
- Bieniawski, Z. T. (1974). "Geomechanics classification of rock and its application in tunnelling". In: *Proc. 3rd ISRM Congress, Denver, vol. II-A*.
- Bieniawski, Z. T. (1976). "Rock mass classification in rock engineering". In: *Proc. Symp. Exploration for Rock Engineering, Johannesburg*.
- Bieniawski, Z. T. (1989). *Engineering Rock Mass Classifications: A Complete Manual for Engineers and Geologists in Mining, Civil, and Petroleum Engineering*. John Wiley, New York. isbn: 978-0-471-60172-2.
- Chang, Y. and H. Stille (1993). "Influence of early-age properties of shotcrete on tunnel construction sequences". In: *Shotcrete for Underground Support*, pp. 110–117.
- Deere, D. U. (1963). "Technical description of rock cores for engineering purposes". In: *Felsmechanik und Ingenieurgeologie 1*, pp. 16–22.
- Deere, D. U. (1968). *Chapter 1: geological considerations*. In: *Stagg KG, Zienkiewicz OC, editors, Rock mechanics in engineering practice*. London, pp. 1–20.

- DS/EN-14487-1 (2005). *Sprayed concrete - Part 1: Definitions, specifications and conformity*. Danish standards.
- DS/EN-1990 (2007). *Eurocode 0: Basis of structure design*. Danish standards.
- DS/EN-1992-1-1 (2005). *Eurocode 2: Design of concrete structures - Part 1-1: General rules and rules for buildings*. Danish standards.
- Fib (2013). *fib model code for concrete structures 2010*. eng. Ernst & Sohn, Wiley, pp. XXXI, 402. isbn: 9783433604090. url: <http://dx.doi.org/10.1002/9783433604090>.
- Goricki, A. (2003). “Classification of Rock Mass Behaviour based on a Hierarchical Rock Mass Characterization for the Design of Underground Structures”. PhD thesis. Graz University of Technology.
- Hoek, E. (1994). “Strength of rock and rock masses”. In: *ISRM New Journal* 2(2), pp. 4–16.
- Hoek, E. (2004). *Unpublished notes - Numerical Modelling for Shallow Tunnels in Weak Rock*. url: <https://www.Bentley.com/assets/resources/learning/papers/Numerical-Modellingfor-Shallow-Tunnels-in-Weak-Rock.pdf>.
- Hoek, E. (2006). *Practical rock engineering*. Lecture notes, University of Toronto.
- Hoek, E. and J. Bray (1977). *Rock slope engineering*. Institution of Mining and Metallurgy: London.
- Hoek, E. and E. T. Brown (1980). “Empirical strength criterion for rock masses”. In: *Rock mechanics Geotech. Engng Div., ASCE* 106 (GT9), pp. 1013–1035.
- Hoek, E. and E. T. Brown (2018). “Hoek-Brown failure criterion and GSI - 2018 edition”. In: *Journal of Rock Mechanics and Geotechnical Engineering* 11, Issue 3, pp. 445–463.
- Hoek, E. and M. S. Diederichs (2006). “Empirical estimation of rock mass modulus”. In: *International Journal of Rock Mechanics & Mining Sciences* 43, pp. 203–215.
- Hoek, E., D. Wood, and S. Shah (1992). “A modified Hoek–Brown failure criterion for jointed rock masses”. In: *Rock Characterization: ISRM Symposium, Eurock '92, Chester, UK, 14–17 September 1992*, pp. 209–214.
- Hoek, E. and E. T. Brown (1997). “Practical Estimates of Rock Mass Strength”. In: *International journal of rock mechanics and mining sciences* 34, pp. 1165–1186.
- Hoek, E., C. Carranza-Torres, B. Corkum, and C. Carranza-Torres (2002). “Hoek-Brown failure criterion - 2002 Edition”. In:
- Hoek, E., T. Carter, and M. Diederichs (2013). “Quantification of the Geological Strength Index Chart”. In: *47th US Rock Mechanics / Geomechanics Symposium 2013* 3, pp. 1757–1764.
- Hudson, J. A. and J. P. Harrison (1997). *Engineering rock mechanics - an introduction to the principles*. Pergamon - An imprint of Elsevier Science. isbn: 0-08-04 19 12-7.
- ISRM (1978). “International Society for Rock Mechanics Commission on Standardisation of Laboratory and Field Tests - Suggested methods for the quantitative description of discontinuities in rock masses”. In: *Int. J. Rock Mech. Min. Sci. & Geomech. Abstr.* 15, pp. 319–368.

References

- Jakobsen, A. (2018). *FagrappportIngeniørgeologi:Nykirke–Barkåker*. url: <https://www.banenor.no/Prosjekter/prosjekter/vefoldbanen/nykirke-barkaker/planerogdokumenter/>. (accessed: 30.04.2020).
- Kanik, M. and Z. Gurocak (2018). “Importance of numerical analyses for determining support systems in tunneling: A comparative study from the trabzon-gumushane tunnel, Turkey”. In: *Journal of African Earth Sciences* 143.

- Kulhawy, F. and R. Goodman (2010). *Foundations in rock, Chapter 55 in Ground engineers reference book, F. G. Bell (ed.)* Butterworths, London.
- Marinos, V. (2012). “Assessing Rock Mass Behaviour for Tunnelling”. In: *Environmental and Engineering Geoscience* 18, pp. 327–341.
- Marinos, V., P. Marinos, and E. Hoek (2005). “Recent developments in rock support estimates by the RMI”. In: *Journal of Rock Mechanics and Tunnelling Technology* 6, pp. 1–19.
- Mayta, E., J. S. Diaz, and R. Brierley (2018). *Design methodology for permanent complex structures: Secondary lining design in junction*. ICE.
- NB (2011). *Norwegian concrete association, publication No. 7: Sprayed concrete for rock support*.
- NGI (2015). *Handbook “Using the Q-system-Rock mass classification and support design”*. Oslo, Norway, pp. 1–54.
- Oke, J., N. Vlachopoulos, and M. Diederichs (2014). “Numerical analyses in the design of umbrella arch systems”. In: *Journal of Rock Mechanics and Geotechnical Engineering* 6, pp. 546–564.
- Palmstrøm, A. (1995). “RMI – a rock mass characterization system for rock engineering purposes”. PhDthesis. University of Oslo.
- Palmstrøm, A. (2000). “Recent developments in rock support estimates by the RMI”. In: *Journal of Rock Mechanics and Tunnelling Technology* 6, pp. 1–19.
- Palmstrom, A. and E. Broch (2006). “Use and misuse of rock mass classification systems with particular reference to the Q-system”. In: *Tunnelling and Underground Space Technology* 21, pp. 575–593.
- Palmström, A. and H. Stille (2010). *Rock engineering*. Thomas Telford Ltd: London.
- Pells, E. J. N. and R. Bertuzzi (2007). “Limitations of rock mass classification systems”. In: pp. 33–34+37.
- Rahmani, N., B. Nikbakhtan, K. Ahangari, and D. Apel (2012). “Comparison of Empirical and Numerical Methods in Tunnel Stability Analysis”. In: *International Journal of Mining, Reclamation and Environment* 26, pp. 261–270.
- Read, J. and P. Stacey (2010). *Guidelines for open pit slope design*. CSIRO Publishing.
- ROBOT (2019). *structural analysis professional, software version: 32.0.2.6571, user manual, Autodesk Inc.* url: <https://knowledge.autodesk.com/support/robot-structural-analysis/products/learn?sort=score>.
- RocData (2019). *software Version: 5.009, user manual, Bentley Inc.* url: https://www.Bentley.com/help/rocddata/#t=rocddata%5C%2FRocData_Overview.htm.
- PLAXIS 2D (2019). *software Version: 5.009, user manual, Bentley Inc.* url: https://www.Bentley.com/help/PLAXIS_2D/#t=getting_started%5C%2FPLAXIS_2D_Applications_Overview.htm.
- Saiang, D. and N. Marshall (2013). “Hoek-Brown VS. Mohr-Coulomb - Results from a three-dimensional open-pit/underground interaction model”. In: *Bergmekanikdagen2014, Stockholm*.
- Vallejo, L. G. de and M. Ferrer (2011). *Geological Engineering*. CRC Press.

Vlachopoulos, N. and M. Diederichs (2009). “Improved Longitudinal Displacement Profiles for Convergence Confinement Analysis of Deep Tunnel”. In: *Rock Mechanics and Rock Engineering* 42, pp. 131–146.

Wittke, W. (2014). *Rock Mechanics Based on an An-isotropic Jointed Rock Model (AJRM)*. Ernst & Sohn (A Wiley Brand). isbn: 9783433030790.

Wyllie, D. C. and C. W. Mah (2006). *Rock slope engineering, 4th edition*. Spon Press, Taylor & Francis Group.

